EXAMINING OF THE BIOPHYSICS OF ULTRASOUND AND ULTRASOUND CONTRAST AGENT INDUCED ANGIOGENESIS

BY

CHENARA A. JOHNSON

DISSERTATION

Submitted in partial fulfillment of the requirements
for the degree of Doctor of Philosophy in Bioenginnering
in the Graduate College of the
University of Illinois at Urbana-Champaign, 2011

Urbana, Illinois

Doctoral Committee:
Professor William D. O'Brien, Chair
Professor Michael F. Insana
Professor David Bunick
Assistant Professor Michael L. Oelze

ABSTRACT

Ischemic diseases affect more than 100 million people in the United States alone (NDFS 2011, Roger et al. 2011). Current interventions include: ablation, angioplasty, revascularization and bypass surgery. The invasive nature of these techniques excludes patients with who are not amenable to surgical intervention. For this reason, alternative methods of revascularization in ischemic cardiac muscle have been explored. Over the past two decades, cellular, molecular, and genetic therapy attempts have been made in order to find a clinically relevant treatment. Ultimately, it is the invasiveness or lack of site specificity that provides the largest obstacle for therapeutic effectiveness of angiogenic treatments.

Current research suggests that ultrasound-ultrasound contrast agent treatment can be therapeutically beneficial, providing a noninvasive way to spatially and temporally target ischemic tissues. This type of angiogenic therapy can be used as an alternative to high risk percutaneous intervention or bypass graft surgery. Several studies report a reparative response to ultrasound-ultrasound contrast agent exposure and state that inertial cavitation, or microbubble collapse, is possibly required for angiogenesis to occur. Numerous small-scale studies have shown promising results; however, when large scale double blind studies were conducted, they showed limited effects. A major impediment for progress to clinical applicability is, perhaps, the lack of understanding the biophysical mechanisms that connect ultrasound-ultrasound contrast agent to neovascularization.

This thesis seeks to explore the biophysics of ultrasound-ultrasound contrast agent-induced capillary angiogenesis, specifically examining the role of the ultrasound contrast agent in creating bioeffects that lead to subsequent angiogenesis. The mechanistic exploration examines both the necessity and concentration of ultrasound contrast agents, bubble dynamics,

the biophysical effects of ultrasound contrast agents and several ultrasound parameters on causing/enhancing ultrasound-induced angiogenesis.

A series of experiments were conducted to examine the biophysics of ultrasound and ultrasound contrast agent induced angiogenesis. The first experiment explores the effect of ultrasound contrast agents on ultrasound-induced angiogenesis with a 3 x 2 x 4 factorial study assessing survival day, infusion media (saline or ultrasound contrast agent) and acoustic pressure, respectively. Then, several exposure-effect studies are presented to examine the specific parameters on the bioeffect and subsequent angiogenic response, both acutely (at 0 day) and at 5 days post exposure. Ultrasound contrast agent concentration is initially explored, followed by a revisit of pressures involvement at a higher contrast agent concentration. In an effort to further understand the biophysical mechanism, a collapse threshold study was conducted, narrowing the pressure range to determine if/ the extent to which collapse was necessary for angiogenesis. Then theoretical models were used to connect the ultrasound contrast agent biophysics to the bioeffects for the therapy. To establish a trail of evidence leading from ultrasound-ultrasound contrast agent induced bioeffects to angiogenesis and characterize the biological motivation, a tissue effect histological study was conducted to establish if the angiogenic response is damage driven. Several other parameters, pulse repetition frequency, exposure duration and the total number of pulses, are also discussed in terms of their influence on the angiogenic response.

All of the data gathered herein lead to several conclusions: 1) ultrasound contrast agents increase the angiogenic response, 2) ultrasound contrast agent collapse is required for the increased angiogenic response, 3) increases in vascular permeability occur acutely with collapse, 4) shear stresses during exposure are likely involved in the induction of acute bioeffects, 5)

acoustic pressures equal to or greater than 1.3 MPa demonstrate a deleterious effect, and 6) there is a concurrent increase in vascular endothelial growth factor expression and capillary density at 5 days post exposure that suggests an peak range of parameters for ultrasound-ultrasound contrast agent induced angiogenesis. For the studies conducted herein, the optimal window for the angiogenic response was a number of pulses $\leq$ 3000, a duty factor on the order of 10^{-2}, acoustic pressure ~ 0.7 MPa, pulse repetition frequency ~ 10 Hz, and exposure duration between 2 to 5 minutes. This compilation of studies not only provides some biophysical mechanistic information but also a bit of predictive information when determining appropriate settings for ultrasound-ultrasound contrast agent induced angiogenesis.

Dedicated to my parents, Loise Smith and Clarence Johnson, Jr, and my sisters: Chelsea, Cacharel and Clarissa Johnson.

ACKNOWLEDGEMENTS

I would like to firstly say a big “thank you” to Dr. William D. O’Brien, Jr. for providing me the opportunity to be a part of the Bioacoustics Research Lab and conduct this research. Without his advice and guidance the work would not have been possible. I’d be remiss not to include an additional thank you for the letters of recommendation, the one-on-one practice presentations and the many, many revisions of manuscripts and fellowship applications. Dr. O’Brien was always available to talk, even when I knew he was busy with other obligations; I have always been baffled by how he seemingly creates time.

I also would like to thank my doctoral committee: Dr. David Bunick, Dr. Michael Oelze, and Dr. Michael Insana. They have been with me since the beginning and have each given me valuable advice and insight regarding this work. I would especially like to thank Dr. Bunick and wife, Carrol Bunick for opening up their lab to me, and making me feel incorporated. Dr. Bunick was always willing to discuss my ideas and theories, and Carrol was always there to help figure out why my experiments weren’t working and offer motherly advice.

I am very grateful for the BRL team, so thank you to: Dr. Rita Miller for her patience with my last minute orders and assistance with experiments, Jim Blue for his help with troubleshooting experiments, Sue Clay for all of the orders, submissions and conference handiwork, and Daniel King, whose work forms the basis upon which my work builds. Jose Sanchez, Zachary Hafez, and Monica Forbes were also members of the lab that I’m thankful for—they provided me with entertaining conversation, valuable life advice and research solutions.

In addition, I’d like to acknowledge my sources of funding for this work: NIH Grants R37EB002641 and F31HL097653.

From the Medical Scholars Program, Dean Carien Williams, Dean Susan Kies, Dr. James Slauch, and Dr. Nora Few are also extremely appreciated. I don't know what I would have done without their support. Thank you for providing a listening ear, for valuing my voice, and for encouraging me when I was frustrated. Also, a special thanks to Dr. Katherine Omueti-Ayoade for her encouragement, uplifting words and advice.

I'd like to acknowledge my family for their support in this endeavor. I thank my mother for her prayers, my father for his wisdom, and my sisters for always reminding me where I came from.

Enyinnaya Egejuru has played a pivotal role in backing me on this path. Words can't even begin to capture the immense gratitude I have for him. He always made sure I had what I needed.

There are several others who offered their support in my journey—I'd like to take the last several lines to acknowledge the positive impact they've had over the past several years, so a warm thank you to: 'Zed', 'Wargus', 'Zay', 'R Breezy', 'Natan', 'JP', and 'Connie'—each of them were there to pick me up when I was down and to celebrate the victories—I will never forget that. I am blessed to have met all of them.

Thank God for seeing me through it all.

TABLE OF CONTENTS

LIST OF ABBREVIATIONS

Ang	angiopoietin
AR	angiogenic response
ARP	angiopoietin related protein
bFGF	basic fibroblast growth factor
CBP	CREB binding protein
CDC	cell division control molecule
CVD	cardiovascular disease
CW	continuous wave
DAG	diacylglycerol
DPE	days post exposure
EBD	Evans blue dye
EC	endothelial cell
ECM	extracellular matrix
ED	exposure duration
FAK	focal adhesion kinase
FGF	fibroblast growth factor
GTP	guanosine-5'-triphosphate
HIF-1α	hypoxia inducible factor-1 alpha
HRE	hypoxia response elements
IC	inertial cavitation
IL	interleukin
IP_3	inositol triphosphate
MAPK	mitogen-activated protein kinase
MI	mechanical index
MMP	matrix metalloproteinase
NADPH	nicotinamide adenine dinucleotide phosphate
NO	nitric oxide
NP	number of pulses
OAc	acetate
PAD	peripheral arterial disease
PD	pulse duration
PDGF	platelet derived growth factor
PHD	proline hydroxylase
PLC	phospholipase C
Pr	peak rarefactional pressure, acoustic pressure
PRF	pulse repetition frequency
ROS	reactive oxygen species
TGF-β	transforming growth factor-beta
TIE	tyrosine kinase immunoglobulin & epidermal growth factor domains
TNP	total number of pulses
Ub	ubiquitin
US	ultrasound
UCA	ultrasound contrast agent

[UCA]	ultrasound contrast agent concentration
USFV	ultrasound focal volume
VEGF	vascular endothelial growth factor
VHL	von Hippel Lindau

LIST OF SYMBOLS

α	absorption coefficient
a	instantaneous radius
a_e	equilibrium radius
B	volume of blood in the US focal volume
c	speed of sound
C_v	heat capacity per unit volume
C_d	drag coefficient of the bubble
d_v	boundary layer thickness
d_o	distance between two bubble centers
ξ	radial displacement
ϵ	compressibility of the bubble
$\dot{}$	first derivative with respect to time
$\ddot{}$	second derivative with respect to time
f	frequency
f_o	undamped natural resonant frequency
f_{res}	damped resonant frequency
F_f	frictional forces from damping
F_L	force on the bubble from surrounding liquid
F_s	force on the bubble surface
F_m	mechanical forces
F_{rad}	radiation force
F_d	drag force
F_{sd}	Stoke's drag force
G_s	shear elastic modulus
Γ	volume fraction
h	enthalpy
i	imaginary number
I	infusion rate
I_{TA}	temporal average intensity
k	wavenumber = $2\pi/\lambda$
K	rate
κ	polytrophic gas exponent
λ	wavelength
m	effective mass
M	added mass of translating bubble
N	number of bubbles
$N_{D\text{-}USFV}$	number of Definity® microbubbles in the US focal volume
$N_{R\text{-}USFV}$	number of RBCs in the US focal volume
η_s	shell dilatational viscosity
ω	angular frequency
p	pressure
Pr, p_r	peak rarefactional pressure
p_s	pressure on the bubble shell

p_o	atmospheric pressure
p_∞	pressure in the liquid far from the bubble
p_v	vapor pressure
p_g	gas pressure in the bubble; equilibrium pressures
p_L	pressure in the liquid
φ	decay constant
P_{opt}	the smallest pressure required for an optimal sized bubble
$P_{r,3}$	derated peak rarefactional pressure
Q	quantity
$\dot{Q}$	amount of heat generated per unit volume
Φ	velocity potential
r	radius
R	mechanical resistance
Re	Reynold's number
S_p	shell elasticity (stiffness)
S_f	shell friction
δ	damping term due to viscosity (δ_{visc}), shell (δ_{shell}), or total (δ_t)
σ	surface tension
Δt	time, exposure duration (ED)
T_{max}	maximal temperature
ΔT_{max}	maximal temperature increase
u	velocity of liquid
μ	shear viscosity
V	volume
V_B	volume of blood
V_{blood}	volume of the blood in the rat
V_D	volume of gas contained in Definity®
V_{focus}	volume of the US focus
V_{rat}	estimated volume of the rat
V_T	total volume
v(t)	velocity of bubble in a steady fluid
v_{grad}	velocity gradient
v_a	velocity of approach
x	shell thickness
y	van der Waals hard core radius
χ	elastic modulus

CHAPTER 1: INTRODUCTION

Ischemic diseases affect more than 100 million people in the United States alone (NDFS 2011, Roger et al. 2011). These diseases include cardiovascular and diabetic complications. The people suffering from such illnesses would benefit from some form of proangiogenic therapy (Lloyd-Jones et al. 2009, Roger et al. 2011). There are presently three scenarios for which proangiogenic therapies are used clinically: chronic wounds, peripheral artery disease and ischemic heart disease (Li et al. 2004, Li et al. 2005), where the goal is to increase neovascularization, or new blood vessel growth, to promote healing. The number of individuals who could benefit from proangiogenic therapy increases drastically when including patients with atherosclerotic disease and hypertension. In addition to these, proangiogenic therapy has another realm of application in plastic surgery and dermatology with the minimization of scars and increased healing time. The benefits of researching novel ways of promoting angiogenesis and the potential impact are tremendous.

1.1 Clinical treatments for ischemia

Ischemia is currently treated by either amputation or restoration of blood flow. Because amputation is undesirable, efforts are made to restore blood flow. Clinically, blood flow restoration is accomplished mechanically or with surgical intervention.

Mechanical stimulation methods involve methods that apply shear stress, perturb the vessel walls or produce muscle contractions. Mechanical stimulation is typically a treatment for mild forms of ischemia resulting from diabetic complications or patients with intermittent claudication of limbs. Generally the mechanical stimulation comes in the form of exercises to increase blood flow, tissue perfusion, and to some extent muscle hypertrophy (which necessitates angiogenesis). Recently, the clinical use of ultrasound (US) as an external mechanical stimulus

has been used to enhance bone healing, presumably via angiogenesis. Its exact mechanism of action, however, remains unclear. Both exercise and US are used in mild ischemic scenarios, but are not useful when blood supply has been severely diminished. Therefore, surgical intervention is another method for treating ischemia.

Surgical interventions include endovascular surgery such as by-pass and revascularization by way of wounding (where angiogenesis occurs secondary to wounding) (Estvold et al. 2010, Lucas et al. 2011). In by-pass surgery a vascular graft is either manufactured or removed from the veins of the patient and a conduit allowing blood to by-pass the occluded vessel is attached. By-pass surgery involves maximal invasiveness because it requires not only open heart surgery, but often times additional surgery to be performed on the limb from which the venous graft is taken.

Endovascular surgery includes angioplasty and the placement of stents to fortify and widen vascular lumens in an effort to increase blood flow and cause capillary growth. The endothelial cells of vasculature are sensory cells that respond to increases and decreases in flow, and at the capillary level growth and regression, respectively. While endovascular techniques are minimally invasive, not all patients qualify for the procedure. Also angioplasty increases risk of other complications like arterial dissection, aneurysms, and general weakening of the vascular wall.

Revascularization was introduced for patients who did not qualify for bypass or angioplasty. Revascularization can be direct or transmyocardial, where an incision is made to expose the heart and a laser is used to drill a series of holes in the left ventricle. This procedure uses secondary wound healing angiogenesis to treat pain caused due to ischemia, where damage

is created to boost the normal wound healing response and cause capillary growth. Revascularization is associated with the risk of death, stroke and MI.

Currently clinical methods for inducing angiogenesis in cardiac and skeletal muscle remain invasive, and are contraindicated for certain populations as a result. Typically the procedures require reintervention that ultimately has more risks. Therefore less invasive and less exclusive methods have been researched.

1.2 Research-based methods for treating ischemia

Research-based techniques for increasing angiogenesis include: the use of growth factors, genes, or stem cells and mechanical stimulation. Stimulation by growth factors, genes, or stem cells typically involves direct injection or infusion of proangiogenic molecules. Infusion is challenging because factors can diffuse throughout the body, having a nontargeted effect. Similarly, direct muscular injection may cause complications with absorption (it may diffuse away) or discomfort associated with multiple injection sites. In the last few decades other forms of therapeutic stimulations evolved, including cellular and genetic methods where stem cells or DNA are injected at the ischemic site (Messina et al. 2002, Halkos et al. 2008). These injections also pose difficulty with absorption and stability of the injected substance. It is therefore important to explore spatially specific, noninvasive methods for treating ischemia.

Mechanical stimulation has been the most promising method for the induction of noninvasive spatially specific angiogenesis. Literature dating back to the 1970s showed US to provide spatial specificity and a noninvasive way of treating ischemia. This enhancement of wound healing was hypothesized to be angiogenesis driven (Dyson et al. 1968). With the advent of ultrasound contrast agents (UCAs), researchers were able to spatially distribute angiogenesis promoting factors and track their absorption into the tissue. While some researchers use UCAs

to deliver growth factors or stem cells to ischemic areas, others utilize UCAs for noninvasive secondary wound healing angiogenesis. Secondary wound healing angiogenesis, in this case, is defined as the local, focal cause of damage to the peripheral vasculature of the ischemic area in an effort to boost the normal wound healing responses and cause an ingrowth of capillaries. A limiting factor of applicability with using US and UCAs to induce angiogenesis is that there remains a lack of consensus regarding dosage that ultimately prevents its transition to clinical use. Specifically, a wide range of peak rarefactional pressures (Pr) and UCA concentrations have been used and demonstrated some level of effect. Pr is of particular importance when UCAs are used because as Pr increases the UCAs responses change from a regime of oscillation to collapse. These physical microbubble responses affect the surrounding medium leading to a range of bioeffects. Potentially, it is these bioeffects that motivate the angiogenic response noted with US and UCA therapy. However, no investigation of the biophysical mechanism by which US and UCA-induced angiogenesis occurs has been conducted. Therefore the biophysical mechanism of bubble dynamics that lead to the bioeffects and result in an angiogenic response are explored herein.

1.3 Overview

This thesis seeks to explore the biophysics of US and UCA-induced capillary angiogenesis, specifically examining the role of the UCA in creating bioeffects that lead to subsequent angiogenesis. The scope of this study is confined to using a normal rodent model *in vivo* to explore mechanisms of the UCA effects. The mechanistic exploration examines both the necessity and concentration of UCAs, bubble dynamics, the biophysical effects of UCAs and several US parameters on causing/enhancing US-induced angiogenesis.

This thesis will begin by discussing angiogenesis, its primary molecular motivators and its various stages. Next, there will be a discussion of current proangiogenic techniques, the angiogenic stage at which the procedure acts and the short comings of current techniques. The thesis will then shift focus to a discussion of US and UCAs, and in particular the physical responses of UCAs to US exposure. Mathematical models for free and shelled bubble dynamics will be discussed as well as experimental models for oscillation and collapse. A brief introduction to complex clouds of bubbles with a particular volume fraction is also included. After introducing US and UCAs, a discussion of the current understanding of how US-UCAs relate to the induction of angiogenesis will be given followed by identification of areas that remain unexplored.

This thesis will provide the methods used for the seven experiments presented herein, and then detail each of those seven experiments. The overall goals of the experiments are to explore the role of the UCA and then examine the mechanism of US and UCA induced angiogenesis. The first experiment explores the effect of UCAs on US-induced angiogenesis with a 3 x 2 x 4 factorial study assessing survival day, infusion media (saline or UCA), and acoustic pressure (Pr), respectively. Then, several exposure-effect studies are presented to examine the specific parameters on the bioeffect and subsequent angiogenic response, both acutely (at 0 day) and at 5 days post exposure (DPE). UCA concentration ([UCA]) is initially explored, followed by a revisit of Prs involvement at a higher [UCA]. In an effort to further understand the biophysical mechanism, a collapse threshold study was conducted, narrowing the Pr range to determine if/ the extent to which collapse was necessary for angiogenesis. In order to establish a trail of evidence leading from US exposure to angiogenesis and characterize the biological motivation, a tissue effect histological study was conducted to establish if the angiogenic response is damage

driven. Finally, several other parameters, pulse repetition frequency, exposure duration and the total number of pulses, are also discussed in terms of their influence on the angiogenic response. The final chapter provides a summary of all experiments, and then contextualizes and interprets the results.

1.4 Clinical significance

Understanding the biophysical mechanism by which UCAs operate to induce acute bioeffects that lead to angiogenesis is integral to not only therapy optimization, but also aids in its transition to clinical use. Currently various UCAs with varying [UCA]s and wide ranges of US exposure parameters are used. The attempt herein is to control the variation, such that not only can a physical mechanism be elucidated, but also to determine which of the tested parameters motivate the angiogenic response. In addition, a biological mechanism is explored. Understanding the mechanistic motivators and investigating the extent to which UCA and US parameters interact to cause angiogenesis is of importance in gauging adequate exposure parameters. Ultimately this information will be vital to figuring out how to clinically implement US and UCA induced angiogenesis.

CHAPTER 2: ANGIOGENESIS & CURRENT PROANGIOGENIC TECHNIQUES

This chapter discusses angiogenesis beginning with its definition, followed by the mechanistic triggers, angiogenic stages and the molecules involved in potentiating new blood vessel formation. The chapter will extend the discussion of angiogenesis and its importance to ischemic diseases and cover the use of proangiogenic techniques as a method of restoring blood supply to hypoxic and nutrient deprived tissues. These techniques will be discussed with respect to their current use, invasiveness, specificity, and effectiveness.

2.1 Angiogenesis

Angiogenesis is primarily defined as the sprouting of blood vessels from preexisting vessels, but can also involve nonsprouting mechanisms called intussusceptive microvascular growth (Augustin et al. 2001). In angiogenesis there are several overlapping stages including: inflammation, formation of granulation tissue, reepithelialization, matrix formation, and remodeling (Barrientos et al. 2008).

The protagonists in angiogenesis are the endothelial cell (EC) and extracellular matrix (ECM) components. ECs serve as sensory cells for vasculature ultimately controlling constriction, dilation, and growth. These sensory cells respond to the demand of growing or healing tissues in response to angiogenic triggers.

The triggers for angiogenesis include: metabolic stressors, mechanical forces, and inflammatory cells. Metabolic stressors include low oxygen tension, low extracellular pH and low glucose concentration (Mariotti et al. 2006). One study found that angiogenesis is triggered by low oxygen levels itself as opposed to hypoxia-dependent events in energy metabolism (Pugh et al. 2003). Mechanical forces from the shear stress of blood flow also play an important role providing perfusion feedback, where poorly perfused vessels undergo regression, and highly

perfused vessels proliferate (Reynolds et al. 1998). Finally, most inflammation cells are proangiogenic and their specific role in angiogenesis is contingent upon the balance of mechanistic modulators including endothelial cells and angiogenic markers.

For all angiogenesis triggers, the pathways merge at the increased production of vascular endothelial growth factor (VEGF). In the case of wound healing, both the low oxygen and inflammatory cell pathways motivate angiogenesis. When the blood vessel lumen is disturbed homeostasis is the initial objective. Platelets degranulate to release VEGF, platelet derived growth factor (PDGF) and transforming growth factor-beta (TGF-β) (Mariotti et al. 2006, Barrientos et al. 2008). These growth factors attract neutrophils and monocytes (inflammation cells) to the area and release nitric oxide (NO). Monocytes mature to macrophages that initiate granulation tissue development. These macrophages infiltrate the perturbed tissues and secrete angiogenic factors such as HIF-1, IL-8, and matrix metalloproteinase 1, 2, and 9 (MMPs) to aid in potentiating angiogenesis (Mizrahi et al. 2007, Barrientos et al. 2008). The trigger for angiogenesis in wound healing is primarily the result of low oxygen levels leading to hypoxia inducible factor (HIF-1α) upregulation.

HIF-1α is normally manufactured in the EC (Figure 2.1). It is regulated by proline hydroxylases in the presence of oxygen. In normoxia, HIF-1α is hydroxylated by proline hydroxylases (PHD 1, 2 and 3) in the presence of O_2, Fe^{2+}, 2-oxoglutarate (2-OG) and ascorbate. Hydroxylated HIF-1α (OH) is recognized by pVHL (the product of the von Hippel–Lindau tumor suppressor gene), which, together with a multisubunit ubiquitin (Ub) ligase complex, tags HIF-1α with polyubiquitin; this allows recognition by the proteasome and subsequent degradation. Acetylation of HIF-1α (OAc) also promotes pVHL binding (Carroll et al. 2005).

However, in the absence of oxygen, proline hydroxylation is inhibited and HIF-1α accumulates. VHL is no longer able to bind and target HIF-1α for proteasomal degradation, which leads to HIF-1α accumulation and translocation to the nucleus. There, HIF-1α dimerises with HIF-1β, binds to hypoxia-response elements (HREs) within the promoters of target genes and recruits transcriptional co-activators such as p300/ CREB-binding protein (CBP) for full transcriptional activity (Carroll et al. 2005). Initiation ends with the production of the critical driver of angiogenesis: VEGF (Figure 2.1).

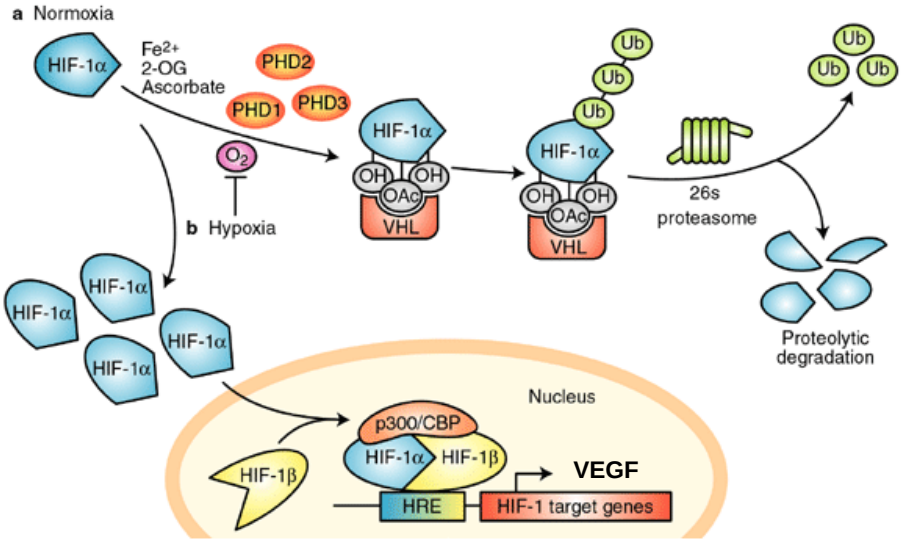

Figure 2.1: HIF-1α regulation in a) normoxic and b) hypoxic conditions (Carroll et al. 2005).

VEGF can also be mechanically stimulated. The mechanical stimulation of VEGF can be categorized as internal or external. Limited work has been performed on internal stimulation via shear stressors, but external stimulation has not been well characterized at all with respect to angiogenesis. With regard to internal stimulation, one study demonstrated that endothelial proliferation was correlated to high rates of blood flow in the female reproductive system (Reynolds et al. 1998), and others have noted the shear stress induction of reactive oxygen species (ROS), Rac-1, CDC-42, $\alpha_v\beta_3$, and Akt increasing VEGF expression (Girard et al. 1995, Gavard et al. 2006, Frey et al. 2009, Kasten et al. 2010).

These factors, in turn, attract endothelial and other cells contributing to the formation of new vessels (Figure 2.4). VEGF is also secreted from the endothelial cells in response mechanical perturbation not involving blood flow and metabolic stress (Mariotti et al. 2006).

VEGF causes the activation of four stages that culminate in angiogenesis: increased vascular permeability, EC remodeling, EC proliferation and migration, and EC survival for the newly formed vasculature. Increased permeability most often occurs via MMPs causing dissolution of the basement membrane to allow for the remodeling and migration of ECs. Vascular permeability is accomplished by the angiopoietin-2 (Ang-2) activation. Ang-2 binds to a TIE-2 receptor to block the steady state Ang-1 receptor that maintains the activity of vascular endothelial (VE) cadherin (an adhesion molecule between ECs) (Mukherjee et al. 2006, Mizrahi et al. 2007). VEGF assists in the inactivation of VE-cadherin by causing β-arrestin to form a complex with actin subunits (Gavard et al. 2006) (Figure 2.2).

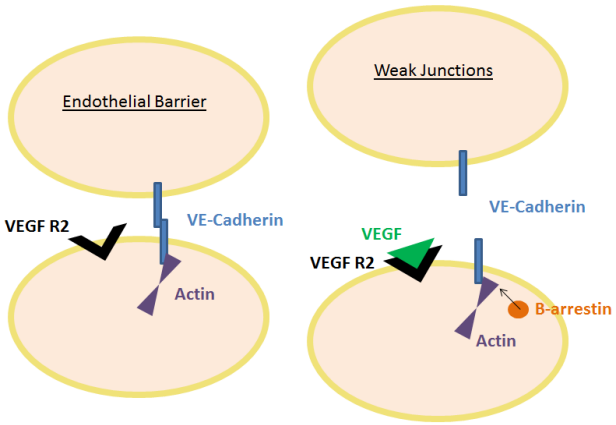

Figure 2.2: Vascular endothelial (VE) cadherin's role in destabilizing the endothelial barrier (adapted from Gavard et al. 2006, Mukherjee et al. 2006, and R&D Systems 2007).

EC remodeling occurs through several pathways, but of importance is the focal adhesion kinase (FAK) enzyme pathway. VEGF, along with PDGF, activates FAKs. FAK disassembles the structural proteins (vinculin, talin) of cell-cell and cell-ECM junctions. FAKs include cell division and control (CDC) and transcription factors (ie. Rac-1) that allows for filopodal

extension and actin rearrangements (Figure 2.3). Upon activation, CDC-42 activates PAK-1 (protein activating kinase) which binds to actin fibers within the cell and at the adhesion junction to increase their activity (Jimenez et al. 2000). Stress fibers are cytoskeletal structures, tensile actomyosin bundles which allow sensing and production of force, provide cells with adjustable rigidity and participate in various processes such as wound healing. Focal adhesions anchor the EC to the ECM and serve to direct signals to the EC via integrins. CDC-42 also activates N-Wasp (Wiskott-aldrich syndrome proteins) that rearranges actin to motivate filopodial extension through the action of actin-related protein (ARP) 2 & 3 (an actin filament component) (Klemke et al. 1997) (Figure 2.3). Rac-1 acts similarly (activated by GTP) promoting basement membrane equivalents of filopodia (Jones et al. 2000). (Rac-1 also generates ROS via NADPH oxidase, and stimulates more CDC-42 production) (Figure 2.3). All of these actin rearrangements and remodeling lead ultimately to cell migration, which is part of the next step of angiogenesis.

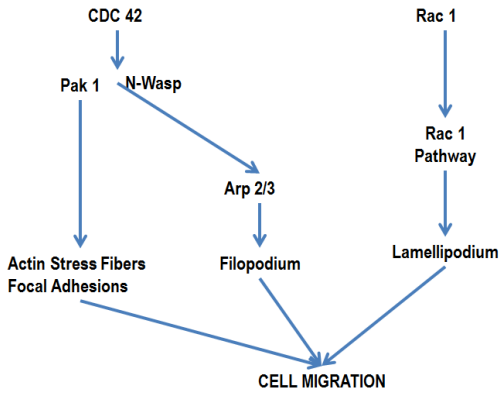

Figure 2.3: EC remodeling, and cellular migration molecular involvement of cell division control (CDC 42) and transcription factor Rac-1 (adapted from Klemke et al. 1997, Sells et al. 1997, Jimenez et al. 2000, Jones et al. 2000, Biocarta 2001).

As alluded to previously, VEGF causes activation of PDGF and basic fibroblast growth factor (b-FGF) to cause endothelial cell proliferation and capillary growth (Sunderkotter et al.

1994, Mariotti et al. 2006). These growth factors are the key players in EC proliferation and migration via phospholipase C (PLC, an enzyme). PLC is cleaved into second messengers, diacylglycerol (DAG) and inositol triphosphate (IP3). DAG activates mitogen activating protein kinase (MAPK) through protein kinase C (PKC) (Figure 2.4). IP3 increases the intracellular calcium and NO. The final substances, calcium, NO and MAPK, potentiate the mitogenic proliferation and cellular contraction to facilitate movement (Brown et al. 1992, Wahl et al. 1994, Liekens et al. 2001, Ferrara et al. 2005). Finally, once the vessel is established the Akt (also called the protein kinase B) pathway prevents apoptosis and promotes Ang-1 binding and vascular stabilization (Figure 2.4).

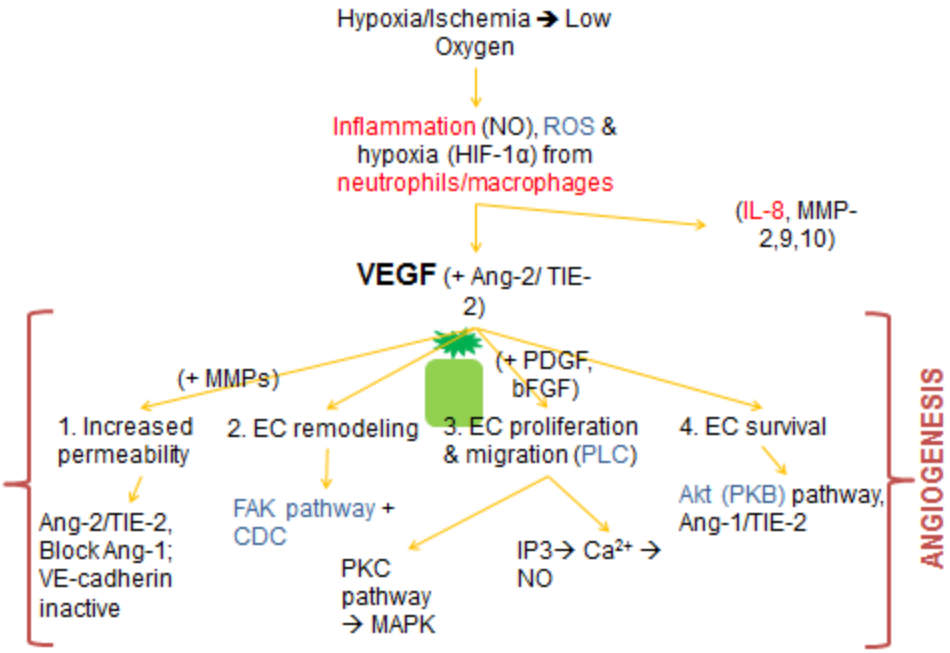

Figure 2.4: Flow chart of events in angiogenesis. Low oxygen pathway is shown in black, mechanical forces in blue, and inflammation's role is shown in red.

Numerous researchers study the importance of VEGF and bFGF in mediating wound angiogenesis. Mariotti, Ferrara and Dvorak assert that VEGF is a predominant, necessary, and essential regulator of angiogenesis (Dvorak et al. 1995, Ferrara et al. 1996, 2005, Mariotti et al.

2006, Mizrahi et al. 2007). In wound healing, capillary density exponentially increases in time then decreases, with VEGF playing the key role, and then endothelial cell survival signals are maintained to ensure adequate blood supply. It is speculated that antiangiogenic factors are expressed once healing has resolved to prevent excess angiogenesis and its complications (Tandar et al. 2002).

Ultimately, angiogenesis is a balancing act between proangiogenic and antiangiogenic molecules to ensure that the body maintains adequate oxygen and nutrient supply. See Figure 2.5.

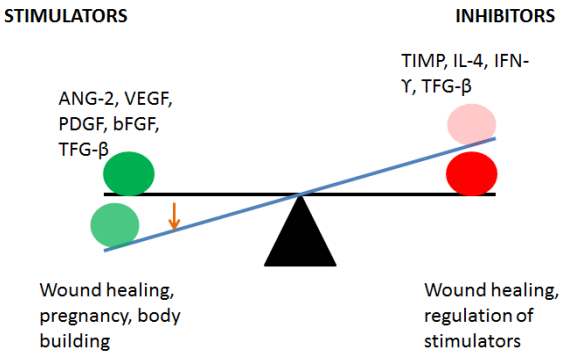

Figure 2.5: Balancing of proangiogenic (stimulators) and antiangiogenic (inhibitors) molecular signals. Blue bar indicates biological response to ischemia/hypoxia.

2.2 Overview of current proangiogenic therapies

Typically, in ischemic cases such as peripheral arterial disease (PAD) or cardiovascular disease (CVD), surgery or endovascular methods are used (Tandar et al. 2002, Sabti et al. 2007) to restore blood flow in the clinic. As discussed previously, these include by-pass, stent placement and angioplasty (Landolfo et al. 1999, Chu et al. 1999, Leon et al. 2000, Yamamoto et al. 2000, Dallan et al. 2008, Estvold et al. 2010, Lucas et al. 2011). Surgical techniques like by-pass promote angiogenesis by providing an alternate route for blood flow such that the downstream endothelial cells sensing more shear stress due to blood flow. This increase in shear may promote angiogenesis to the ischemic area through the pathways discussed in 2.1. For early

PAD or CVD, exercise shows promise, but this treatment is contraindicated for advanced disease (Hansen et al. 2010). Exercise would lead to muscular development, creating a hypoxic environment which would facilitate new blood vessel growth.

Other techniques that show promise include laser revascularization and radiofrequency ablation (Burkhoff et al. 1996, Yamamoto et al. 2000). These techniques utilize the method of secondary wound healing angiogenesis—revascularization prompted by minor wounding, again promoting the hypoxic trigger for blood vessel growth. Because of the associated risk due to the invasive nature of the procedures, many patients do not qualify for any of the mentioned procedures, and others may be nonresponsive to the surgery (Bridges et al. 2006). For these reasons, alternative methods of revascularization in cardiac and skeletal muscle ischemia have been explored. The delivery of growth factors (Hershey et al. 2003, Idirs et al. 2004, Efthimiadou et al. 2006), cellular, molecular, and genetic therapy attempts have been made in order to find a clinically relevant treatment (Takeshita et al. 1996, Assmus et al. 2002, Messina et al. 2002, Iwaguro et al. 2002, van Royen et al. 2002, Lebherz 2003, Grines et al. 2003, Hiasa et al. 2004, Halkos et al. 2008, Kang et al. 2008).

Table 2.1 summarizes the surgical, cellular, molecular and genetic techniques represented in the literature over the last 15 years. Takeshita et al. (1996), Yamamoto et al. (2000), Lebherz et al. (2003), Hershey et al. (2003), and Kang et al. (2008) all used growth factors known to be involved with angiogenesis (Table 2.1 and Figure 2.4). Of them, only Yamamoto et al. (2000) combined the growth factor with transmyocardial revascularization which demonstrated a greater level of effectiveness than the others. In Chapter 1 it was noted that growth factor infusion alone shows minimal effectiveness. The table also shows that over time, the effectiveness of transmyocardial revascularization has decreased by about 50% (Table 2.1). Though part of the

apparent decrease is attributable to differences in experimental setup and controls, there is also variation in the type of revascularization (ie. direct, mechanical, the addition of growth factors) that makes a one to one comparison difficult. The majority of the techniques used to treat ischemia by inducing angiogenesis are invasive, site specific and temporal, but effectiveness varies from 0 to 80% (Table 2.1). The trends show that the less invasive procedures have not been as effective. Chapter 1 discussed that the invasiveness of current procedures like bypass are contraindicated for certain populations, therefore these alternatives do not provide a feasible alternative for those patients. It is generally the invasiveness or lack of site specificity that provides the largest obstacle for therapeutic effectiveness with angiogenesis. As a result, a noninvasive, spatially specific technique that is safe and effective would be highly medically significant.

Table 2.1. Surgical, cellular, molecular, genetic techniques and effectiveness. Effectiveness is measured in percent increase in perfusion or increased capillary/vessel density from control.

Citation	Technique	Invasive	Site Specific	Temporal	Effectiveness
Takeshita et al. 1996	Gene transfer of VEGF	Yes	No	No	~40%
Landolfo et al 1999	Transmyocardial revascularization	Yes	Yes	Yes	0%
Chu et al 1999	Mechanical transmyocardial revascularization	Yes	Yes	Yes	~80%
Leon et al. 2000	Direct myocardial revascularization	Yes	Yes	Yes	0%
Yamamoto et al. 2000	Transmyocardial laser revascularization + bFGF	Yes	Yes	Yes	75%
Lebherz et al. 2003	IV bFGF infusion	No	No	No	~33%
Hershey et al. 2003	Adenovirus-delivered VEGF	No	Yes	No	~43%
Dallan et al 2008	Cell therapy + Transmyocardial revascularization	Yes	Yes	Yes	50%
Halkos et al 2008	IV infusion of stem cells	No	No	No	~30%
Kang et al 2008	Nanosphere-mediated delivery of VEGF (gene therapy)	No	Yes	No	~67%
Estvold et al 2010	Transmyocardial laser revascularization	Yes	Yes	Yes	~40%
Lucas et al 2011	Bypass & Endovascular surgery	Yes	Yes	Yes	~45%

This chapter gave an overview of angiogenesis and defined its protagonists and mechanistic triggers. It also expounded upon the importance of VEGF as the critical driver of angiogenesis. Supplemental involvement of PDGF, TGF-β, MMPs, and HIF-1α were discussed

to show the progression of blood vessel formation. Next, a flow chart (Figure 2.4) placed the key elements in order of their appearance in the angiogenic process. Finally, a brief discussion of current proangiogenic treatments including: gene transfer, transmyocardial revascularization, and growth factor infusion was presented in an effort to demonstrate that the development of a noninvasive, spatially specific therapy for angiogenesis induction is warranted.

CHAPTER 3: ULTRASOUND & ULTRASOUND CONTRAST AGENTS

This chapter defines and gives a brief history of ultrasound (US). It discusses US bioeffects and relevant calculated quantities. Further, this chapter gives an overview of ultrasound contrast agents (UCAs) and their responses to US as a segue to US-UCA induced bioeffects.

3.1 Ultrasound

Ultrasound (US) is a general term for sound with frequencies greater than 20 kHz, which is the upper limit of the audible range for most people. The concept of sound existing above the range of human hearing has been known since the late 1800s (Rayleigh et al. 1945, O'Brien et al. 1998). Initially, US was developed to echo-locate icebergs (French et al. 1951, Hunt et al. 1982). Interestingly, in the mid-1910s, Langevin observed two unique events with US: a detrimental effect where fish in the beam of the source were killed immediately, and the development of cavitations in water (Hunt et al. 1982, O'Brien. et al. 1998). From this observation, it was noted that US has the ability to induce biological effects. Though the bioeffects of US were noticed in the 1910s, the research to examine the biophysical mechanisms of these effects did not begin until several decades later (Harvey et al. 1930, O'Brien et al. 1998).

3.2 Ultrasound bioeffects

The biological effects (bioeffects) of US include tissue but are not limited to ablation (Xu et al. 2005), lung lesions (O'Brien et al. 2001), hemorrhage (Miller et al. 2008), and arrhythmias (Fujikura et al. 2006). US is also capable of inducing cellular level events such as changes in diffusion rate, increased protein synthesis, membrane damage, mast cell degranulation and histamine release (Miller et al. 2007, Paliwal et al. 2008). Bioeffects were found to result from varying ultrasonic parameters such as: acoustic pressure (Pr), pulse repetition frequency (PRF),

and exposure duration (ED). A few acute studies have looked at relationships between the exposure parameters in the lung, muscle, intestine and in cell-based models.

Pr is an important parameter of ultrasound; it has been positively correlated with the severity of bioeffects in both tissue and cellular models. Muscle erosion was found to occur with pressures of exposure above 10 MPa at 0.8 MHz (Xu et al. 2005), but membrane damage was reported at a much lower Pr = 0.07 MPa with 1 MHz exposure (Miller et al. 2004). In another cellular study, membrane damage was determined to increase with increasing Pr from 0.6 to 3.0 MPa (Guzman et al. 2001). An *in vivo* study using frog heart found that Prs from 5 to 10 MPa during systole and diastole caused reduced aortic pressure and premature ventricular contractions, respectively (Dalecki et al. 1993). Unlike Pr, PRF does not demonstrate as strong of a correlation to bioeffects.

In rat lung, O'Brien et al. used a range of PRFs (50 – 1700 Hz) and demonstrated that PRF by itself was insignificant (O'Brien et al. 2001, O'Brien et al. 2003). Contrary to O'Brien et al., it was found that there was a significant PRF dependence with the cell viability and free radical formation *in vitro* when 0.5 to 100 Hz was examined; this study found that lower values (5 Hz) were associated with less bioeffects (Buldakov et al. 2008). In a rat ex vivo cardiac muscle, lesion width, but not size was positively correlated with PRF (Fujikura et al. 2006). With various experimental models and US settings, PRFs role in inducing bioeffects remains unclear. However, the product of PRF and ED, the total number of pulses (TNP) does reveal trends.

Several studies have demonstrated a positive correlation between TNP and bioeffects. In vitro studies on blood clots showed that TNP was positively correlated to thrombolysis rate (1 MHz, duty cycle = 10%, PRF = 1Hz) (Frenkel et al. 2006). A renal model (PRF = 100 Hz, PD =

20 μs) found that low TNP (10 or 100) was correlated to focal hemorrhage and cellular injury and large TNP (1000 or 10000) showed complete destruction (Roberts et al. 2006). Other research performed a study on PRF and ED that demonstrated significance for the interaction term, TNP (6.1 MPa, 2.8 and 5.6 MHz) (O'Brien et al. 2005). Likewise ED demonstrated a positive trend with bioeffect generation, although this trend only emerges in excess of 3 minutes (O'Brien et al. 2005, Miller et al. 2008). However, this threshold seems to be lower for in vitro models. A prostate cancer cell viability study found that ED was positively correlated with prostate cancer cell viability (0.1 to 10 s) at Pr = 0.1 to 1 MPa (Cochran et al. 2001). Ultrasound was found to completely eradicate gram negative bacteria like E. coli with ED > 5 min, but gram positive bacteria like S. aureus were more resistant to US exposure, demonstrating only moderate declines at EDs up to 60 minutes (Monsen et al. 2009). Longer EDs allow for more US energy to be absorbed by the tissue that is exposed. This energy absorption can produce heating.

3.2.1 Thermal effects of US

US bioeffects are generally categorized as thermal or non-thermal (mechanical) in nature. Thermal effects result from the interaction of the applied Pr, PRF and ED are considered to play a role in bioeffect induction. The thermal dose is a concept that was introduced by Sapareto et al. (1984) and is comprised of both the temperature applied and ED, where with higher temperature, less time is necessary to create a bioeffect (O'Brien et al. 2007, ter Haar et al. 2009). With US, thermal effects can be exacerbated by increasing Pr. Higher Prs place more energy into the system and therefore can cause more heating. The maximal temperature increase for no heat removed processes (ΔT_{max}) from US exposure can be approximated by (Fry and Fry et al. 1953, O'Brien 2007, NEMA 2009a):

$$\Delta T_{max} = \frac{\dot{Q}\Delta t}{C_v} \tag{3.1}$$

$$\dot{Q} = 2\alpha I_{TA} \tag{3.2a}$$

$$I_{TA} = \frac{\alpha P_r^2}{\rho c} \tag{3.2b}$$

where $\dot{Q}$ is the amount of heat generated per unit volume, I_{TA} is the temporal average intensity, α is the absorption coefficient, Δt is the ED, C_v is the heat capacity per unit volume, ρ is the density, c is the speed of sound, and Pr is the applied acoustic pressure.

3.2.2 Mechanical effects of US

One of the mechanical effects of US is due to radiation force. (Nyborg et al. 1953, 1965, 1975, Hoff et al. 2001, Yang and Church 2005, ter Haar 2009). Radiation force is contingent upon the amount of US energy absorbed. The absorbed energy manifests as force on the object. Radiation force is defined as a small, steady force that is produced when a sound beam strikes a reflecting or absorbing surface. It is exerted on any body immersed in the acoustic field and may cause bulk movement of cells and tissue displacement (Nyborg et al. 1965, Nightingale et al. 1995, Postema et al. 2004). Dyson et al. (1971) demonstrated that red blood cells in large vessels formed bands when exposed to continuous wave US. Dalecki et al. (1997) showed that radiation force caused reduced aortic pressure and disturbed cardiac rhythm in a frog heart. Radiation torque, related to radiation force, is a twisting action that may be caused when a sound wave hits a suspended object. Symmetrical objects have been shown to rotate, while others will tend toward a preferred orientation. This phenomenon is not as well characterized.

Another mechanical effect is due to acoustic cavitation. Cavitation is defined as the formation of gas filled cavities or 'free bubbles' in a medium exposed to an ultrasonic field (ter Haar et al. 1986). These free bubbles can oscillate with the applied pressure. One form of

oscillation is stable cavitation. Stable (linear) oscillation displays equal magnitude expansion and contraction phases in response to the applied pressure (Pr and Pc, respectively).

A basic approximation to bubble dynamics views a bubble as a linear oscillator, where forces are both internal and external (Figure 3.1). These forces include the force on the bubble surface, F_s, the force on the bubble from the surrounding liquid, F_L, and the frictional forces from damping, F_f. Beginning with instantaneous radius, $a(t)$, equilibrium radius, a_e, and equilibrium volume, V:

$$a(t) = a_e + \xi(t) \tag{3.3}$$

$$V = \frac{4}{3}\pi a^3 \; and \; \Delta V = 4\pi a^2 \xi \tag{3.4}$$

where ξ is radial displacement, which is assumed to be much smaller than the bubble equilibrium radius, a_e. Equations 3.3 and 3.4 show that changes in the radius will cause volume changes.

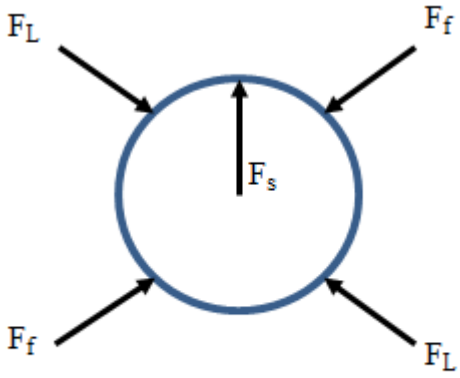

$$F_f + F_s + F_L = 0$$

Figure 3.1: Forces acting at the bubble surface at equilibrium radius.

The volume change causes a change in pressure, Δp, inside the bubble.

$$\Delta p = -\frac{3\kappa p_g \xi}{a} \tag{3.5}$$

where κ is the polytropic gas exponent, p_g is the equilibrium (gas) pressure inside the bubble. The force on the bubble surface, F_s, is equivalent to the integral of pressure inside the bubble on the surface:

$$F_s = \iint_S p_s \, dS = 4\pi a^2 p_s = -12\pi a \kappa p_g \, \xi = s \, \xi \tag{3.6}$$

$$s = -12\pi a \kappa p_g \tag{3.7}$$

where s is the "spring constant" of the bubble.

The pressure radiating from the oscillating bubble at radius r, $p_s(r)$, is determined from:

$$p_s(r) = \; p_s(a) \frac{a e^{i(\omega t - kr)}}{r} \tag{3.8}$$

where $p_s(a)$ is the pressure at the surface of the bubble, ω is the frequency, *t* is time, *k* is the wavenumber, and *r* is the radius. Relating this pressure outside the bubble to the radial displacement can be accomplished by using the Euler equation:

$$\rho \ddot{\xi} = \; -\nabla p = \frac{p_s(a)}{a}(1 + ika) \tag{3.9}$$

$$p_s(a) = \; \dot{\xi} \omega \rho a \; (i + ka) \tag{3.10}$$

where ρ is the density of the liquid, $\dot{\xi}$ is the velocity, $\ddot{\xi}$ is the second time derivative of ξ, and ∇p is the partial derivative of p_s with respect to radius. These equations assume linearity and *ka* << 1. Then the mechanical force on the bubble, F_m can be solved from the integral of p_s over the bubble surface:

$$F_m = -4\pi a^2 p_s = \; -4\pi a^3 \dot{\xi} \omega \rho a \; (i + ka) \; = -R\dot{\xi} - m\ddot{\xi} \tag{3.11}$$

$$F_f = -R\dot{\xi} \tag{3.12}$$

$$F_L = -m\ddot{\xi} \tag{3.13}$$

where F_f are the frictional forces from radiation and viscosity, F_L is the force from the liquid, $m = 4\pi a^3 \rho$ is the effective mass of the oscillating bubble, and the mechanical resistance is defined as: $R = 4\pi a^2 \rho c (ka)^2$. With an applied acoustic pressure, p_A, this force balance becomes:

$$F_s + F_f + F_L = s\xi + R\dot{\xi} + m\ddot{\xi} = \iint_S p_A(t)\, dS = -4\pi a^2 p_A \tag{3.14}$$

This equation describes a free bubble as a linear mechanical oscillator. It does not incorporate surface tension at the gas-liquid interface.

Another way to theoretically describe bubble dynamics is to begin with an equation to describe liquid flow, the Bernoulli equation (3.15), and the continuity equation (3.16):

$$\frac{\partial \psi}{\partial t} + \frac{1}{2}(\nabla \psi)^2 = -h(r) \tag{3.15}$$

$$u(r,t) = \frac{f(t)}{r^2} \tag{3.16}$$

$$\psi(r,t) = -\frac{f(t)}{r} \tag{3.17}$$

where $\psi(r,t)$, is the velocity potential, $h(r)$ is the enthalpy, $u(r,t)$ is the velocity of the liquid, and $f(t)$ is an arbitrary function of time. From the continuity equation we see that $u(r,t)$ can be derived from $\psi(r,t)$ as described by:

$$u = \nabla \psi \tag{3.18}$$

The enthalpy term was described in terms of pressure and density by Prosperetti et al. (1984), and simplified by assuming an incompressible liquid (ρ = constant) by Hoff (2001) as:

$$h = \frac{p(r) - p_\infty}{\rho} \tag{3.19}$$

where $p(r)$ is the pressure at radius, *r*, and p_∞ is the pressure in the liquid far from the bubble. Therefore, the Bernoulli equation can be rewritten as:

$$\frac{\partial \psi}{\partial t} + \frac{1}{2}(\nabla \psi)^2 = -\frac{p(r) - p_\infty}{\rho} \tag{3.20}$$

which describes a relationship between the velocity potential and pressures (in the surrounding media and at the bubble surface). To solve these equations in terms of radius varying with time, boundary conditions must be set:

$$u(r = a) = \frac{\partial \psi}{\partial r}|_{r=a} = \dot{a} \tag{3.21}$$

$$p(r)|_{r=a} = p_s \tag{3.22}$$

where $\dot{a}$ is the radial velocity and p_s is the pressure at the bubble surface. From Eq 3.17 and 3.21 we find that:

$$a^2\ddot{a} + 2a\dot{a}^2 = f'(t) \tag{3.23}$$

Placing Eq. 3.23 into 3.20 with:

$$\frac{\partial \psi(r,t)}{\partial t} = -\frac{f'(t)}{r} \tag{3.24}$$

(from Eq 3.17), and noting that $\nabla\psi = u = \dot{a}$, from Eq. 3.18 and Eq. 3.21. If Eq. 3.24 is evaluated at r = a, we find the Rayleigh-Plesset equation (Plesset et al. 1949, Hoff et al. 2001):

$$a\ddot{a} + \frac{3}{2}\dot{a} = -\frac{p_\infty - p_s}{\rho} \tag{3.25}$$

This equation describes the relationship between the radius and pressure. It assumes spherical symmetry and purely radial and irrotational flow. Stable linear cavitation describes the steady, continuous oscillation (expansion and contraction) of bubbles in response to US (Figure 3.2).

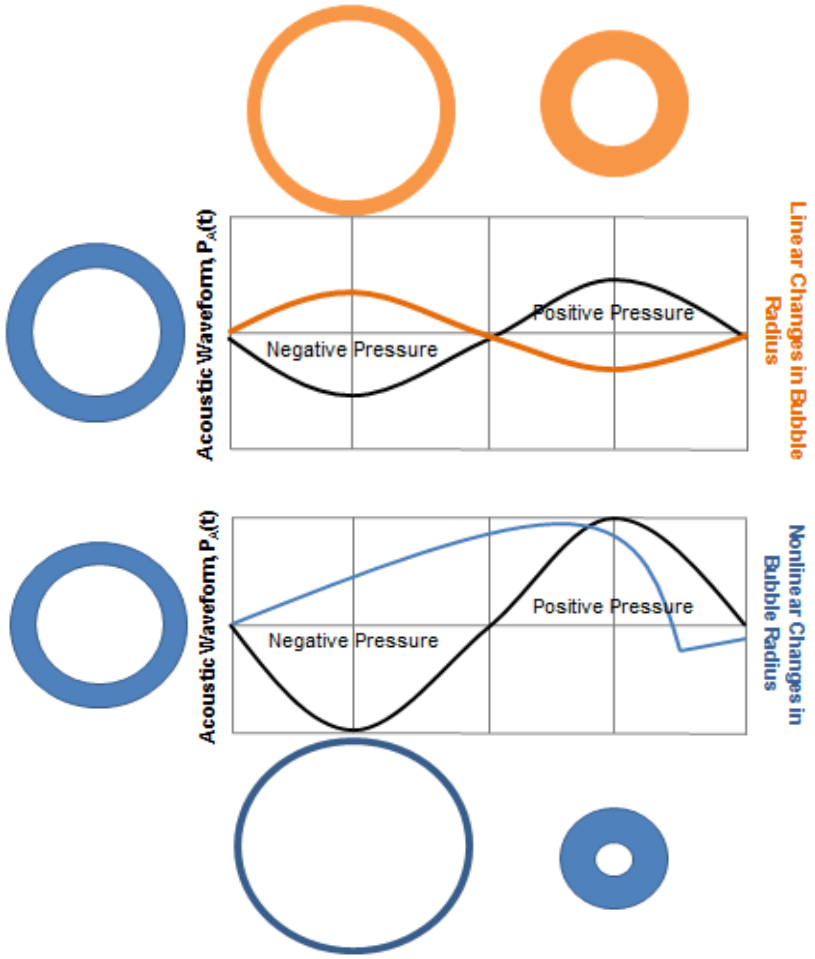

Figure 3.2: The changes in bubble radius with applied acoustic pressure. The linear case is valid when the acoustic amplitude is low, and the nonlinear case is for high amplitude waveforms, though only one waveform is depicted here.

This type of cavitation progresses to a nonlinear regime when the Pr is further increased, where there is a slow expansion caused by the peak rarefactional pressure, followed by a rapid contraction phase (peak compressional pressure) as seen in Figure 3.2 in blue. Equation 3.25 allows for the derivation of theoretical models that describe both linear and nonlinear oscillation.

Incorporating a driving acoustic field (Plesset et al. 1949) $p_\infty = p_o + p_A(t)$, the Raleigh-Plesset equation for an oscillating free bubble becomes:

$$a\ddot{a} + \frac{3}{2}\dot{a}^2 = -\frac{p_o + p_A(t) - p_s}{\rho} \tag{3.26a}$$

where $p_A(t)$ is the driving acoustic pressure, p_o is the atmospheric pressure. In response to an applied acoustic field bubbles will oscillate with the pressure wave (Figure 3.2). Equation 3.26a assumes spherical symmetry, purely radial and irrotational flow. It neglects the contribution of viscosity in the bulk of the liquid. This equation also does not directly account for contributions from the acoustic radiation, gas, viscosity, or surface tension, and assumes an incompressible liquid.

Other models like Trilling et al. (1952) or the Keller-Miksis et al. (1980) added a constant speed of sound in the liquid, linear compressibility and acoustic radiation damping advantages over the Rayleigh-Plesset model. The left side of Eq. 3.26a was later modified to include the radiation damping term from the Trilling and Keller-Miksis models; the modified Rayleigh-Plesset equation is described by:

$$a\ddot{a} + \frac{3}{2}\dot{a}^2 = -\frac{p_o + p_A(t) - p_s}{\rho} + \frac{a\dot{p}_s}{\rho c} \tag{3.26b}$$

Understanding bubble dynamics began with the derivation of an equation to describe radius, a, in terms of pressure with respect to time. This equation was further modified to include viscosity of the liquid, μ (Leighton et al. 1994):

$$\rho\left(a\ddot{a} + \frac{3}{2}\dot{a}^2\right) = p_s - p_A(t) - p_o - \frac{4\mu\dot{a}}{a} \tag{3.27}$$

When including the contributions of surface tension, σ, and constant vapor pressure, p_v, we find (Leighton et al. 1994):

$$\rho\left(a\ddot{a} + \frac{3}{2}\dot{a}^2\right) = \left(p_o + \frac{2\sigma}{a_e} - p_v\right)\left(\frac{a_e}{a}\right)^{3\kappa} + p_v - p_o - \frac{2\sigma}{a} - \frac{4\mu\dot{a}}{a} - p_A(t) \tag{3.28}$$

This equation, like Eq. 3.27, defines the change in bubble radius with time when acoustic pressure is applied. It assumes the following: the bubble radius is small with respect to the acoustic wavelength, spherically symmetrical oscillation of a free bubble in an incompressible liquid, and that the density of the liquid is large compared to the gas.

As the acoustic pressure is further increased, the nonlinear expansion and contraction may transition to inertial cavitation (IC)**.** At high pressures, IC is described by a slow expansion followed by a rapid contraction when the free bubble is dominated by the inertia of the surrounding fluid; this rapid contraction approaches the speed of sound (Flynn et al. 1975, Forbes 2009). Highly localized, short duration (nanosecond) collapses cause high temperatures (> 4300 K) and high pressures (Didenko et al. 1999). The fluid volume above the bubble can be accelerated and focused during the collapse to produce a microjet (Postema et al. 2004). Also this bubble collapse is associated with generation of free radicals (NCRP 2002, Miller and Thomas et al. 1994).

Several parameters have been investigated with respect to the effect on IC. The Pr threshold for which IC occurs has been shown to be positively correlated with frequency (Ammi et al. 2006b, King et al. 2010, King et al. 2011), viscosity (Coakley & Nyborg et al. 1978), and weakly with pulse duration (Church et al. 2005, Haak & O'Brien 2007) and number of cycles (Flynn & Church 1988, Forbes 2009). The occurrence of IC has been negatively correlated with PRF (Buldakov et al. 2008), temperature and gas content (Coakley & Nyborg 1978). Numerous studies have demonstrated the dependence of IC on a bubbles change in radius, noting that the threshold is reached when the microbubble expansion reaches two times its equilibrium radius (ie. $a_{max}/a_e \geq 2$) (Flynn et al. 1975, Church et al. 2005, Forbes 2009).

While posed as separate entities, there is the potential for considerable overlap with thermal and mechanical bioeffects. One can see that the two are not perfectly disjointed because the calculation estimates for both types of effects involve Pr (Fry and Fry 1953, Nyborg et al. 1981, Cavicchi and O'Brien 1984, O'Brien 2007, ter Haar et al. 2009). Both thermal and mechanical bioeffects were implicated in the mentioned studies and research continues to be conducted regarding the safety limits of ultrasound.

This section described US and US-induced thermal and biological effects. US was linked to both local temperature increases and free bubble development that induces mechanical effects. Section 3.2 began by listing the quantified bioeffects to US exposure. These phenomena have been studied since the 1950s, but the connection of the physical mechanisms to biological effect has not been examined. Theoretical equations were presented such that US's physical effects could be linked to bioeffects. Hemorrhage, lesions, arrhythmias, membrane damage, and protein synthesis changes were discussed to be initiated via thermal or mechanical effects of US. The theoretical models and maximal temperature estimate allow one to assess a likely mechanism.

3.3 Ultrasound contrast agents

In the early 1990s, shelled bubbles were developed to improve contrast in acquired images. These shelled bubbles were called ultrasound contrast agents (UCAs). UCAs opened many new fields of US research, namely UCA responses to US, UCA bioeffects and UCA therapeutic effects/applications. UCAs can generally be described as a thin elastic shell approximately 1-200 nm thick encapsulating a gas core. UCAs are microbubbles that range from 2-20 μm in diameter. There are two commercially available UCAs in the United States: Definity® and Optison™. Definity® is a lipid shell microbubble encapsulating

octafluoropropane with a median diameter of approximately 2 μm. Optison™ is an albumin shell contrast agent encapsulating octofluoropropane with a median diameter of approximately 4 μm. Due to recirculation, both Definity® and Optison™ are detectable for up to 10 minutes and have a mean half-life of 1.3 minutes in humans (Definity Package Insert, Optison Package Insert). Definity® was the UCA chosen to be used in this thesis because commercially available UCAs have been characterized, and Definity® was the only UCA consistently available for purchase.

3.4 UCA responses to US

Spontaneously formed free bubbles (cavitation) were described previously. Here the discussion is extended to shelled bubbles introduced into the system. UCAs fundamentally behave like free bubbles (Section 3.2), however the shell and enclosed gas make additional terms necessary to describe the bubble behavior. Along with US exposure, UCAs, like free bubbles, have been shown to oscillate, expanding in response to peak compressional pressure and contracting in response to peak rarefactional pressure. As Pr increases, UCAs progress from linear oscillation, to nonlinear oscillation, to inertial cavitation (IC).

For linear oscillation *undamped* natural resonant frequency, f_o, of encapsulated bubbles is described as (Goertz et al. 2007):

$$f_o = \frac{1}{2\pi}\sqrt{\frac{3\kappa p_o}{\rho a^2} + \frac{2S_p}{\rho a^3}} \tag{3.29}$$

where S_p is a shell restoring force accounting for shell elastic (stiffness) effects, p_o is the atmospheric pressure (101 kPa), κ is the polytropic exponent, and a is the bubble radius. UCAs typically oscillate most efficiently (resonate) at frequencies from 1 to 8 MHz at relatively low Prs. The resonant frequency is dependent upon the UCA size and capsule composition (Moran et

al. 2002, Wu et al. 2008). Because there is a shell, the effective surface tension changes as a function of the bubble radius, and the shell of a UCA both constrains and raises the resonant frequency, which, in turn, affects the collapse threshold. Also, commercially available UCAs bubble diameters vary in size (Goertz 2007, Overvelde et al. 2010). For microbubbles with small diameter, surface tension adds to the restoring force along with the shell stiffness making collapse require higher Prs (AIUM 2000). Wu et al. (2002) derived an equation to determine the resonant frequencies for exposures in the MHz ranges where viscous forces dominate. Incorporating damping terms that result from the shell surface tension and viscosity we find the *damped* resonant frequency (Wu et al. 2002, Goertz et al. 2007):

$$f_{res} = \frac{1}{2\pi}\sqrt{\frac{3\kappa}{\rho a_o^2}\left(p_o + \frac{2\sigma}{a_o}\right) + \frac{2S_p}{\rho a_o^3} - \frac{2\sigma}{\rho a_o^3}} \tag{3.30}$$

$$\cong f_o\sqrt{1 - \frac{(\delta_{visc} - \delta_{shell})^2}{2}} \tag{3.31}$$

where the shell elastic parameter is $S_p = 6G_s x \approx 1.1$ N/m, G_s is the shear elastic modulus, x is the shell thickness, σ is the surface tension, and f_o is described in Eq. 3.29. The Goertz equation includes the damping terms:

$$\delta_{visc} = \frac{4\mu}{\omega\rho a^2} \tag{3.32}$$

$$\delta_{shell} = \frac{S_f}{4\pi\rho\omega a^3} \tag{3.33}$$

and the shell friction effects, $S_f = 48x\pi\mu_{shell} \approx 0.5 \times 10^{-6}$ (Goertz et al. 2007). The two equations above yield similar results as seen in Figure 3.3 for Definity® with a median bubble diameter range of 1.1 – 3.3μm, f_{res} = 0.3 – 2 MHz:

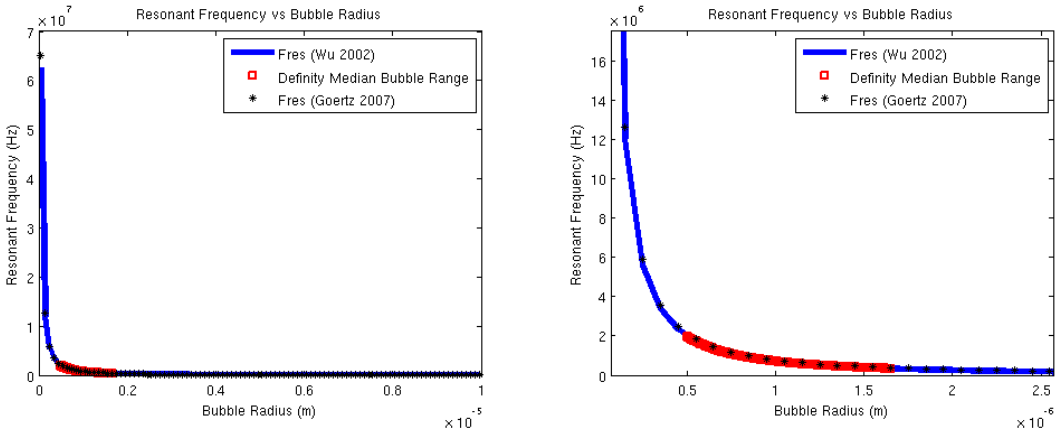

Figure 3.3: Resonant frequency for a range of diameters. The red portion represents the median range for Definity® microbubbles (ρ = 1060 kg/m for blood, p_o = 101.3E3, σ = 0.073 N/m (Wu et al. 2002), S_p = 1.1 N/m (Goertz et al. 2007)). The black asterisks are f_{res} from Goertz 2007. The right figure is a zoomed in version of the left figure.

In addition, a UCA's robustness for oscillation is affected by other US parameters. The resonance describes the frequency at which the bubble oscillates most efficiently, or linearly. The resonant frequency is dependent upon the applied pressure, because, as discussed before linear oscillation is only valid for low pressures. For example, when a range of microbubbles (2 to 11 µm) was exposed to 1.7 MHz, oscillation started at 30 to 120 kPa, below which, little or no oscillation was observed (Emmer et al. 2007).

For this thesis, UCAs are infused intravenously. Research has shown that cylindrical confinement may affect resonant frequency due to viscous and thermal damping. Energy is absorbed from acoustic field that goes into random motion and internal molecular energy. Oguz et al. (1998) demonstrated that the exact confinement conditions play a role in how the resonant frequency is affected. For the infinitely thin, pen vessel with a 0.5 bubble radius to blood vessel radius ratio (which is most similar to capillaries) the f_{res} drops by ~ 50%, but this model does not consider the biomechanics of capillary blood vessels. Another study showed that if the initial bubble radius is much smaller than the blood vessel radius, f_{res} remains relatively constant, even

when assuming that the capillary is relatively rigid due to the surrounding tissue (Sassaroli et al 2004). It should be noted that Definity® 's mean radius is ~ 1 μm and the mean capillary radius is ~ 4 μm. However, Definity® radii ranges from 1—10 μm and capillaries *in vivo* can have diameters smaller than the diameter of a red blood cell (~7 μm) at rest. Since cylindrical confinement can affect the resonant frequency researchers continued to study how the confinement affects the progression of a bubble from oscillation to collapse and the elicitation of bioeffects.

Sassaroli et al. (2004) wrote, "… it is extremely difficult to make *in vivo* measurements in these small blood vessels…to check bubble dynamics" therefore mathematical modeling at the micron scale or large scale models has been used. One such mathematical model found that decreasing tube thickness and tube radius, while increasing Pr lead to increased stress and microvascular rupture (Miao et al 2008). The Miao et al (2008) study studied peak hoop stress with vessel wall thickness of 1 μm, f = 1 MHz and a Pr = 0.5 MPa; at these settings, the hoop stress was found to be greater than the strength of the capillary (Young's modulus of capillary ~ 2 MPa (Smaje et al. 1980)). When hoop stress exceeds capillary strength, it's postulated that capillary rupture occurs (Miao et al. 2008). Recent studies with UCA radii smaller than the confining vessel argue that in capillaries the collapse threshold is not considerably affected because the Young's modulus of capillaries is low (compliant tubing), and the wall thickness is less than the bubble diameter (minimal damping) (Miao 2008, Martynov 2009). Existing literature maintains that the average sized capillary does not significantly change the resonant frequency; therefore cylindrical confinement is not of particular concern with regard to its effect on bubble dynamics. However, other research shows that as pressure is increased, nonlinearity

and collapse occur, regardless whether the driving frequency is resonant or not (King et al. 2011).

Progressing from oscillation to collapse, a study on Optison™ and Definity® shell rupture found that the collapse threshold for postexcitation acoustic emissions (a rebound signal proposed to occur with an inertial cavitation event) increased with frequency and decreased with pulse duration (Ammi et al. 2006, King et al. 2010). Studies also report that the most likely destruction process for Definity® is that exposure produces a defect in the microbubble shell and breaks the microbubble into smaller bubbles (daughter bubbles) (Moran et al. 2000, Sarkar et al. 2009).

Various models have been generated for shelled bubbles; they account for inner and outer radii (for an incompressible shell) (Church et al. 1995), shell thickness with constant volume (Hoff et al. 2000), and equations to express shear loses (Church et al. 1995, Leighton et al. 2008). The Church et al. (1995) model included shear modulus and shear viscosity shell terms, but neglected surface tension for an albumin shelled UCA. When a gas is encapsulated by a lipid shell, the hydrophobic nature of the shell requires surface tension be included. Also lipid shells cause the bubble to undergo higher amplitude oscillations with increases in pressure. Shell properties aside, the main limitation of the previously described equations is that they do not incorporate collapse. As previously stated, when Pr is increased the expansion slows reaching large amplitudes and is followed by a rapid contraction.

In 2005, Marmottant defined a model for large amplitude oscillations that lipid shelled bubbles undergo that includes rupture of the microbubble. This model includes surface tension, surrounding liquid viscosity and the surface dilatational viscosity from the bubble's shell. These terms are incorporated by the boundary condition (Marmottant et al. 2005):

$$p_g(t) - p_L(t) = \frac{2\sigma(a)}{a} + 4\mu\frac{\dot{a}}{a} + 4\eta_s\frac{\dot{a}}{a^2} \tag{3.34}$$

where p_g is gas pressure in the bubble, p_L is liquid pressure, η_s is the shell surface dilatational viscosity, and σ is surface tension. Equation 3.34 assumes that the shell is thin with respect to the bubble radius and therefore not included. Thickness measurements of phospholipid monolayers range between 1 – 2 nm (Minones et al. 2002, Goertz et al. 2007) so a thin shelled approximation (neglecting the inner radius) for UCAs is appropriate.

Assuming an ideal polytropic gas with $p_g\, \alpha\, a^{-3\kappa}$, where κ is the polytropic gas exponent, and combining Eq. 3.28 with Eq. 3.34 the Marmottant equation to describe lipid shelled bubbles in a surrounding liquid is described with:

$$a\ddot{a} + \frac{3}{2}\dot{a}^2 = \frac{1}{\rho}\left\{\left[p_o + \frac{2\sigma(a_e)}{a_e}\right]\left(\frac{a}{a_e}^{-3\kappa}\right)\left(1 - \frac{3\kappa\dot{a}}{c}\right) - \frac{2\sigma(a)}{a} - \frac{4\mu\dot{a}}{a} - \frac{4\kappa_s\dot{a}}{a^2} - p_o - p_A(t)\right\} \tag{3.35}$$

Marmottant also defined shell surface tension in terms of bubble radius:

$$\sigma(a) = \begin{cases} 0\ if\ a \le a_{buckling} \\ \chi\left(\frac{a^2}{a_{bucking}^2} - 1\right)\ if\ a_{buckling} \le a \le a_{breakup} \\ \sigma_{water}\ if\ ruptured\ and\ a\ \ge a_{ruptured} \end{cases} \tag{3.36}$$

$$with\ a_{rupture} = a_{buckling}\sqrt{\left(1 + \frac{\sigma_{water}}{\chi}\right)} \tag{3.37}$$

Equation 3.35 has been popular in describing Definity®, because it closely approximates the experimental bubble behavior (King et al. 2010). The Marmottant equation also takes into consideration the thin shell behavior during oscillation.

One property the Marmottant equation neglects is the initial gas pressure in the bubble. While fluorocarbons are common to UCAs, other gases like sulfur hexafluoride have been used (SonoVue package insert). Because of their low solubility in blood and high vapor pressure, various types of perfluorochemical gases like perfluorocarbon, perfluorobutane, perfluoropropane, and perfluorohexane are used to improve the stability and plasma longevity of the agents. The properties of the internal gases partially determine the oscillatory patterns.

King et al. (2011) proposed a modified Marmottant equation to include a van der Waals gas rather than an ideal gas:

$$a\ddot{a} = \frac{1}{\rho}\left[\begin{array}{c}\left(p_o + \frac{2\sigma(a_o)}{a_o}\right)\left(\frac{a^3 - y^3}{a_o^3 - y^3}\right)^{-\kappa}\left(1 - \frac{3\kappa a^3 \dot{a}}{c(a^3 - y^3)}\right) \\ -\frac{2\sigma(a)}{a} - \frac{4\mu\dot{a}}{a} - \frac{4\kappa_s \dot{a}}{a^2} - p_o - p_A(t)\end{array}\right] - \frac{3}{2}\dot{a}^2 \qquad (3.38)$$

where *y*, the van der Waals hard core radius, accounted for large amplitude responses such as inertial cavitation and rebound. Experimentally, the King equation did not fit well with the 1 MHz driving frequency that will be used in this thesis, therefore the standard Marmottant equation will be used to investigate the physical mechanisms with $a_e = 1.0\ \mu m,\ \chi = 0.85\ \frac{N}{m}$ and with $\sigma_{blood} = 0.046\ \frac{N}{m}$ instead of σ_{water} (Harkins et al. 1929, Marmottant et al. 2005, Definity® Package insert).

3.5 Physical regimes of bubble responses

3.5.1 Radiation forces

A bubble in a sound field experiences the spatial variation of the change in pressure. In theory, the pressure is greater on the side facing the acoustic pressure than the other. Therefore the pressure drop can cause translation. UCAs are often much smaller than the acoustic wavelength, with UCA diameters ~2 μm and the wavelength, λ = c/f = 1500 μm for a 1 MHz

driving frequency. When the amplitude of the acoustic pulse is low, both the UCA and the sound wave oscillate sinusoidally. The magnitude of the radiation force is dependent upon the bubble radius for a traveling wave; the direction is in the propagation of the wave. These waves depend on both bubble radius and location, because the amplitude of the sound wave varies with location. Therefore bubbles that are less than the resonant size are translated in the direction of pressure maxima, and bubbles that are larger than resonant size are translated toward pressure minima (AIUM 2000). As acoustic pressure is increased, the force on the smaller bubbles is increased (as they have been translated to pressure maxima), and the pressure on larger bubbles is decreased.

Radiation force is also responsible for UCA coalescence. UCAs scatter energy affecting other nearby UCAs and tissues in vivo. Secondary radiation forces (Bjerknes forces) cause microbubble translations toward each other. When two bubbles are both either above or below the resonance sized bubble, these bubbles are attracted together. When a larger than resonance bubble is near a smaller than resonance bubble, they oscillate out of phase and the net force between the two bubbles is repulsive (Leighton et al. 1994, Postema et al. 2004). For biological structures (which are normally denser than blood plasma) the force is directed toward the bubble, perhaps causing cells to accumulate on the UCAs surface increasing the likelihood of cellular lysis.

The calculation of the radiation force acting on a UCA to cause translation is defined by (Postema et al. 2004):

$$F_{rad} + F_d - \frac{d(Mv)}{dt} = 0 \tag{3.39}$$

averaging over one acoustic cycle, $F_{rad} = \frac{\frac{P_r^2 a_e \delta_t \frac{fres}{f}}{}}{\rho c f\left[\left(\frac{fres}{f}\right)^2 - 1\right]^2 + \left(\frac{\delta_t fres}{f}\right)^2}$ (3.40)

$$M \cong \frac{2\pi}{3}\rho a_e^3 \tag{3.41}$$

$$F_d = \frac{\pi\mu}{4} C_d Re a_e v(t) \tag{3.42}$$

where M is the added mass of the translating bubble, F_{rad} is the primary radiation force, F_d is the drag force, v is the velocity of a bubble in a steady fluid in an US field, c is the speed of sound, Pr is the peak rarefactional pressure, δ_t is the dimensionless total damping coefficient (Medwin et al. 1977), f_{res} is the bubble resonant frequency, μ is the shear viscosity of the liquid, $Re = \frac{2\rho a_e |v(t)|}{\mu}$ is the Reynolds number, and $C_d = \frac{24}{Re}(1 + 0.15\ Re^{0.678})$ is the drag coefficient of the contrast agent (Postema et al. 2004).

Miri et al. (2011) investigated radiation force on UCAs near a porous vessel and demonstrated that the radiation force increased with increasing UCA shell thickness and with driving frequencies up to about 15 MHz. Also larger bubble radii were associated with larger radiation forces up to 5 MHz. At 1 MHz (the approximate frequency used in this thesis) shell thickness changed the radiation force by less than 5%. A 2 μm-diameter bubble demonstrated no radiation force, while a 10 μm bubble showed ~ 0.5 N radiation force at a distance-to-radius ratio of 1.5 and a reflection coefficient of 0.5 (Miri et al. 2011). Extending these findings to the median range distribution of Definity®, the increase in radiation force, when near a boundary, is only moderate.

3.5.2 Microstreaming

US not only exerts an effect on the UCA causing oscillation or collapse, but also exerts an indirect effect upon the media through the contrast agent. Microstreaming is a major effect of

insonation in which the fluid around the vibrating bubble forms eddies of flow, or turbulence, adjacent to an oscillating bubble (Gormley and Wu 1998, Baker et al. 2001, Sarkar et al. 2009). The pulsation amplitude of a bubble in a traveling wave field varies with bubble radius, being greatest for resonant bubbles and less for either larger or smaller ones. Oscillating bubbles that are also being translated by the acoustic pressure may produce shearing flow in the surrounding medium. Both microstreaming-induced and translation-induced shear is greatest near the bubble surface (where the fluid velocity is greatest). Thus biological tissues experience a stronger velocity gradient when they are closer to the UCA resulting in shearing stresses that can distort a tissue's endothelium provided the stress exceeds some minimal time or shear stress level.

Because oscillation was shown to produce microstreaming, it has been theorized to be involved with cellular changes and/or damage. Microstreaming has been under investigation since the late 1960s, though induction was typically via a vibrating wire or needle (Hughes & Nyborg 1962, Rooney et al. 1970, 1972, Williams et al. 1971, Crowell et al. 1977). Bioeffects of the vibrating wire or needle included high shear stress responsible for hemolysis (Williams et al. 1970), injury to bacteria and E. coli (Hughes & Nyborg 1962). Microstreaming was also found to induce membrane damage in Elodea leaves with the critical shear stress being on the order of 50 Pa for 100 second exposures (Miller et al. 1985). Studies have shown that microstreaming generates stress from the tens of Pascal's (Wu et al. 2002) to hundreds of Pascal's (Williams et al. 1971), with exposure duration being negatively correlated to critical shear stress (Miller et al. 1985). Theoretical models for estimating shear stress induction with UCAs predicted shear stress to be greater than the stress that causes hemolysis in blood and several orders of magnitude (1000 times) greater than the physiological stress induced on the blood vessel wall by blood flow (Krasovitski et al. 2004). These stresses induced by an acoustic frequency of 4 MHz and a

pressure of 20 kPa generated a steady shear stress of several kiloPascals (Krasovitski et al. 2004).

Microstreaming has been associated with a range of shear stresses, and the theoretical model for adding UCAs exacerbates the effect. Therefore, it is suggested that the endothelium in blood vessels may be particularly prone to disturbance. It remains unknown if the negative correlation between shear stress and ED exists in vivo, but because biological tissues demonstrate viscoelasticity it could remain valid.

To theoretically describe shear stress,τ, first we must consider the boundary layer. A pulsating bubble near a boundary has a sharp velocity drop across the boundary layer with thickness, d_v, this is also known as a viscous boundary layer (Nyborg et al. 1958, Wu et al. 2002):

$$d_v = \sqrt{\frac{2\mu}{\rho\omega}} \tag{3.43}$$

To calculate the shear stress from microstreaming we also need to know the velocity gradient across the boundary. The velocity gradient across the boundary layer associated with microstreaming is denoted v_{grad} (Lewin & Bjorno 1982, Wu et al. 2002):

$$v_{grad} = \frac{\omega(a - a_e)^2}{a_e d_v} \tag{3.44}$$

Now the shear stress,τ, can be found by:

$$\tau = \mu v_{grad} = \frac{\mu\omega(a - a_e)^2}{a_e d_v} \tag{3.45}$$

where μ is the viscosity of the liquid, τ is the shear stress, ρ is the density of the liquid, ω is the frequency, a is the instantaneous radius, and a_e is the equilibrium radius. This equation was developed to describe the shear stress associated with a pulsing bubble near a living cell as a

solid boundary (Lewin & Bjorno 1982). It should be noted that smaller than resonant bubbles exhibit particularly strong changes in oscillatory patterns in response to slight pressure increases, therefore the shear stress dependence upon the bubble radius is a direct result of the underlying physics. For Definity® $a_e \approx d_v = 1$ μm, which means that the streaming speeds are similar for both a free bubble and a bubble resting on a solid boundary (Davidson et al. 1971, Leighton et al. 1994).

The shearing stresses may be exacerbated when oscillation becomes nonlinear. Nonlinearity may be induced by off-resonance oscillation, or by the microbubble being near a boundary. While most of the theory represented in this chapter assumes spherical symmetry of oscillation, UCAs that are near a semi-rigid boundary (ie. vascular endothelium) do not oscillate symmetrically Figure 3.4. The pressure difference across the bubble is asymmetrical because the surface restricts the motion of fluid on that side of the UCA. This asymmetry results in the formation of a microjet, an invagination of fluid on the UCA side that is opposite the boundary. With increasing pressures, the invagination flows through the UCA and may violently hit the boundary. Microjets have been demonstrated to cause significant damage (Kodama & Takayama 1998, Fletcher et al. 2002). These microjects (overpressure = 10.5 MPa) caused liver parenchymal cells to split in the direction of the liquid jet (Kodama & Takayama 1998). Microjets have also been shown to travel at more than 60 m/s to penetrate, but not perforate the wall of a small diameter blood vessel (Fletcher et al. 2002).

Although liquid microjets have been observed, they are difficult to predict. The force generated from the inertia is dependent not only upon the bubble but the bubble's location and the pressure gradient that develops across the bubble. Even when a boundary is present a liquid microjet may or may not occur, as some inconsistency has been seen near the threshold

(Prosperetti et al. 1997). Liquid jets have been visualized with high speed cameras and have been shown to behave erratically. Tomita and Shima (1990) captured a series of photograph showing the development in bubbles collapsing very close to a wall and with a bit of separation from a wall. The bubble adjacent to the wall demonstrated the invagination seen in Figure 3.4, but the bubble with separation demonstrated invagination then collapse disintegration. Because the exact location of a UCA cannot always be known, predicting jetting is difficult in biological scenarios.

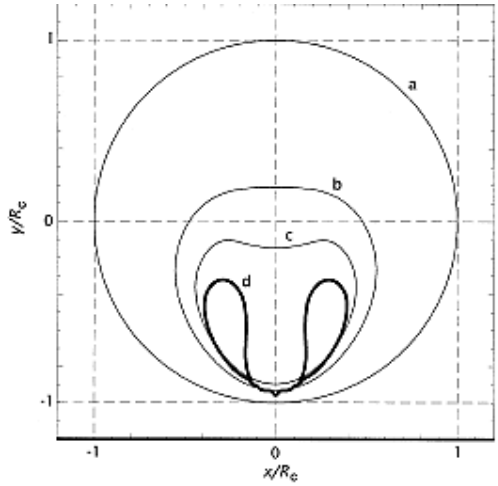

Figure 3.4: Asymmetric collapse profile of a microbubble near a semi-solid boundary. Reproduced from (Postema et al. 2004).

3.5.3 Inertial cavitation

When a UCA is exposed to sufficiently high acoustic pressure it induces high amplitude nonlinear oscillations. These oscillations occur as a slow maximal expansion to a rapid contraction. Because this radial max to min occurs quickly, the surrounding liquid may build up inertia that exceeds that within the bubble resulting in collapse. Collapse can produce mechanical shock waves in the bubble and surrounding fluid, more powerful perforating liquid jets, high temperatures, free radical production, and high velocity shell fragments. Holland and Apfel (1989) and Apfel et al. (1991) examined bubble responses to one cycle of acoustic

pressure with respect to the effect of the liquid's viscosity and surface tension including a criterion of the generation of a 5000 K temperature inside the bubble. The likelihood that cavitation would occur (in terms of a pressure threshold) was derived from their original work (Apfel et al. 1991, Holland et al. 1996):

$$0.06 = \frac{\left(P_{opt}\right)^{1.67}}{f} \tag{3.46}$$

where P_{opt} is the smallest peak negative pressure threshold required for an optimal sized bubble, at a given frequency, f (MHz), and 1.67 and 0.06 are constants for blood. This equation underwent further modification to be normalized to pressure and frequency (1 MPa and 1 MHz, respectively). Then the following index was obtained (Apfel et al. 1991):

$$I = \frac{P^2}{f} \tag{3.47}$$

where P is the peak negative pressure (MPa). In 1998 AIUM/NEMA described the following as the mechanical index (AIUM/NEMA 1998, NEMA 2009b):

$$MI = \frac{P_{r,3}}{\sqrt{f}} \tag{3.48}$$

defined as the likelihood of nonthermal biological effect with an intervening tissue path, where $P_{r,3}$ is the derated peak rarefactional pressure measured in water. The FDA recommends the MI not exceed 1.9. The mechanical index was devised for US exposure only in the induction of cavitation; it assumes the existence of stabilized gas pockets or free bubbles as nuclei of cavitation. Therefore the MIs usefulness is questioned when UCAs are added, given that UCAs can respond differently to US than do free bubbles. A few other researchers have experimented with integrating viscoelastic properties into the MI (Jimenez-Fernandez et al. 2005) or

determining the IC threshold using shell chemistry (Dicker et al. 2010), but these incorporations are not standardized or used frequently.

Shock waves resulting from IC are generated from the speed of the gas-liquid interface estimated to be 40 m/s (Brujan et al. 2005). Shock waves are on the order of a few nanoseconds but may reach pressures up to 40 MPa (Brujan et al. 2005). Therefore, biological tissues that are exposed to the shock may briefly (nanosecond time scale) experience large stresses as a result of IC.

Free radical production results from the contraction phase of collapse where the pressure inside the bubble reaches several megapascals and the temperature may reach thousands of Kelvin. In a UCA's core there exists a fluorocarbon gas; however the shell is comprised of several components containing nitrogen, hydrogen, phosphates and oxygen. High temperatures may lead to the chemical dissociation of these elements to form hydride and hydroxide (Verral & Sehgal 1988). The typical lifetime of these free radicals *in vivo* are ~10 ns, and thus should not affect the surrounding tissue. However, hydrogen peroxide, which can be produced by the combination of these free radicals has a substantially longer lifetime and has been shown to induce DNA damage (Miller et al. 1995). Kondo et al. (1988) observed cell killing induced by 1.0 MHz CW US at 5.8 W/cm^2 and determined that a small percentage of the killing was caused by the production of free radicals. A 300 kHz US exposure induced the production of hydroxyl radicals, hydroperoxyl radicals and hydrogen peroxide (Merouani et al. 2010). Miller et al. (1995) also demonstrated DNA breaks when exposing Chinese hamster ovary cells to 2.17 MHz US at 0.82 MPa. In producing free radicals there does not appear to be an association with acoustic pressure or US frequency per se, but rather a direct link to collapse.

Also, with IC daughter bubbles may be generated that oscillate add to the range of bubble sizes represented in a system. Daughter bubbles are primarily the result of fragmentation followed by shell coalescence. As with the formation of smaller daughter bubbles, there are also other theories regarding changes in the bubble size population. One suggests that microbubble fusion occurs with the expansion of adjacent bubbles (Postema et al. 2004). Dayton et al. (1997b) constructed a velocity of approach equation to describe the speed at which two bubbles exposed to US approach one another, at an equal distance from the transducer due to the radiation force. Equating Stokes drag force

$$F_{sd} = 6\pi\mu a_e v_a \tag{3.49}$$

to the secondary Bjerknes force:

$$F_{2r} = -\frac{2\pi\rho(\omega p_A)^2\epsilon^2 a_1^3 a_2^3}{9d_o^2} \tag{3.50}$$

The velocity of approach for two equal sized bubbles would be:

$$v_a = -\frac{(2\pi f p_A)^2\rho\epsilon^2 a_e^6}{27\mu d_o^2} \tag{3.51}$$

where ϵ is the compressibility of the bubble, and d_o is the distance between the centers of the bubbles. This equation assumes the bubbles are of the same size, which is the resonant size. Chesters et al. (1982) and Postema et al. (2004) state that bubbles will fuse only when the Weber number is greater than 0.5. The Weber number is a dimensionless number used to describe fluid flows between two fluids. It is defined as the inertial force relative to the surface tension force:

$$We = \frac{\rho v_a a}{\sigma} \tag{3.52}$$

when $a_1 = a_2$.

Because collapse may occur as fragmentation or simply be due to gas leakage (Chomas et al. 2001, Bouakz et al. 2005), which changes the size of the bubble and pressure inside the

bubble, oscillation and collapse regimes are affected. Bouakaz et al. (2005) found that after intense compressions, the shell fissures and gas escapes (sonic cracking (Postema et al. 2004)), and found a correlation between exposure and the dynamic change in microbubble diameter. Other research details another bubble event that counteracts diffusion: rectified diffusion, where a bubble may grow by active pumping of gas, initially dissolved in the liquid surrounding the bubble, into the bubble by the energy of the sound field (Eller et al 1965, Leighton 1997). UCAs size population can affect the surrounding tissue because of the acoustically active nature of exposure (Figure 3.6).

While the effects due to oscillation and IC are not entirely separable, determination of the IC threshold is useful for establishing mechanistic motivation for therapy or bioeffects. To date, there exists a range of bioeffects for which a particular mechanistic motivation is unknown.

3.6 Uncategorized bioeffects of US and UCAs

The bioeffects of US alone were discussed previously. This section extends the discussion to include bioeffects of US and UCAs. Because it is difficult to monitor bubble dynamics *in vivo*, some of what is known about bubble behavior is derived from *in vitro* experiments. The bioeffects of US-UCAs, have been observed *in vivo*, but typically without mechanistic motivation—where an effect is observed, with no discussion of the role of the UCA. Various factors interact to produce the observable biological, chemical and/or physical manifestations of US-UCA interaction (Figure 3.6).

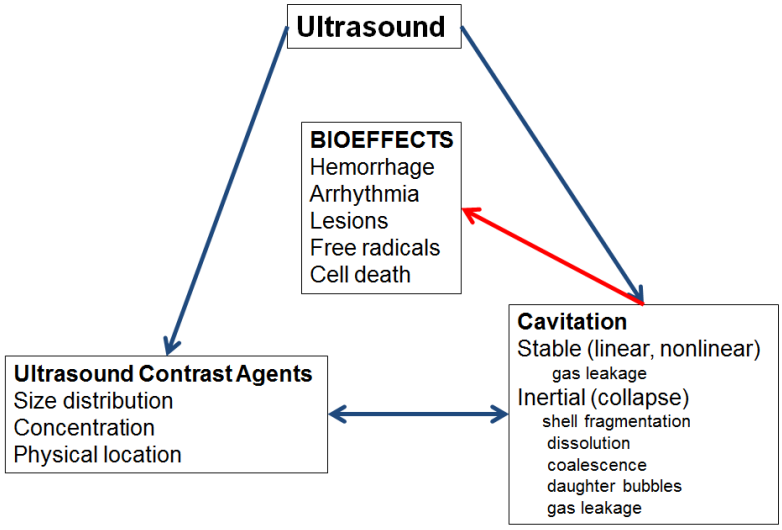

Figure 3.5: The interaction of US with UCAs to produce cavitation-induced bioeffects.

UCAs have the potential to exacerbate bioeffects due to the increased number of cavitation bodies. Research shows that adding UCAs diminishes the pressure threshold for bioeffects (Hwang et al. 2005). Albunex®, an albumin shelled UCA, was shown to increase petechial hemorrhage in mouse intestine when used in conjunction with pulsed US with respect to US alone (Miller et al. 1998c). This study noted that the hemorrhage increased with UCA addition showing 30 times more hemorrhage than when UCAs were not used (Pr = 2.8 MPa, US frequency = 1.09 MHz) (Miller et al. 1998c). In a review published by Miller et al. (2008), bioeffects induced by US and UCAs on skeletal and cardiac muscle ranges from Pr = 1.0 to 2.8 MPa for Optison™, and a narrower range of Pr = 1.1 to 1.6 MPa for Definity® (Miller et al. 2008). Bioeffects ranged from microvessel rupture to cell killing to arrhythmias in cardiac muscle. Miller et al. (2008) reported that petechiae were positively correlated with UCA concentration [UCA] for Definity®, Imagent and Optison™ with a Pr = 1.9 MPa and US frequency of 1.7 MPa. Definity® also caused glomerular capillary hemorrhage and blood filled urinary tubules when the porcine kidney was exposed (Miller et al. 2010). Song et al. (2004) used a rat hindlimb model with 1 MHz ultrasound and found that capillary disruptions were

positively correlated with UCA concentration (Pr = 0.7 MPa). These observations demonstrate that not only is the addition of UCAs important to bioeffects, but also the [UCA] can increase the magnitude of the bioeffect.

Ultrasound pressure (Pr) has been shown to be highly correlated with petechaie and hemorrhage when Definity® UCAs are involved (Miller et al. 1998, Song et al. 2004, Miller et al. 2008). Also, in mice, Albunex® and Optison™ behaved similarly, showing more hemorrhage at higher Pr values (Miller et al. 1998). Therefore Pr (and IC, while not directly stated) has been correlated to bioeffects.

Numerous other bioeffects have been observed to be intensified by the use of UCAs. These include increases in temperature (ns duration) (Stride et al. 2004), production of free radicals (Wu et al. 2008), arrhythmias in cardiac muscle (Kobayashi et al. 2002), endothelial cell damage (Rota et al. 2006).

These findings, however, may be tissue dependent because a study performed on rat lungs, showing that Optison™, per se, did not increase lung damage (O'Brien et al. 2004). When Albunex® was used hemorrhage was found to depend on the tissue type, with fat being the most susceptible to damage, followed by muscle, stomach, skin and mesentery tissue (100 pulses, Pr = 3.6 MPa) (Dalecki et al. 2000). Similarly, bioeffect with MIs ranging from 0.31 to 1.7 with a variety of UCAs have been associated with hemorrhage in skeletal or cardiac muscle, whereas wider MI range (0.1 to 1.9) exists for other tissues (ie. intestine, mesentery, brain, kidney, liver, lung, and tumor) (Miller et al. 2008).

Aside from possible tissue differences, in a study on membrane permeability it was found that albumin bubbles cause more cellular lysis than lipid under the same conditions, but that lipids induce apoptosis and affect cellular stability to a lesser extent (Korosoglu et al. 2006).

There is limited research stating major differences in bioeffect induction using commercially available UCAs. Some researchers use non-commercial UCAs, but do not characterize their inertial cavitation thresholds or other important properties; therefore there may be greater variation in effects. Because the non-commercial UCAs are not characterized to the extent to which commercially available UCAs are, comparisons between studies are difficult.

Cellular damage, changes in permeability, and hemorrhage are recurring themes in the study of US and UCA induced bioeffects, and many of these studies suggest that bioeffects occur as a result of US-UCA interactions involving cavitation (Dalecki et al. 2000, Song et al. 2002, Rota et al. 2006, Wu et al. 2008). But Church et al. (2001) pointed out that IC requires high Pr, but hemorrhage occurs in skeletal muscle at 0.6 MPa at 2.5 MHz (below the IC threshold). Because cavitation is a property that depends on microbubble properties, it is important to control the type of microbubble used to ascertain mechanistic information for the induction of bioeffects.

To examine the collapse threshold for the UCA used in this thesis, a logistic regression analysis on single bubble experiments was conducted to analyze the dependence of ruptured contrast agent occurrence rates as a function of $Pr_{(\text{in vitro})}$. The 5% occurrence rate was used to quantify the shell rupture, or inertial cavitation, threshold *in vitro*. A postexcitation signal (PES) was used as the qualifier of shell rupture, because it was found that this type of rebound signal occurs for free (unshelled) gas bubbles emitted during rebound of the UCA and consequently is linked to shell rupture and transient collapse of the UCA (King et al. 2010). At an approximate US frequency of 1 MHz, the collapse threshold of Definity® was determined at a PD of 3 cycles (Haak et al. 2007, King et al. 2010) (Figure 3.6). Definity® was found to demonstrate a 5% occurrence rate of collapse at approximately 0.2 MPa.

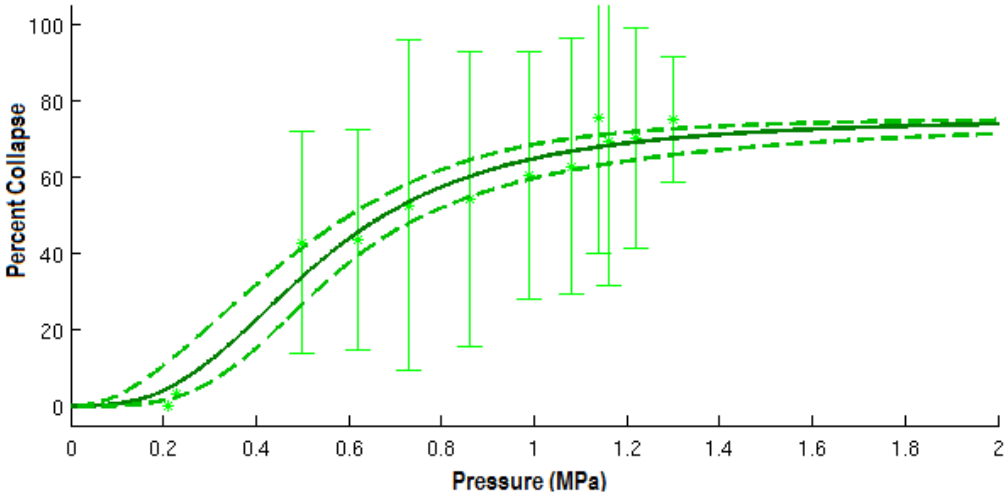

Figure 3.6: Percent collapse versus Pr: Definity® inertial cavitation thresholds (MPa) at 1.0 MHz. (King et al. 2010).

The data in Figure 3.6 represents repeated experiments conducted by three separate individuals, as such, the variance in the data is quite large. As a guide, however, the logistic regression fit can be used to discern a collapse trend. The 5% and 100% (~0.9 MPa, the point where the regression plateaus) collapse occurrence was consistent amongst trials.

3.7 Bubble clouds

A complexity of modeling US and UCAs interaction are the population effects or bubble clouds that are often present *in vivo*. Inertial cavitation depends on several parameters: the acoustic frequency, the acoustic pressure *at the bubble*, and the equilibrium size (Leighton et al. 1994). Previously discussed was the wide variation in potential bubble sizes with US interaction. The acoustic frequency herein has been set to approximately 1 MHz per previous research, but the Pr at the bubble is difficult to control when there are multiple bubbles in the sonicated area. Bubble aggregations are acoustically active; they may shield, channel, or scatter the acoustic field (Leighton et al. 1994) (Figure 3.6).

A few researchers have attempted to construct theoretical models for bubble clouds. Some of these studies observe the effects that two bubbles have on one another in terms of primary and secondary Bjerknes forces (Mettin et al. 1997), while others examine these forces between bubble clouds (Yasui et al. 2008). The results gathered from each of these studies vary significantly, and even within a single study two separate bubble clouds display different levels of radial expansion and responses to the applied US. Because, as Leighton (1994) described, the acoustic energy can be shielded, channeled or scattered, the pressure *at* an individual bubble's surface may be significantly lower than or equal to the measured output pressure. In addition, these types of studies have, to the knowledge of the author, not been conducted with shelled bubbles.

Shelled microbubbles are injected (bolus) intravascularly *in vivo*, and subjected to flow. The modified Rayleigh Plesset Equation is difficult to solve for bubbly cavitating flow. Hoff et al. (2001) stated that: "[it] can, in theory, be solved to find unknowns for any bubbly cavitating flow. However, in practice the nonlinearities in the equation present difficulties except when simple geometry is used".

Experimentally optical methods (LIDAR) and nonlinear US scattering have been explored for exploring size distribution and concentration of bubbles (Mari et al. 2007, Li et al. 2009). Estimating the acoustic activity of bubble clouds has been attempted mathematically using numerical simulations of bubble pulsations exposed to an acoustic horn (Yasui et al. 2008), but even quantifying concentration in in vitro flow systems remains elusive. The spatial temporal dynamics of bubble clouds has been experimentally studied and it was shown that bubble activation has a spatial preference. Chen et al. (2006) found that the focal region followed by the post then pre-focal region was the order in which bubbles were activated using 1.2 MHz focused

US. The conclusions from such studies are that bubble pulsation *can be* strongly reduced by the interaction with the surrounding bubbles. Yasui et al. (2008) found that the isolated bubble model (modified Keller equation, Mentin et al. 1997) predicted bubbles expanding up to 120 μm, whereas when the bubble-bubble interactions were considered, this expanded radius dropped to 40 μm, while these findings are not directly applicable to Definity microbubbles one can note how drastically a cloud of bubbles can affect bubble dynamics.

From Eq. 3.51 and 3.52, the distance that is necessary between two bubbles for the attractive velocity within a non-coalescent Weber number is 0.021 μm (using f = 1 MHz, ρ_{blood} = 1060 kg/m^3, a = 1 μm, p_A = 0.1 MPa, μ_{blood} = 0.005 Pa-s, $\sigma_{definity}$ = 0.025 N/m, ϵ = 5 x 10^{-7} m^2/N, (de Jong et al. 1993). The volume fraction (volume of gas/mL) is often calculated to estimate the distance between two bubbles. This fraction needs to be less than 0.001% for the attractive velocity to not spontaneously coalesce (see calculation in Chapter 5: Materials and Methods). While setting bubble coalescence as the determinant of bubble-bubble interaction does not account for the dynamic movements of the bubbles, it is used here to illustrate the spread of bubbles *in vivo*. This thesis uses an infusion of UCA solution, which is allowed to reach a steady state volume. The resulting volume fraction of the Definity® microbubbles to blood volume was calculated to be a maximum of 0.00008% for the infusion used herein, which represents a sufficiently low volume fraction that is within limitations (see details in Chapter 5: Materials and Methods). Therefore, the single bubble approximation used herein explores mechanistic motivation, because, to date, no models exist to accurately describe the effects of multiple bubbles. The main purpose of this thesis is to gain insight to the mechanisms, not necessarily to obtain concrete values.

3.8 Therapeutic effects of US and UCAs

Though bioeffects are reported from US exposure (via thermal and nonthermal effects), therapeutic effects of US have been shown as well (Porter et al. 2001, Kost et al. 2002, Chappell et al. 2006, Pang et al. 2010). The nondestructive effects (increased cell permeability, minor hemorrhage, slightly increased temperature, etc.) could be used to motivate therapeutic treatments. US has been used in the treatment of diabetic ulcerations (Dyson et al. 1976) to stimulate tissue regeneration (Dyson et al. 1968), and for bone regeneration (Hasuike et al. 2011).

UCAs have opened up the possibility to provide more types of therapy through bioeffects. Surprisingly, limited work has been done to connect the known UCA responses to US to bioeffects, and no work to establish the link between bioeffect and therapy has been explored. Studies have shown that UCAs are involved in sonoporation, sonothrombolysis, increasing perfusion and permeability (Postema et al. 2005, Forbes 2009, Choi et al. 2010, Hitchcock et al. 2010, Hernot et al. 2010). Sonoporation, for example, has been used for over 10 years to aid in drug delivery with ultrasound, yet the physical mechanism of it remained unexplored until recently (Bednarski et al. 1997, Forbes 2009, Forbes et al. 2011).

One study linked inertial cavitation to blood vessel rupture at high Pr (Ohl and Ikink 2003, Chen et al. 2010) which could be the mechanism by which drugs are locally introduced *in vivo*. IC has also been linked to increased nitric oxide (NO), calcium permeability, and cell-cell permeability (Juffermans et al. 2008, Juffermans et al. 2009, Shang et al. 2010).

While there has been extensive research on the therapeutic effects of US and UCAs, most of the studies were conducted *in vitro* and only assess acute effects. A few studies have used animal models to study other therapeutic effects such as blood brain barrier disruption for drug delivery (Yang et al. 2010) and arteriogenesis (Song et al. 2004). Nonthermal mechanisms have

been proposed to aid in tissue regeneration, and soft tissue repair (Paliwal et al. 2008). At the cellular level it has been hypothesized that changes in diffusion rates and membrane permeability due to microstreaming stimulates cells to increase protein synthesis essential for repair (Paliwal et al. 2008). One study even suggested that the acute bioeffect studied, hemorrhage, initiated a reparative response (Chappell et al. 2006), but no UCA mechanisms were discussed.

This chapter began by discussing US and associated bioeffects. Then UCAs were introduced and the physical and biological effects of UCA responses to US explored. While US bioeffects have been studied for quite some time, the advent of UCAs opened many new areas of research. All of the same underlying physical mechanisms remain (thermal and nonthermal effects) but UCAs introduce more cavitational bodies that behave differently than free bubbles. UCAs have been studied to understand bioeffects and utilized to promote therapy. However, the connection between the UCA behavior has not been correlated to the bioeffects or therapy, nor has the bioeffect been related to the therapy.

CHAPTER 4: ULTRASOUND & ULTRASOUND CONTRAST AGENT-INDUCED ANGIOGENESIS AND SPECIFIC AIMS

This chapter focuses on ultrasound alone, and with the addition of ultrasound contrast agents in the induction of a specific therapy, angiogenesis. It extends the discussion to include an overview of the wide range of parameters used in this therapeutic application, and describes the areas of research that remain open as possible reasons for the slow transition to clinical use. Next, this chapter states a hypothesis for the biophysical mechanism with respect to ultrasound contrast agents, and potential mechanistic motivation of US-UCA-induced angiogenesis. Concluding the chapter are the specific aims to be addressed in this thesis, along with a flow chart of proposed events.

4.1 US-induced angiogenesis

Ultrasound was first researched as a means for inducing vascular changes, and in particular angiogenesis, in the late 1960s (Dyson et al. 1968, 1976, Hogan et al. et al. 1981, Dyson et al. et al. 1987). It provided a way to spatially target ischemic tissue. US disturbs tissue by bulk streaming, and was initially used for its ability to accelerate healing, presumably by proangiogenic methods (Dyson et al. 1976). Conflicting levels of angiogenic responses have been noted with the various techniques—none of which have transitioned well into the clinic. US-induced angiogenesis is an existing phenomenon that has been documented for over 50 years. However, a major impediment to progress in the field is the deficit in biophysical understanding apparent from the lack of unified exposure conditions. Therapeutic applications typically use 1—3 MHz for US exposure (Dyson et al. 1976, Hogan et al. 1982, Young & Dyson 1990, Barzelai et al. 2005, O'Brien 2007). Though US frequency is consistent, Pr, repeated exposure conditions, pulsed vs. continuous, and even the day at which the angiogenic effect is observed all vary (Table 4.1). Exposure conditions with peak rarefactional pressures (Pr) ranging

from 40 kPa to 5 MPa, continuous US to pulsed US, and EDs ranging from 30 seconds to 20 minutes have been used and increased angiogenic effects to some extent. How these parameters influence the response has not been assessed (Table 4.1). The extent to which US affects the tissue for therapeutic benefit is also undetermined, as exposure conditions are influenced by whether or not there is overlaying skin during the exposure, the area of exposure, and the tissue being exposed. With that stated, several studies report a reparative response to US with *repeated* exposures (Dyson et al. 1976, Hogan et al. 1982, Barzelai et al. 2005, Sugita et al. 2008). The significance of understanding the biophysics of the mechanism to establish a standard protocol for exposure is therefore of importance.

Table 4.1: Ultrasound–mediated angiogenesis and effectiveness

Citation	Transducer Frequency	Pulsed/ Continuous	Pressure	Angiogenic effect @	Repeated Exposures	Effectiveness
Dyson, et al. 1976	3 MHz	Pulsed (2ms on; 10ms off)	0.18 MPa	28-d	3 times/week	~28%
Hogan, et al. 1982	1 MHz	Pulsed (100us, DC=50%)	0.2, 0.3, 0.4, 0.6 MPa	3 wks	~3 times/week	~10%
Young & Dyson 1990	0.75, 3 MHz	Pulsed (2ms on, 8ms off)	0.06 MPa	5-d	7 times/week	~40%
Reher et al. 1999	1 MHz	Pulsed (2ms on; 8 ms off)	0.5 – 5 MPa	18 hours	Not repeated	~50%
Barzelai, et al. 2005	2 MHz	Continuous	0.04 MPa	7-d	3 times	30%

Johns et al. (2002) hypothesized that angiogenesis is induced by a mechanical effect of low-intensity US based on radiation force and cavitation bubbles acting on the cellular membrane and the molecular structures within the cell. Another study stated that because bovine aortic endothelial cells display an angiogenic phenotype in response to US stimulation in bubble minimizing media, there is a mechanism other than cavitation that promotes angiogenesis (Mizrahi et al. 2007). Yet another hypothesis is that the US radiation force promotes inflammation and apoptosis to encourage angiogenesis (Barzelai et al. 2005).

The induction of angiogenesis with US has only been directly studied by Young and Dyson et al. (1990) and Barzelai et al. (2005). Both studies examined ischemic models that were relatively well calibrated. Other studies (Hogan et al. 1982, Reher et al. 1999) focused on the wound healing—which involves new blood vessel growth, but angiogenesis was not necessarily quantified. The US Prs used vary from 40 kPa to 5 MPa, pulsing regimes vary, and there is variability with the time point which the angiogenic effect was observed. Therefore, there still remains a disconnect assessing 'appropriate' exposure conditions. One reason for this disconnect could be that the US physical parameters and their connection to the biological response remains systematically uninvestigated.

4.2 US-UCA-induced angiogenesis

With the development of UCAs, research seeking to establish models for the use of microbubble-enhanced ultrasound induced angiogenesis surfaced (Korpanty et al. 2005, Chappell et al. 2006). US and UCAs have been used for site specific delivery of factors and/or controlled damage, where the logic was to cause controlled damage to areas peripheral to the ischemia such that the normal angiogenic response caused an ingrowth of vasculature. With the deposition of angiogenic factors, this response would presumably be enhanced. Upon US irradiation the UCA would oscillate or collapse and release a proangiogenic agent (Zen et al. 2005, Yoshida et al. 2005). Various agents have been used in cardiac or skeletal muscle models. Korpanty et al. (2005) destroyed (UCAs underwent IC) microbubbles to offer site specific delivery of VEGF to the myocardium. In addition, endothelial progenitor cells were delivered to the myocardium and it was found that via an angiogenic response, cardiac function was improved (Zen et al. 2005). Bone marrow derived stem cells (BMSCs) have also been used to

promote blood vessel growth by being attached to UCAs (Song et al. 2008). These studies use a one-time exposure to induce the reported effects (Table 4.2).

The most recent work using contrast agents shows promising results for a future lacking ischemic diseases and myocardial degeneration. Note that the effectiveness has improved over the past several years with the addition of growth factors or DNA plasmids (Table 4.2). The literature also suggests that inertial cavitation is required for angiogenesis to occur or for angiogenic factors to be deposited (Song et al. 2002, Korpanty et al. 2005, Chappell et al. 2006, Hwang et al. 2005, Miyake et al. 2007, Leong-Poi et al. 2007).

Table 4.2: Ultrasound–mediated angiogenesis and effectiveness

Citation	Transducer Frequency	Pulsed/ Continuous	Pressure	UCA Type	Angiogenic effect at	Effectiveness
Song, et al. 2004	1 MHz	Pulsed (100us, 5Hz)	0.5 MPa	Albumin shelled UCA	7-d	~33%
Korpanty, et al 2005	1.3 MHz	Pulsed	1.8 kPa	hVEGF tagged lipid shell	10-d	33%
Zen, et al. 2005	1 MHz	Pulsed (50% DC)	0.25 MPa	BM-MNC+Optison	20 wks	~5%
Chappell, et al. 2006	1 MHz	Pulsed (100us, 5Hz)	0.79 MPa	Albumin shelled UCA	3-d	~15%
Leong-Poi et al. 2007	1.3 MHz	Pulsed (5s)	Not Provided	VEGF tagged MP1950	4 wks	~30%
Song et al. 2008	1 MHz	Pulsed (50% DC)	1 MPa	SonoVue + BMSC	28-d	~20%
Chappell et al. 2008	1 MHz	Pulsed	0.8 MPa	bFGF tagged lipid shell	7 & 14-d	~50%
Fuji et al. 2009	8 MHz	Pulsed	4.5 MPa	Definity + DNA	21-d	~44%
Kobulink et al. 2009	1.3 MHz	Pulsed (5s)	2.1 MPa	VEGF tagged lipid shell	17-d	~50%

In comparing US-induced (Table 4.1) with US-UCA induced angiogenesis (Table 4.2) we note several things: the necessity for repeated exposures to achieve similar levels (if not more) of effectiveness has been eliminated, the therapeutic range for US transducer frequencies when UCAs are involved is about 1-2 MHz, the average pressure of US exposure is higher, and

stem cells or growth factors were added. For researchers using contrast agents to elicit a response, understanding how the US and UCA parameters influence the response is important.

As mentioned in Chapter 3 of this thesis, ultrasound contrast agents undergo dynamic responses when exposed to ultrasound. Part of understanding an effect is determining the mechanism by which the effect is occurring. With sufficiently high Pr, UCAs undergo collapse, but some researchers expose at a pressures well below the UCA collapse threshold, where microstreaming is the dominating bubble response (Korpanty et al. 2005, King et al. 2010). When UCAs are used, Table 4.2 shows that Pr = 0.18—4.5 MPa have been used to elicit an angiogenic response. There is no discernable for effectiveness with Pr, but the use of this range of Pr supports the suggestion that IC is required. However, microstreaming has been correlated to increases in shear stress that may activate FAK and Akt stress pathways in angiogenesis induction.

Davies et al. (1986) found that turbulent fluid shear stress induces vascular endothelial cell turnover or proliferation—an important step of angiogenesis. Further, high shear stress has been linked to increased permeability and enhanced EC biosynthetic capabilities (DeForrest et al. 1980, Davies et al. 1986, Paszkowiak et al. 2003). This increased shear stress could be caused by microstreaming. Also the wall shear stress of blood vessels has been linked to decreased EC alignment resulting in increased pore size (Paszkowiak et al. 2003). Figure 4.1 shows the proposed sequence of events (Hudlicka et al. 2006). Capillary shear stress promotes EC cell growth by activating VEGFR-2 and VEGF (Hudlicka et al. 2006, Jin et al. 2003, Shay-Salit et al. 2002, Urbich et al. 2003, Wang et al. 2004) and has a critical role in initiating angiogenesis. ECs sense shear stress via cytoskeletal elements, microfilaments and shear stress response elements. Normal vascular shear is ~ 1.5 Pa, but as little as 0.075 Pa can transiently activate transcription

factors for VEGF, PDGF and MAPK (Braddock et al. 1998) (Figure 2.4). Therefore it remains unknown whether inertial cavitation (or a particular amount of cavitation) induced damage/turbulence or if microstreaming induced shear stresses potentiate the angiogenic response.

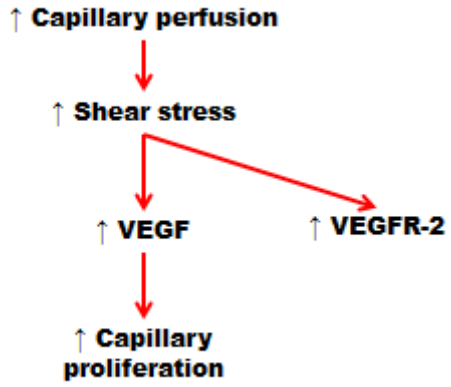

Figure 4.1: Hypothesized biological mechanisms resulting from physical effect of microstreaming. Adapted from Hudlicka et al. (2006).

With UCAs involved, infusion rate and UCA concentration ([UCA]) should also be considered. Infusion rate and [UCA] are related in that if there is a bolus injection many microbubbles reach a particular portion of the vasculature all at once, and the simultaneous collapse of several could result in massive damage to the capillary walls; this is analogous to infusion of high doses of contrast agent.

Other non-UCA parameters may also affect the response. Pulsed US has been widely used over continuous exposure (presumably to minimize heating) of inducing angiogenesis, but the ED and PRF vary significantly (Song et al. 2004, Leong-Poi et al. 2007, Kobulink et al. 2009). A mouse model using UCAs had an ED of 3 minutes (Chappell et al. 2006), but another mouse study (same strain) used an ED of 20 minutes (Fuji et al. 2009) (Table 4.2). US-UCA-induced angiogenesis also shows a range of effectiveness from 5 to 50%. The range could be

because of the different time points at which angiogenesis was observed (Johnson et al. 2010), ED, PRF, [UCA], the type of contrast agent used, or the involvement of UCA collapse (ie. Pr).

To the knowledge of the author, only two studies have been conducted without the use of proangiogenic agents (Song et al. 2004, Chappell et al. 2006), and only one of these two used a normal animal model (Chappell et al. 2006). Both Song et al. (2004) and Chappell et al. (2006) report relatively low effectiveness for reasons that remain unknown. If the mechanism is explored in a normal model, the effectiveness of all studies can potentially increase. For the purposes of this thesis, only one UCA, Definity® was explored, as others were inconsistently available for purchase.

None of the studies displayed in Table 4.2 linked the acute bioeffects to the subsequent angiogenesis or exposed the UCA behavior for mechanistic motivation. The goal of this thesis is to explore the role of the UCA and the mechanism by which angiogenesis is induced beginning with the bioeffects.

4.3 Hypothesis

From the literature, the hypothesized physical mechanism for the angiogenic response occurs through inertial cavitation. Precautions were taken to eliminate the thermal effects such that the nonthermal bioeffects leading to angiogenic response could be investigated. Therefore it is proposed that in the normal rat model ICs lead to capillary damage/rupture and controlled tissue damage. This damage elicits the VEGF (and hypoxia) that potentiates angiogenesis. See Figure 4.2.

4.4 Specific aims

Numerous studies demonstrate the real, reproducible proangiogenic therapy that US provides; however, the mechanism has not been elucidated. Barzelai et al. (2005) states that

"lack of consensus regarding the optimal dose needed to produce maximal protective effect is evident from different studies that have used a wide range of US energy and intensities."

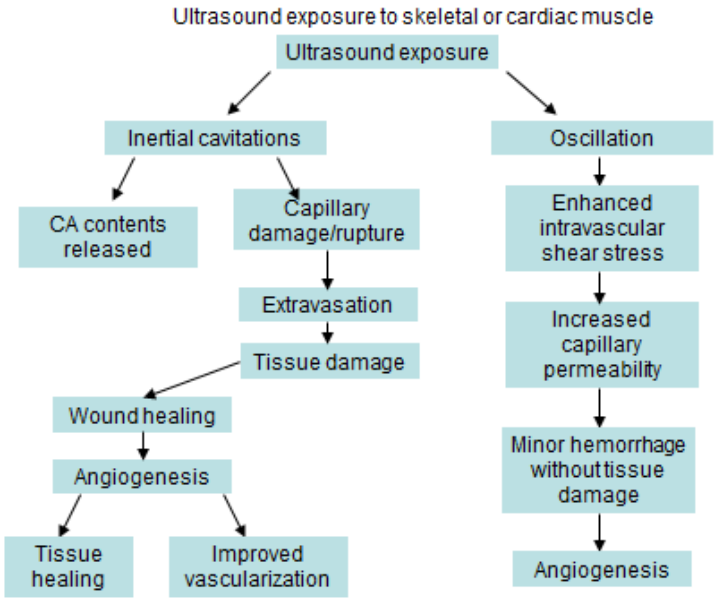

Figure 4.2: Hypothesized effect of ultrasound exposure to muscle

For proangiogenic US therapy to transition to clinic, minimally an exposure-effect understanding must be known with some basis for an operative mechanism. Therefore, the objective of this project is to explore the physical and biological mechanisms of US-UCA induced angiogenesis via exposure-effect studies. Specifically, the objective is to explore the biophysics of the UCA in inducing angiogenesis including the role of UCAs, some US parameter optimization and connecting the bioeffects to the therapy for potential predictive and mechanistic motivation value. These aims will be assessed using capillary density, vascular endothelial growth factor (VEGF), and EBD extravasation (vascular permeability measurement) as measurement end points.

4.4.1 Specific aim #1. To determine the role of UCAs in US-induced angiogenesis

Whether UCAs are necessary for an angiogenic response is unclear. A variety of UCA concentrations have been used in the literature (no UCAs to bolus injection) (Barzelai et al. 2006, Chappell et al. 2006, Zen et al. 2005, Miller et al. 2008); effects noted may have been contingent upon [UCA]. Therefore it is important to understand how the angiogenic effect varies with increasing number of microbubbles. It is hypothesized that as UCA concentration increases, the angiogenic effect will increase. Also, it is hypothesized that an angiogenic response can occur without UCAs, but UCAs enhance the angiogenic response above that of US alone.

4.4.2 Specific aim #2. Explore the mechanism of US and UCA induced angiogenesis

US-induced angiogenesis can be affected by multiple parameters, and their dependencies on angiogenesis will provide insight into biophysical mechanisms. The objective of this aim is to correlate the acute bioeffects of US-UCA with the physical behavior of the UCA. This objective will examine collapse and microstreaming as potentiating factors for bioeffects. The secondary goal is to assess the biological mechanism by correlating the acute bioeffects to the angiogenic response.

Sub-Aim A: To connect the acute bioeffects to UCA behavior (physical mechanism)

If UCAs are needed, whether or not microstreaming or IC (increased shear stress, eddies in flow, local turbulence) are essential to neovascularization is unknown. It is hypothesized that IC causes a reduction in capillary density, hemorrhage, and tissue damage necessary for an angiogenic response. Whereas microstreaming, along with increased shear stress causes increases in permeability, but not angiogenesis.

Sub-Aim B: To assess the biological mechanism

The literature, to date, has either focused on the acute effects of US, US and UCAs, or the angiogenic response (AR) at some time point. The initial effect of US and UCA that potentiates the AR has not been studied. Thus far possible mechanistic motivators of angiogenesis have been speculated to be damage induced by the combined effect of US and UCAs. Literature hypothesizes inflammation, apoptosis, hemorrhage, cellular membrane perturbation/disruption, stimulation of molecular structures within the cell to be involved in the process. This aim seeks to specifically determine if damage, defined as coagulative necrosis and/or a reduction in capillary density precedes the angiogenic response (Figure 4.3). It is hypothesized that a reduction in capillary density that boosts the normal wound healing response precedes the angiogenic response. This connection is not only important to understanding the mechanism, but also provides risk/benefit and potential predictive information.

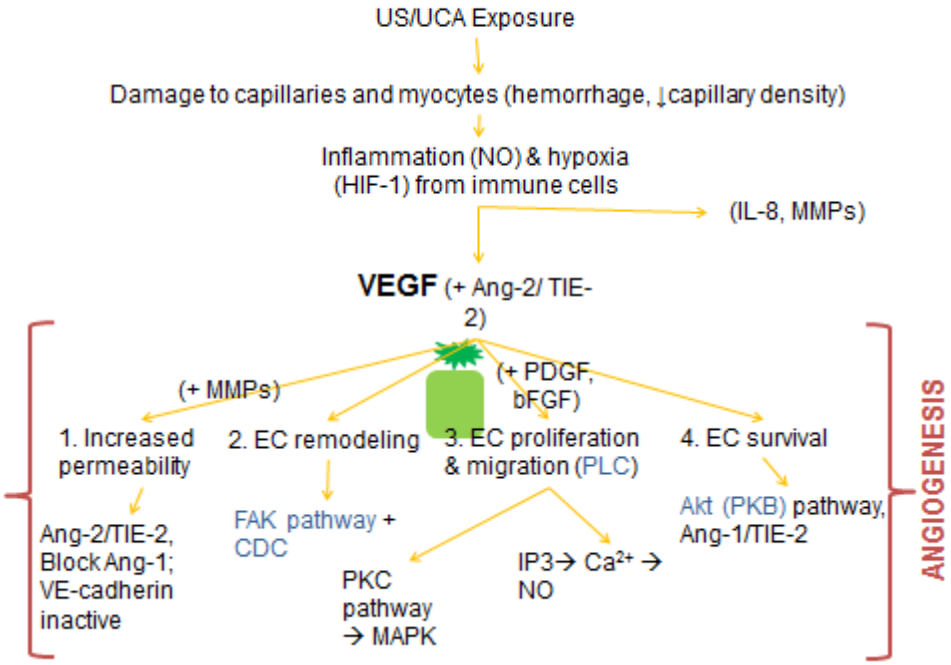

Figure 4.3: Proposed mechanism for US and UCA induced angiogenesis. The blue items indicate shear stress activated pathways.

4.4.3 Specific aim #3: US parameter optimization: examine the effects of PRF and ED

Conflicting results concerning the PRF and ED on bioeffects have been reported (Song et al. 2002, Fujikura et al. 2006, O'Brien et al. 2005, Miller et al. 2008). Below 3 minutes, bioeffects are generally uncorrelated to ED, however as this value increases a positive trend emerges (Miller et al. 2008, O'Brien et al. 2005). The interaction of PRF and ED, the total number of pulses, was significant for all studies in which it was tested (Song et al. 2002, O'Brien et al. 2005). It is therefore hypothesized that the total number of pulses will be positively correlated with the angiogenic effect and that ED and PRF will not be significant.

CHAPTER 5: MATERIALS AND METHODS

5.1 Experimental Setup

A 1.0 MHz single element focused (f/3) transducer (Valpey Fisher E1051, 0.75" diameter, 2.25 S.F; Hopkinton, MA) connected to a power source (RAM5000, Ritec, Inc., Warwick, RI) was used for the exposures. The base was removed from a cylindrical bowl, and Syran® wrap placed securely around the bowl with large rubber bands. A custom built plastic holder for the bowl was constructed such that the bowl could be suspended from a square post. The bowl was filled with degassed water for ultrasonic transmission (see Figure 5.1). The water was heated to approximately 35 ^{o}C using a proportional temperature controller (Yellow Springs Instrument Co./Cole Parmer Instrument and Equipment Co. Model 72). Mineral oil was then used as a coupling agent at the point of contact (between skin and Syran® wrap) to ensure an air-free interface.

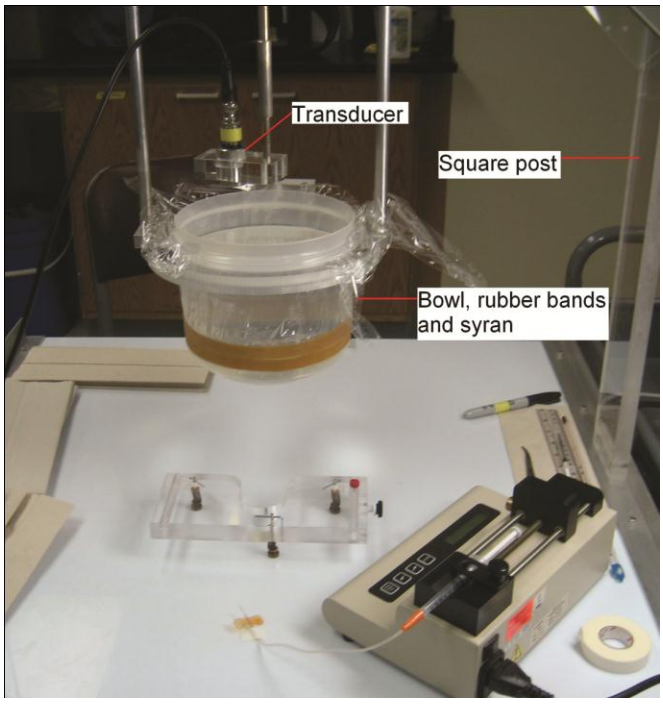

Figure 5.1: Experimental Setup

5.2 Exposimetry

5.2.1 Calibration

An automated procedure, based on established standards (AIUM/NEMA 2000, ODS 1998, NEMA 2009a, 2009b), was used to routinely calibrate the ultrasound fields (Semsprott et al. 1999, Zachary et al. 2001).

All calibrations were performed with calibrated hydrophones [PVDF membrane hydrophones (Perceptron Model 804, Plymouth Meeting, PA) and Marconi Model Y-34-6543, (Chelmsford, UK)], both before and after experiments were conducted. The Marconi M1 hydrophone was placed in a custom built tank containing degassed water attached to a positioning system. The transducer was placed perpendicular to the hydrophone in the tank. Using the RITEC® power supply, electrical pulses were sent to the transducer. To calibrate, the transducer was manually moved until the signal produced on the Agilent scope reached its maximal intensity. Once the transducer was manually centered, the Daedal positioning system (Daedal Systems, Inc.) was used to ensure symmetry. The hydrophone was then placed in the lower left corner of the focus, such that the Daedal positioning system could scan through the focus to find the pressure output (Sempsrott and O'Brien, 1999; Sempsrott, 2000). Routine calibrations resulted in approximately 10% error in all calibrations. See block diagram in Figure 5.2.

The transducer calibration procedure yielded the following quantities: pulse duration (μs), *in vitro* peak compressional pressure at global maximum (MPa), *in vitro* peak rarefactional pressure at global maximum (MPa), and Mechanical Index (MI).

While calibrations were performed in degassed water, *in situ* (at the muscle surface) estimation of the US exposure quantities was required to assist in evaluating exposure-effect

responses and basic physical mechanisms. The *in situ* peak rarefactional pressure was estimated from Pr (*in situ*) = Pr (*in vitro*) e^{-Ax}, where Pr (*in vitro*) is the global-maximum water based value.

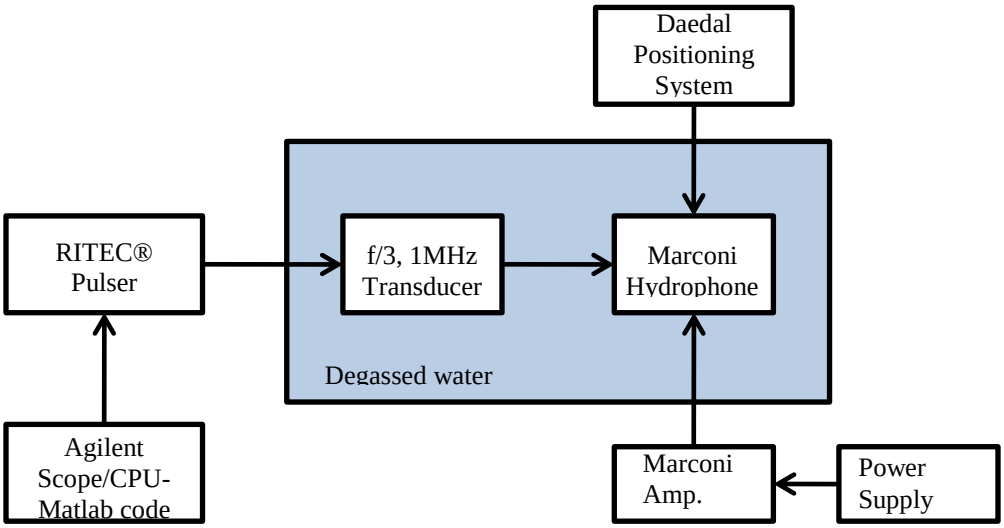

Figure 5.2: Calibration setup, including a pulser, transducer, hydrophone, amplifier, power supply and oscilloscope.

"A" is the attenuation coefficient of the skin (A ≈ 2 dB/cm at 1 MHz) (Riederer-Henderson et al. 1988) overlaying the gracilis muscle, which had a thickness, x, of approximately 1 mm. Attenuation of US by intervening tissue is negligible (0.98 of *in vitro* Pr) and thus the reported Pr is that of the in vitro value. The parameters tested herein include: Pr ranging from 0 to 1.9 MPa, PRF = 0 to 40 Hz, ED = 0 to 5 min, DPE = 0 to 6 DPE, and [UCA] = 0 to 10x. The PD was set at 10 μs for all exposures. The US parameters are stated before the results section of the chapter for each experiment.

5.2.2 Transducer alignment

Before exposures, the transducer's peak signal was aligned with the marked exposure site. The peak signal was found visually using an attached oscilloscope (500 MS/s, LeCroy Model 9354TM Oscilloscope, Chestnut Ridge, NY, USA). For transducer alignment, a low Pr value (50 kPa) was used to ensure minimal US-induced damage. Parameters used during

alignment were a pulse duration (PD) of a 10 cycle sine wave (10 μs), and pulse repetition frequency (PRF) of 10 Hz.

5.3 Animals

A total of three hundred thirty three female Sprague Dawley rats (Harlan, Indianapolis, IN, USA) were used in this study. Animals ranged in age from 11 to 13 weeks old and weighed between 190 and 215 grams.

Rats were weighed and anesthetized with ketamine hydrochloride (87 mg/kg) and xylazine (13 mg/kg) administered intraperitoneally. Hind limb hair over the gracilis muscle was removed with an electric clipper, followed by a depilatory agent (Nair® Carter-Wallace, Inc., New York, NY, USA) to maximize sound transmission. The rat was then placed in a custom built holder. Bilateral sites on the lateral sides of the left and right gracilis muscle were marked with a black dot to denote the US exposure location. Medial sections of the gracilis muscle served as the sham (Pr = 0 MPa) for exposed animals. The US transducer was visually aligned with the black dot using a custom build laser pointer that was spatially registered with the beam focus. For both US-UCA and US-saline infused groups, the 0 DPE rats were euthanized within 1hr following exposure, and rats assessed at other time points were euthanized on their respective recovery day (ie. 3, 5 or 6 DPE).

The experimental protocol was approved by the Institutional Animal Care and Use Committee of the University of Illinois and satisfied all campus and National Institutes of Health rules for the humane use of laboratory animals. Animals were housed in an Association for Assessment and Accreditation of Laboratory Animal Care, Rockville, MD-approved animal facility and provided food and water *ad libitum.*

5.4 Microbubble preparation

The manufacturer's recommended dosage for infusion was used to establish the 1x concentration of Definity® (Bristol-Myers Squibb Medical Imaging, North Billerica, MA) for UCA infused groups.

For 0 DPE animals, 1.5 mL of Definity® solution (containing 0, 0.07, 0.25, or 0.75 mL Definity® brought up to volume with saline, for the saline (0x), 1x, 5x, and 10x concentrations, respectively) was prepared in a 3 mL syringe. The 1x UCA concentration [UCA] was determined from the package insert (1.3 mL of Definity® in 50 mL saline).

5.5 Evans blue dye

Evans blue dye (EBD) was discovered in 1917 as a method to estimate blood volume (LeVeen et al. 1947). EBD binds to serum albumin, and is not normally secreted from blood vessels; particularly those that do not have large inter-endothelial cell gaps like skeletal muscle. Albumin is approximately 70 nm in diameter, whereas the pores in undisturbed skeletal muscle are ~ 4 nm. Therefore leakage of the albumin bound dye indicates capillary disruption. Since 1917, EBD has been the choice dye marker for vascular permeability (LeVeen et al. 1947, Jackieqicz et al. 1998). In this study EBD (10 mg/mL) was dissolved in the volume of saline prior to addition of UCA. For the 5 DPE animals, the same procedure was followed, but without the addition of EBD due to diffusion to peripheral tissues and potential dye toxicity. EBD has been shown to modify the ultrastructure of regenerating blood vessels in rats (Jackieqicz et al. 1998).

5.5 Infusion

5.5.1 Initial manual injection of UCAs or saline

Prior to US exposure, the rat tail vein was manually injected for 30 seconds with 0.5 mL of Definity® solution (at 1x, 5x, or 10x [UCA]) such that UCAs were introduced into circulation. The saline infusion group received 0.5 mL of saline for 30 seconds prior to US exposure.

5.5.2 Infusion of UCAs or saline

After manual infusion, 1.0 mL of Definity® solution or saline was infused with an infusion pump (model 780100; KD Scientific, Holliston, MA) for 15 minutes into the rat tail vein at a rate of 4.0 mL/hr. The resulting infusion rate was a maximum of 3.3×10^8 microbubbles/min (at 10x [UCA]). The following infusion regimes was used: the first of two ultrasound-exposed sites was started approximately 5 seconds after the infusion pump was started (ie. 5 minutes per exposed site, 3 minutes for realignment with the next site, and 2 sites per rat = 13 minutes). The exposures were completed before the infusion pump was stopped such that Definity® solution was present during each exposure.

The saline infusion groups received the same treatment but without UCA addition.

The following was used to model the *in vivo* quantity of Definity as a function of time:

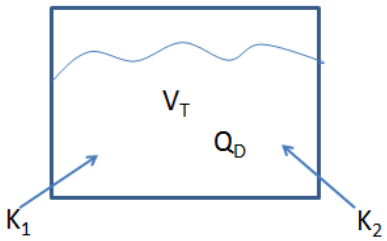

Figure 5.3: Model of the total volume (V_T), quantity of Definity® (Q_D), initial (K_1) injection rate (0.5 mL in 30 seconds), and infusion rate (K_2) (1.0 mL over 15 minutes).

The quantity of Definity®, Q_D, for the initial injection is the number of microbubbles at time, t (minutes), plus the infused amount entering at rate K_1. Such that:

$$\Delta Q_D = \Delta t C + \Delta t K_1 \tag{5.1}$$

$$\frac{dQ_D}{dt} = I \cdot C(t) + K_1 \tag{5.2}$$

$$Q_{D1}(t) = -\mathrm{K}_1(1 - e^t) \quad (5.3)$$

where K_1= 5 x 10^9 microbubbles/minute, and t = 0.5 minutes. To account for the 5 second delay between injection and infusion where monoexponential decay (Definity® package insert) occurs:

$$Q_{D2}(t) = Q_1(0.5)e^{-\varphi t} \quad (5.4)$$

where t = 0.083 minutes and φ is the decay constant calculated from the half-life of Definity®. The mean lifetime of Definity® in humans is ~ 3 minutes (Definity package insert), but because the package insert demonstrated an increase in half-life with changes in respiration, the following was noted:

(1) Normal respiration rate for humans ≈ 12 breaths per minute

(2) Chronic obstructive pulmonary disease (COPD) (where the respiratory rate is > 36 breaths per minute) increased Definity's® half-life by 0.6 minutes (Definity Package Insert)

(3) Rat respiration rate under anesthesia is ~ 3 times greater than humans (assessed while sedated)

(4) COPD is an obstructive disorder which increased the half-life; the rat's oxygen exchange would be normal, but higher than humans. Thus the half-life should decrease by an amount approximately equal to but opposite that of the COPD case, where $t_{1/2}$ ≈ 0.7 min and φ = 0.99.

Then, for the 15 minute infusion, which will include decay:

$$Q_{D3}(t) = \left[Q_{D2}(0.083) - \left(K_2(1 - e^t)\right)\right]e^{-\varphi t} \quad (5.5)$$

where K_2 = 3.3 x 10^8 microbubbles/minute. Because Definity® accumulated in the syringe near the plunger and the UCA floats, the initial injection was designed such that the initial injection

rate was higher than the infusion rate. This set of equations assumes that the recirculation rate is equal to the collapse (disintegration) of the UCAs.

Determining the quantity of microbubbles *in vivo* was integral for determining the volume fraction of Definity®. The volume fraction of Definity® was calculated using the following:

$$\Gamma = \frac{V_D}{V_B - V_D} \tag{5.6}$$

$$V_D = \frac{4}{3}(Q_{D3})\pi a^3 \tag{5.7}$$

where V_D is the total volume of gas contained in Q_{D3} bubbles of Definity®, V_B is the total volume of blood, and a is the bubble radius. Because the UCA was infused over 15 minutes, calculating the volume fraction using only the amount in the syringe is an inaccurate estimator for the bubble distribution in vivo. The Sprague Dawley rat's cardiac output is approximately 100 mL/min/100g, so there is ~ 200 mL of blood in a 200g rat (Gotshall et al. 1987). Because $Q_D{}'$ (the steady state quantity) = 3.8 x 10^8 microbubbles/min, we find that V_D = 1.6 x 10^8 μm^3, V_B = 2 x 10^{14} μm^3 and Γ simplifies to V_D / V_B because V_B >> V_D, and Γ = 0.0000008 or 0.00008%. To calculate the volume fraction necessary to minimize bubble coalescence a Weber number of 0.5 was used to calculate the maximum approach velocity ($v_a < 3.43\ \frac{m}{s}$) using Eq. 3.52. This velocity was used to calculate the minimum distance needed for bubbles to not coalesce using Eq. 3.51 ($d_0 = 0.021\ \mu m$). This distance was added to the mean radius of a Definity® microbubble to increase the effective diameter of the bubble, and then used to calculate V_D' and Γ', where the prime indicates the effective diameter was used in the estimate ($\Gamma' = 0.00085\%$). Therefore, a single bubble approximation is appropriate for theoretical estimates.

The saline infusion groups received the same treatment but without UCA addition. The volume fraction of Definity as a function of time is shown in Figure 5.4:

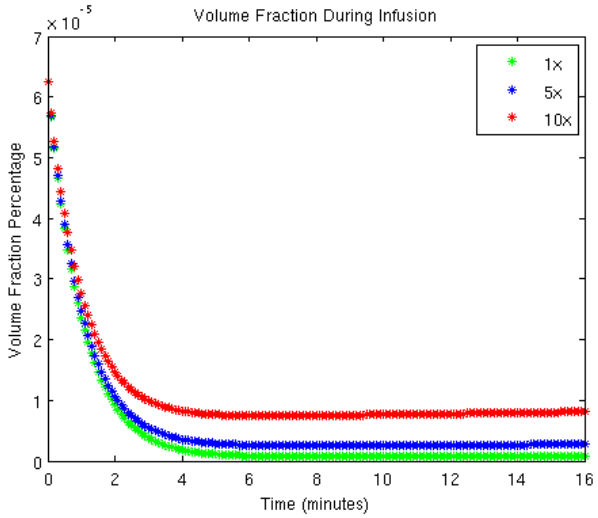

Figure 5.4: The volume fraction (%) of Definity® as a function of time at 1, 5, and 10x [UCA] showing relative consistency over 15 minutes.

5.6 Photographic log of leakage

Once the diameter of leakage was measured, the animal was mounted on a custom built stage. Using a Canon PowerShot SD 880 iS camera; digital pictures were taken of the exposed sites. A ruler was placed on the animal when the pictures were taken for size estimations.

5.7 Post euthanization tissue preparation and processing

A 6 mm biopsy punch (Integra™ Miltex® Plainsboro, New Jersey) was used to extract the exposed region from the gracilis muscle. Because the transducer's beamwidth was sufficiently large (~ 5 mm), one-half of each exposed location was either preserved in RNA*later* (Quiagen, Valencia, CA) (for the 5 DPE animals) or soaked in formamide for 24 hours (for the 0 DPE animals). The other half was formalin-fixed in 10% PBS formalin (Fischer Scientific, USA) for a maximum of 24 hours. See Figure 5.5. The formalin-fixed tissues were then paraffin embedded (Thermo Fisher Scientific, USA). Three-micrometer-thick sections were stained with:

hematoxylin and eosin (H&E) for whole tissue examination, and CD-31 antibody (CD-31, Cell Marque #1A10, Rocklin, CA) for capillary density counts.

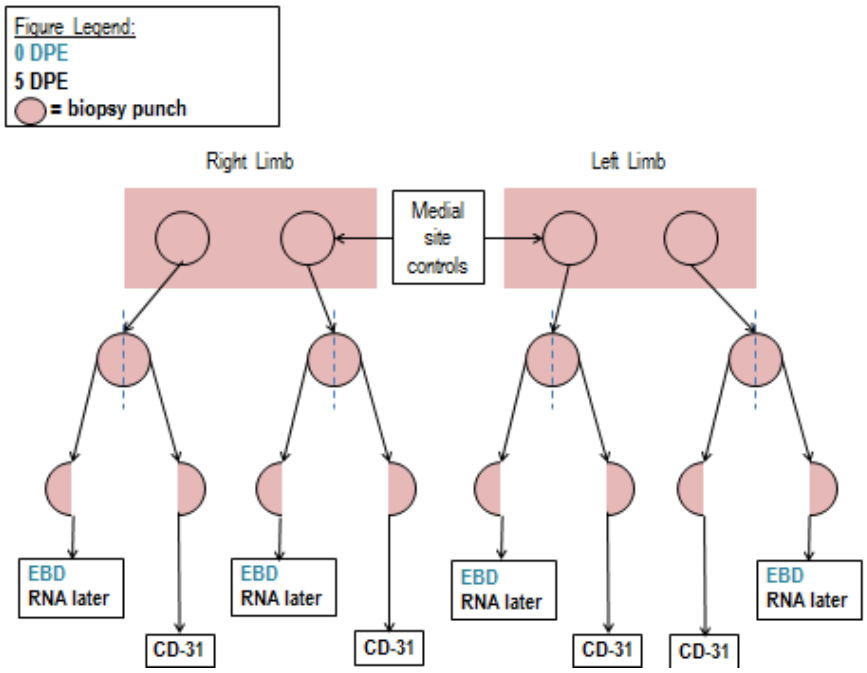

Figure 5.5: Schematic of sample tissue preparation

5.7.1 Histology

The hematoxylin and eosin stain is one of the most widely used stains in histology. These two stains are used in conjunction to visually separate nucleus and cytoplasm. It is a basic stain and counterstain combination used to view a tissue's morphology. H&E stain identifies abnormal features such as hypertrophy, hyperplasia, atrophy, necrosis and apoptosis (provided adequate timing). In addition, accumulation of specific proteins, pigment, and overall structure can be assessed.

There are several stages involved in the H&E tissue staining. The slides were first removed from the heating oven and then placed in xylene three times for two minutes each. Ten dips in 100% ethanol, ten dips in 95% ethanol (twice) follow. The slides were then rinsed with tap water until the water ran off evenly. Hematoxylin was added to the slides for 15 minutes, and then the slides were rinsed. Ammonia water (0.25%) was used to treat the slides prior to ten

tap water dips to allow the hematoxylin to set. Finally, eosin was added to the slides (15 dips), and the slide was then dipped ten times with two changes of 95% ethanol, three changes of 100% ethanol, and three changes of xylene. Cover slips were applied at the end.

In order to look for particular structures however, immunohistochemical (IHC) techniques are employed to specifically stain for capillaries.

For IHC, CD-31 was used. CD-31 is also known as platelet endothelial cell adhesion molecule. Part of its role is to provide a signal medium for the digestion of aging neutrophils via macrophage uptake. CD31, as a result, is normally found on cells that are involved in inflammation or inflammation resolution, such as: endothelial cells, platelets, macrophages, T / NK cells, and neutrophils.

Several stages of slide preparation were involved in the IHC tissue staining. The slides were removed from the drying oven. Then the slides were incubated 3 times in xylene for 10 minutes, twice in 100% ethanol for 2 minutes, and hydrated by placing in 95%, 70%, 50%, 30% ethanol for 2 minutes each. The slides were then placed in buffer for 5 minutes. Buffer: 0.25 M Tris-HCl at pH 7.5. Slides were blocked with CD-31 primary antibody (CD-31, Cell Marque #1A10, Rocklin, CA), incubated for 20 minutes at room temperature in a humidified chamber, and washed in buffer for 5 minutes. Then slides were placed into buffer containing 0.5% BSA and 2% Fetal Calf Serum for five minutes. Once again the slides were incubated in a humidified chamber overnight with secondary antibody (iVIEW^{TM} DAB Detection Kit mouse IgG, IgM and rabbig IgG, Ventana Tuscon, AZ), and the secondary antibody was diluted in the Tris with protein solution above. The antibody was diluted from 1:20. The slides were then rinsed with buffer solution and fitted with cover slips.

For each exposed site the following slides were created: H&E, CD-31, and CD-31 negative control. A CD-31 positive control was made for a batch of slides. H&E was used to observe whole tissue effects. CD-31 slides were used for capillary density counting according to techniques detailed in previously published literature (Johnson et al. 2010). Briefly, each CD-31 slide was divided into 15 random high power fields (HPFs) within the region of interest (the US exposed area) for capillary assessment. Only full lumen capillaries were counted. The Carl Zeiss® Axioscope 2 upright light microscope (Carl Zeiss Microscopy, Thornwood, NY) had a HPF diameter of 0.45 mm in diameter at 40x magnification. Fifteen HPFs were averaged and reported as capillaries/mm^2 ± standard error of the mean (SEM).

5.7.2 Vascular endothelial growth factor (VEGF)

The RNA*later* section was used for VEGF analysis; RNAlater preserved the RNA in the tissue. First, total RNA was isolated using the Quiagen® RNeasy kit (Quiagen, Valencia, CA). The procedure used was a standard protocol (RNeasy Mini Handbook 2006). Then the optical density of the solution was read using the Nanodrop® 2000 Spectrophotometer (Thermo Scientific, Wilmington, DE). The RNA was labeled and stored at -80^{o}C. After isolation, the RNA was reverse transcribed to cDNA.

The real-time PCR was run on the cDNA (Platinum Q PCR Package Insert) with the ABI Prism 7500 (ABI, Applied Biosytems, Foster City, CA) using a *Taq*Man One-Step RT-PCR Master Mix Reagents Kit (ABI) according to the manufacturer's recommendation. Real-time reactions were carried out using pooled RNA samples for both 18S RNA and vascular endothelial growth factor-A (VEGF) RNA. The VEGF primer was designed with the forward sequence: CCACTTCATGGGCTTTCTGCT, and reverse sequence: CACTTGTACCTCCACCATGCCAAG.

The cDNA was loaded into a 96 well plate with the primers (25 µL total) and run on the ABI 7500. Three stages were set in the thermal profile (Stage 1: 1 repetition of 95^0C for 10 minutes, Stage 2: 40 repetitions of step 1: 95^0C for 15 seconds and step 2: 60^0C for 1 minute, Stage 3:1 repetition of 95^0C for 15 seconds, step 2: 60^0C for 1 minute, step 3: 95^0C for 15 seconds) provided fold changes (relative to 18S RNA and control samples). Values for VEGF were normalized to values obtained for 18S RNA in each sample and data were expressed relative to normalized values for controls.

5.7.3 Evans blue dye assessment for permeability

To assess the quantity of extravasated EBD, following experiment, half of the exposed site was removed via biopsy punch, placed on a paper towel for a few minutes to remove excess moisture, weighed and then placed in 100% formamide for 24 hours at 60^oC. This allowed the dye to come to equilibrium with the solution. After soaking in formalin for 24 hours, the supernatant's absorption was measured using the Nanodrop® 2000 spectrophotometer (Thermo Scientific, Wimington, DE) at 620 nm (Jancar et al. 1991). The weight was recorded such that extravasated EBD could be expressed as normalized to the weight of the extracted tissue (µg of EBD leaked per gram of tissue).

5.8 Statistical analysis

For the studies detailed herein, one-way, two-way, or N-way analysis of variance (ANOVA) in Matlab® was used to determine significance for the main effects and interactions. One-way, two-way and N-way ANOVA are special cases of the general linear model: $y = xb + \varepsilon$, where y is a matrix of the observations, x is a design matrix to indicate the independent variables that describe observations in terms of known variables b is a matrix containing estimated parameters, and ε is a matrix containing errors (random disturbances).

ANOVA was chosen because multiple settings were examined in each chapter (ie. acoustic pressure, DPE, [UCA]), where the overall question was: 'Are the fixed effects, parameter x, y, or z, significant for the response? (within the tested range)'; ANOVA is a robust test for statistical difference between two or more groups under the assumption that the sampled populations are normally distributed. ANOVA is useful for comparing two or more means without increasing the type I error (false positive). For all teststhe level of significance was set at $\alpha = 0.05$.

5.8.1 One-way ANOVA

One-way ANOVA is generally represented by:

$$y_{ij} = \alpha_j + \varepsilon_{ij} \tag{5.8}$$

where y_{ij} is a matrix of the observations that are the sum of α_j, a matrix of the group means, and ε_{ij}, a matrix of random disturbances. One-way ANOVA was used for EBD (at 0 DPE) and VEGF (at 5 DPE only) observations (assessments). For these assessments, only one variable, α_j: α_{EBD} or α_{VEGF}, was being tested for significance.

5.8.2 Two-way ANOVA

Two-way ANOVA is generally represented by:

$$y_{ijk} = \mu + \alpha_j + \beta_i + \gamma_{ij} + \varepsilon_{ijk} \tag{5.9}$$

where y_{ijk} is a matrix of the observations with row i, column j, and repetition index k, μ is a constant matrix of the overall mean, α_j is a matrix where the columns are the deviations of the observations attributable to a specific parameter, β_i is a matrix whose rows are the deviation of each observation attributable to a second specific parameter, γ_{ij} is a matrix of interactions, and ε_{ijk}, a matrix of random disturbances. Two-way ANOVA was used for the capillary density assessments, where α_j was DPE (0 or 5 DPE), and β_i was Pr, [UCA], ED, or PRF.

5.8.3 N-way ANOVA

The special case of N-way ANOVA was used only in Chapter 6 where a factorial design study was conducted. Three main effects were varied: DPE (α_j), [UCA] (β_i) , and Pr (γ_k) , and three assessments were made: capillary density ($y_{1,ijk}$), inflammation ($y_{2,ijk}$) and VEGF ($y_{3,ijk}$). N-way ANOVA, in this case was represented by:

$$y_{ijkl} = \mu + \alpha_j + \beta_i + \gamma_k + (\alpha\beta)_{ij} + (\alpha\gamma)_{ik} + (\beta\gamma)_{jk} + (\alpha\beta\gamma)_{ikj} + \varepsilon_{ijkl} \qquad (5.10)$$

where $(\alpha\beta)_{ij}$, $(\alpha\gamma)_{ik}$ and $(\beta\gamma)_{jk}$ are two-way interaction terms and $(\alpha\beta\gamma)_{ikj}$ is a three-way interaction term. Initially when the data is tested the full model is fit (ie. all terms and interactions are tested for significance). When higher order terms did not reach significance they were removed from the model, such that the most prudent representation could be used to explain the output variable *y*.

5.8.4 Follow-up tests

Because the results of ANOVA only determines if there is significance for a particular parameter or combinations of parameters (interactions), it is typically followed with additional tests to determine which groups are different from each other. For example, if parameter 'α_j' is found to be significant, it remains unknown whether α_1 is statistically different from α_2, α_3, … α_n or if all α_j statistically differ from one another. Multiple comparisons (ie. follow-up tests) were made with Tukey's honestly significant difference (Tukey-HSD) criterion. Tukey-HSD simultaneously tests pairwise comparisons for all α_j and identifies where the difference is significant. This test assumes normality, independence and equal variation. The test uses the q-statistic (based on the studentized range distribution), which is similar to the t-statistic, but accounts for experiment-wise type I error increases that occur with multiple testing. The q-statistic, q_s, is defined as:

$$q_s = \frac{Y_A - Y_B}{SE} \tag{5.11}$$

where Y_A is the larger of the two means being compared, and Y_B is the smaller of the two, SE is the standard error of the data. The value of q_s is then compared to a q-value from the studentized range distribution, and when $q_s > q_{critical}$, the means are significantly different.

For the factorial study presented in this thesis, in addition to Tukey-HSD, compound comparisons were made. In the case where main effects did not reach significance with ANOVA, two sets of groups, where one set had two or more groups were compared (e.g., compare average group means of 3 and 6 DPE with 0 DPE, or grouping Pr values into "low" and "high" and comparing low and high). Combining the data in this way minimized the number of test performed and reduced the number of terms in ANOVA.

CHAPTER 6: ULTRASOUND CONTRAST AGENTS AFFECT THE ANGIOGENIC RESPONSE

Microbubbles have been explored as a means of drug delivery in an effort to treat ischemia (Korpanty et al. 2005, Zen et al. 2006, Song et al. 2006). Studies have shown that US and UCAs induce neovascularization (Chappell et al. 2006, Miyake et al. 2007), arteriogenesis (Song et al. 2004, Chappell et al. 2008), and improve cardiac function (Song et al. 2008) in ischemic models. However, an equal amount of literature details the ability of US and UCAs to create damaging bioeffects to various tissues. US and UCAs have been documented to create undesired bioeffects including: premature ventricular contractions (MacRobbie et al. 1997), hemorrhage (Miller et al. 1998), capillary disruptions (Skyba et al. 1998), and lesions (Zachary et al. 2006) in normal animal models. Generally, bioeffects studies focus on 0-day effects in normal models, while methods to induce angiogenesis focus on 3-28 days after US exposure, typically with ischemic models. Acute (0-day) and effect days are rarely addressed in the same study. As such, little is known about the mechanism of US-UCA-induced angiogenesis.

One of the reasons for the disconnect between US's potential adverse biological effects and therapy is that there is a lack of understanding regarding mechanisms initiating the angiogenic response. As such, a wide range of US peak rarefactional pressures (Prs) has been used (Song et al. 2004, Barzelai et al. 2005, Leong-Poi et al. 2007, Song et al. 2008, Fuji et al. 2009) with no dose-effect examination of the therapy. A relatively low Pr (0.25 MPa) was demonstrated to induce an angiogenic response (Zen et al. 2006), but Fuji et al. (2009) found a much higher Pr (4.5 MPa) to be beneficial. When UCAs are used, Pr is the exposure quantity of particular importance because it affects the behavior of the UCA. As incident Pr increases, the UCA's behavior progresses from oscillation to eventual collapse (Marmottant et al. 2005, Ammi

et al. 2006b, King et al. 2010). The UCAs behavior may affect the vasculature and initiate a biological response (Nyborg et al. 1958, Elder et al. 1959).

Therefore, in an effort to connect the 0-day (day of exposure) bioeffects with subsequent therapeutic responses, this study sought to examine the role of the UCAs, and provide insight to the physical mechanism by which US-UCA interaction induces angiogenesis, via a dose-effect study on Pr. This study used either saline or a UCA concentration ([UCA]) of 5x, where 25% Definity® by volume was infused during bilateral exposures for infusion (see Chapter 5). Capillary density, inflammation and vascular endothelial growth factor (VEGF) were used to assess bioeffects and the subsequent angiogenic response at 0, 3 and 6 days post exposure (DPE). One hundred fifty female Sprague Dawley rats were used in this 3 x 4 x 2 factorial study examining DPE, Pr and infusion media. Six rats served as cage controls where no treatment was given; the remaining 144 rats were randomly assigned to one of 24 (3 x 4 x 2) groups with six rats per group. US exposure parameters were: Pr = 0.25, 0.83, 1.4, and 2.0 MPa, PRF = 10 Hz, PD = 10 μs, ED = 5 min.

6.1 Results

Capillary density (CD-31)

Normalized capillary density was determined with US exposures of 0.25, 0.83, 1.4 and 2.0 MPa at 0, 3 and 6 DPE for saline and UCA infusion, respectively (Figure 6.1). Statistical significance was not found with DPE or Pr for capillary density using N-way ANOVA. The general trends of the saline and UCA infused groups were similar; therefore as a further examination of capillary density, the data were grouped into low (0.25 and 0.83 MPa for both saline and UCA infusion) and high (1.4 and 2.0 MPa for both saline and UCA infusion) pressure groups (Figure 6.2). While two-way ANOVA determined that there was no significant

difference for the pressure groups, DPE was a significant parameter. Multiple comparisons showed that the low pressures' acute capillary density was not significantly different from the 3 and 6 DPE capillary density. However, significance is reached when comparing the high pressures' acute capillary density to the combined 3 and 6 DPE capillary densities ($p < 0.05$).

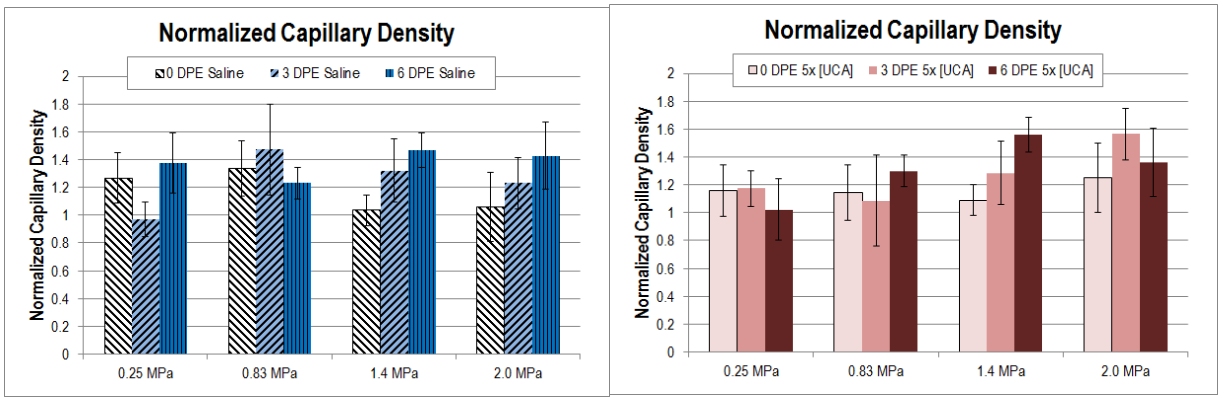

Figure 6.1: Normalized capillary density for exposures, saline (left) and UCA (right). The color darkens as DPE increases, with saline infusion in stripes, and UCA infusion in solids (Johnson et al. 2011)

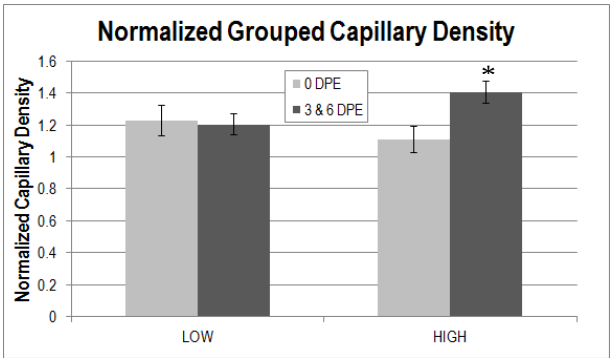

Figure 6.2: Grouped capillary density at low (025 and 0.83 MPa) and high (1.4 and 2.0 MPa) pressures, combining saline and UCA infused groups. * $p < 0.05$ with respect to HIGH 0 DPE.

Inflammation

The IHC slides were digitized and a program to analyze the presence of CD-31 from the images was generated in Matlab®. This program was designed to quantify the presence of the brown stain indicative of inflammation marked by CD-31 (Figure 6.3). The results were normalized to the cage control rats after raw percentages of inflammatory cells were gathered. The program was constructed to read in an image, and using RGB threshold values, highlight

only the pixels of interest. Visual examination of each image confirmed the approximate correctness of the program. The program then returned a percentage (of total pixels in the image, pixel size: 0.5 μm) of inflammatory cells with respect to the total image. This number was used to quantify the extent to which inflammation was occurring.

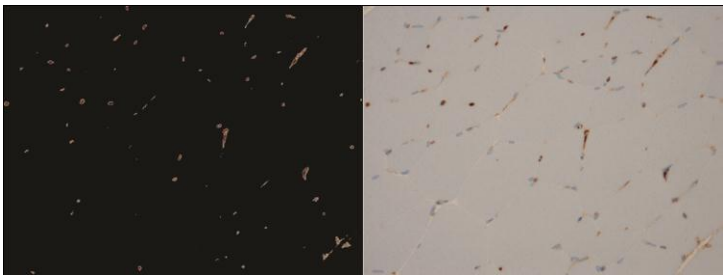

Figure 6.3: CD-31 quantification for inflammation analysis (Johnson et al. 2010).

Figure 6.4 shows the normalized inflammation at 0, 3 and 6 DPE for both saline and UCA-infused groups. Representative IHC images of inflammation are shown in Figures 6.5 and 6.6. In Figure 6.5 and 6.6, acute inflammation (0 DPE) images representing 0.25 to 2.0 MPa show minimal variation for saline and for UCA infusion.

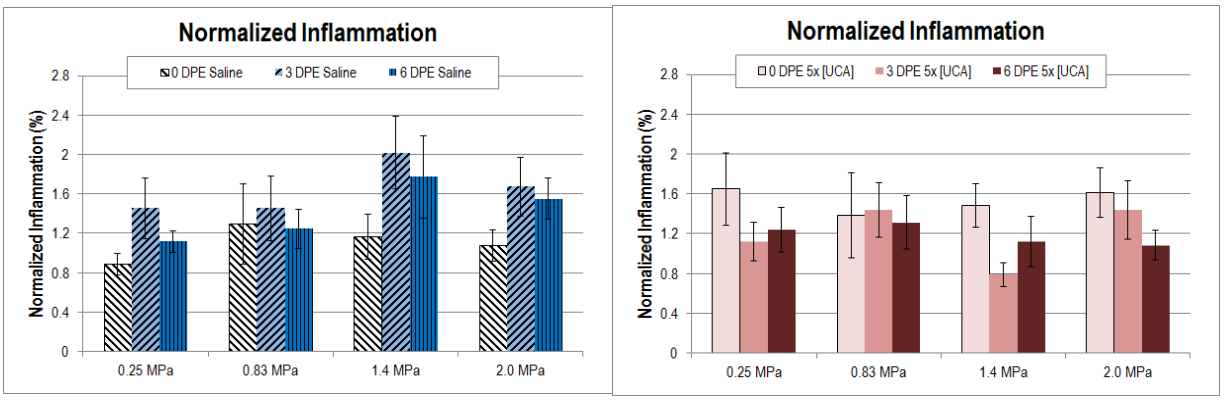

Figure 6.4: Normalized inflammation, saline (left) and UCA (right). The color darkens as DPE increases, with saline infusion in stripes, and UCA infusion in solids (Johnson et al. 2011).

US exposure caused an increase in inflammation with respect to the control. The inflammation did not demonstrate a trend across Pr for neither UCA nor saline-infused groups (Figure 6.3) using N-way ANOVA. DPE was found to be a significant parameter for the saline-infused group only.

Multiple comparisons showed the 3 DPE inflammation to be significantly higher than 0 DPE ($p < 0.02$); however the 3 and 6 DPE groups did not differ.

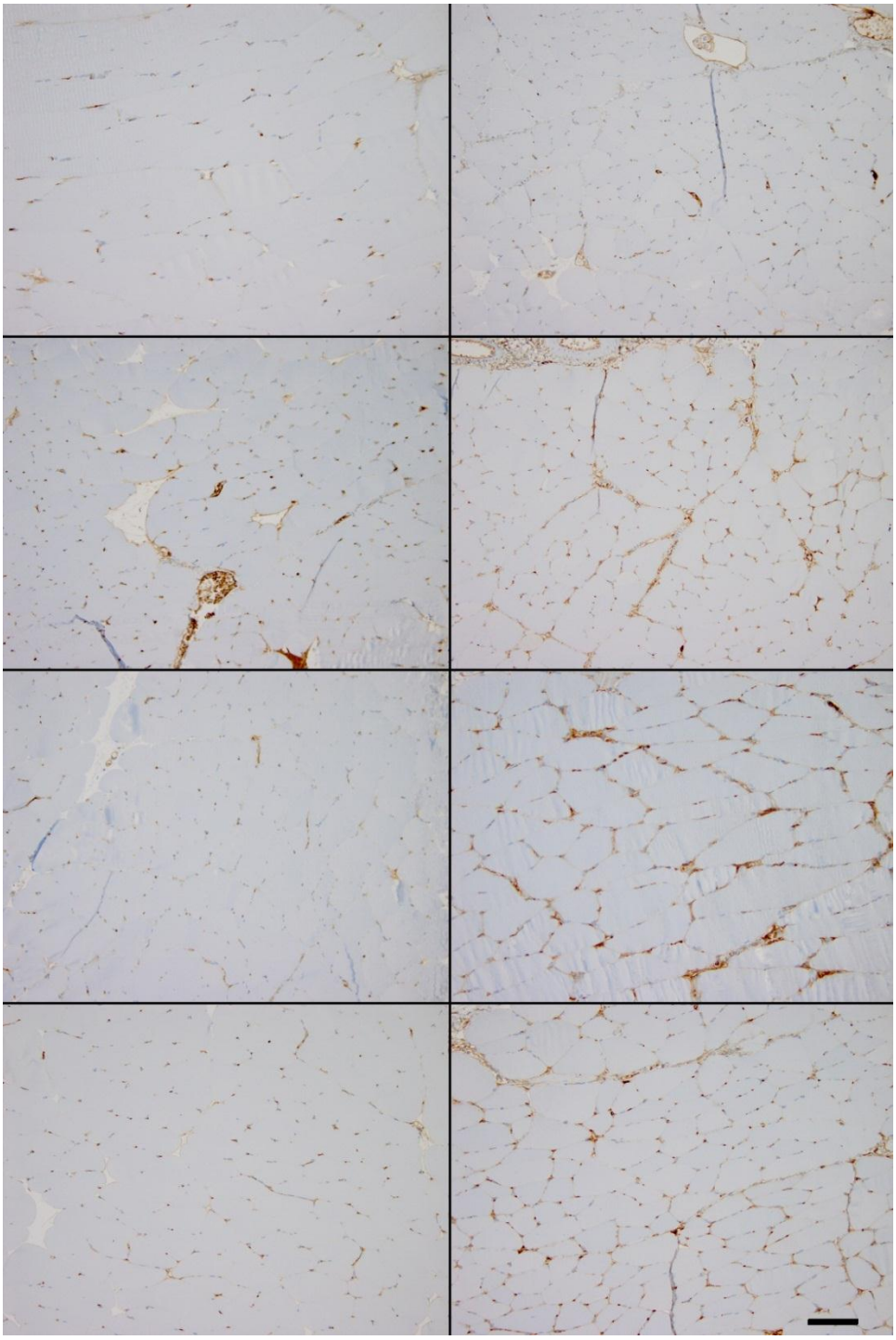

Figure 6.5: Representative images of exposed CD31 stained slides, saline. (Left) 0 DPE, (right) 6 DPE. Top to bottom for each column: 0.25, 0.83, 1.4 and 2.0 MPa, respectively. Bar = 100 μm (Johnson et al. 2011).

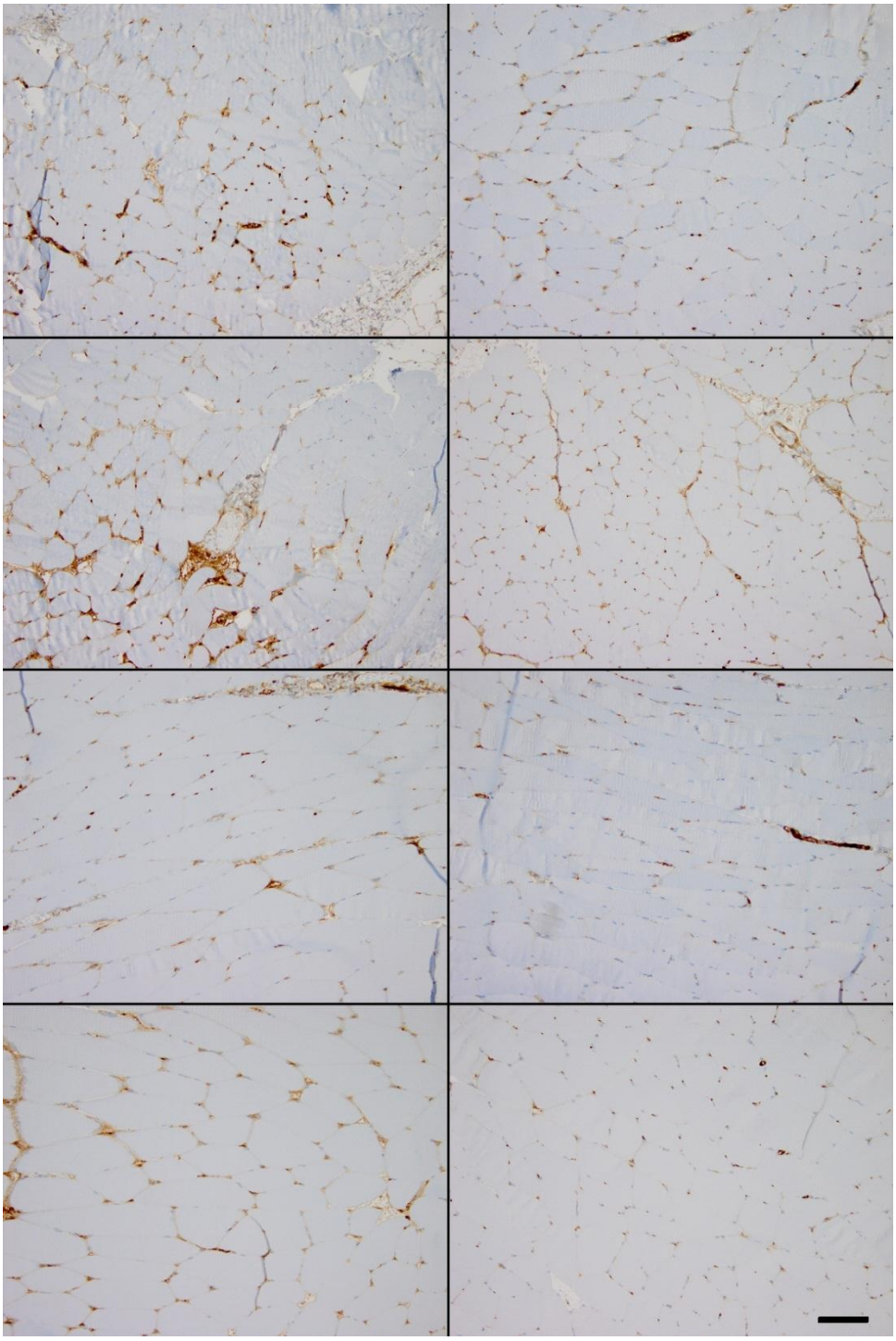

Figure 6.6: Representative images of exposed CD31 stained slides, UCA. (Left) 0 DPE, (right) 6 DPE. Top to bottom for each column: 0.25, 0.83, 1.4 and 2.0 MPa, respectively. Bar = 100 μm (Johnson et al. 2011).

Vascular endothelial growth factor-A (VEGF)

VEGF expression is shown in Figure 6.7 in terms of fold change. Using N-way ANOVA for the saline-infused animals, DPE was significant for VEGF ($p < 0.001$). The 0 DPE mean value of VEGF increases with pressure, but neither 3 nor 6 DPE were significantly different from the control.

N-way ANOVA determined that both Pr and DPE were significant for VEGF when UCAs are used ($p < 0.01$ and $p < 0.001$, respectively). Multiple comparisons determined that the Pr of 2.0 MPa at 0 DPE was significantly different from the control and other pressure settings, indicating a pressure dependency ($p < 0.05$). 0 DPE was not significantly different from 3 DPE; however 6 DPE was significantly lower than 0 or 3 DPE ($p < 0.05$).

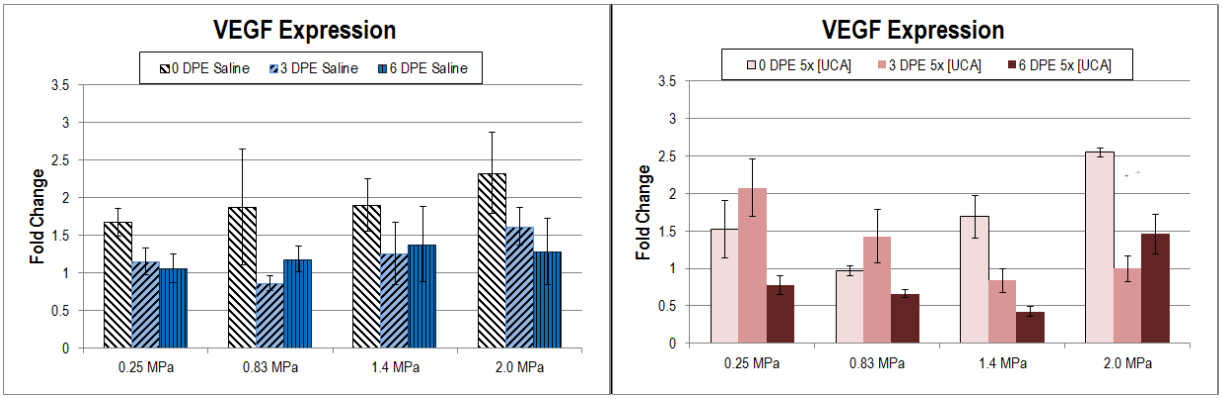

Figure 6.7: Relative VEGF expression for exposures, saline (left) and UCA (right). The color darkens as DPE increases, with saline infusion in stripes, and UCA infusion in solids (Johnson et al. 2011).

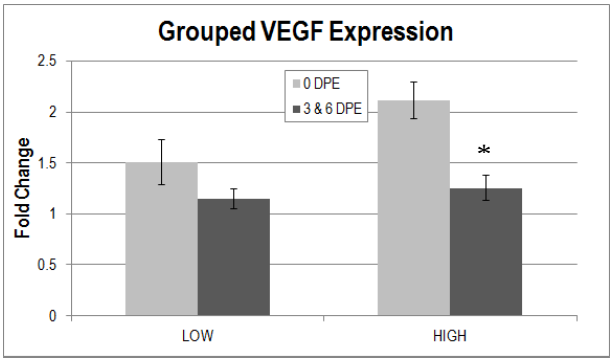

Figure 6.8: Grouped VEGF expression at low (025 and 0.83 MPa) and high (1.4 and 2.0 MPa) pressures, combining saline and UCA infused groups.* $p < 0.05$ with respect to HIGH 0 DPE.

Because both saline and UCA infused groups demonstrated a general trend of acute increase in VEGF expression followed by a decrease at 3 and 6 DPE, the data were grouped for a macroscopic view of the Pr effect of US exposure (Figure 6.8). Like capillary density, the high pressures' acute capillary density was significantly different from the combined 3 and 6 DPE capillary densities ($p < 0.05$).

6.2 Discussion

The intent herein was to ensure that excessive damage did not occur acutely, but also to elicit an angiogenic response such that the mechanism could be explored. With information concerning the mechanism of ultrasound-induced angiogenesis, current treatments can be improved, optimized, or assessed for use in a particular situation.

This study used a range of pressures and three measurements (capillary density, inflammation and VEGF) to explore if US and/or US-UCA interactions could be used to induce an angiogenic effect. The results showed that the angiogenic response was dependent upon infusion media, incident Pr and DPE. The data also suggested that collapse of UCAs resulted in higher acute VEGF expression.

It was expected that as Pr increased the acute capillary density, inflammation and VEGF would decrease, and there would be a subsequent rebound as DPE increased as seen in previous findings (Johnson et al. 2010). Literature supports that there is possibly a range of Prs that may result in beneficial therapy. US pressures ranging from 40kPa to 5 MPa (at a US frequency of 1 MHz) have been used to stimulate healing in varicose ulcers, induce angiogenesis, and treat ischemia both with and without the use of UCAs (Dyson et al. 1976, Hogan et al. 1982, Korpanty et al. 2005, Barzelai et al. 2005, Chappell et al. 2006, Chappell et al. 2008, Fuji et al. 2009).

Ultrasound bioeffects

It is generally assumed that the therapeutic benefits of ultrasound are initiated by damage—as a result of inertial cavitation or cellular changes via mechanical perturbation (Gormley et al. 1998, Leong-Poi et al. 2007, Chappell et al. 2008, Johnson et al. 2010). These effects may or may not result in tissue level damage. Research shows that ultrasound can induce petechiae *in vivo* without tissue destruction (Miller et al. 1998). For this study, to assess US bioeffects the saline infused group was used. For this group, a rise in VEGF and inflammation was expected to occur prior to any increase in capillary density as seen in the literature (Bates et al. 2003, Chappell et al. 2006, Mariotti et al. 2006). Analysis of this study agreed with VEGF appearing with exposure to US, and inflammation increasing above the control. The acute VEGF increase suggests that US exposure activated the expression of VEGF to initiate an angiogenic response by increasing vascular permeability (as discussed in Chapter 2). US caused inflammation that demonstrated an onset peaking at 3 DPE. The 3 DPE peak of inflammation was not unexpected as angiogenesis is known to involve both early and late stage inflammation (Bates et al. 2003).

Ultrasound contrast agents

UCAs increase the potential for damage by introducing cavitational bodies intravascularly. While the general progression of angiogenic response elicited from US-UCA was similar to US-saline, the UCA group demonstrated acute inflammation that possibly occurs due to the increased level of vascular perturbation. For therapeutic applications, typically, UCA concentrations have exceeded the standard recommendations for imaging (Chappell et al. 2006, Chappell et al. 2008, Fuji et al. 2009). For bioeffect and therapy, however, [UCA]s range from 0 to 60% UCA by volume. With greater [UCA] the likelihood for damage is presumably

increased, due to the presence of clouds of bubbles undergoing a range of dynamic behavior. To minimize damaging effects, this study used a relatively low concentration of UCAs (~ 25% Definity® by volume).

Interestingly, when UCAs are used, Pr is one of the most relevant parameters for determining bubble dynamics. UCAs progress from oscillation to collapse with increasing Pr. In separate *in vitro* experiments, this lab determined that the 5% collapse pressure threshold of Definity® occurs at approximately 0.2 MPa (King et al. 2010). The occurrence rises to 50% at approximately 0.5 MPa, and 100% of bubbles exposed to US collapse at about 1.0 MPa with oscillation co-occurrence (King et al. 2010). Thus the range of Prs chosen for this experiment was from 5% to 100% collapse occurrence with exposure to US.

In this study, 0.25 MPa represents a predominantly oscillation inducing pressure. As Pr increases, UCAs slowly expand and rapidly contract resulting in collapse and shell fragmentation (Pr = 0.83, 1.4 and 2.0 MPa). This collapse potentially damages the vascular endothelium and surrounding tissue. In this study, there was no decrease in acute capillary density as seen previously (Johnson et al. 2010) signifying that the vascular endothelium was not ruptured. These data show that oscillation (at 0.25 MPa) causes a change in the VEGF expression possibly due to continual local hemodynamic disturbance (Figure 6.7). As Pr increases, collapse eliminates the constant oscillatory disturbance in the US beam focus, but infusion replenishes the UCAs. While locally circulating red blood cells may be damaged the vessel lumen remains intact as determined by acute capillary density (Figure 6.1 and 6.2). Because capillary density does not decrease acutely with exposure to US and UCA, the increased VEGF expression seems to be mechanical, not damage induced. Inflammation did appear acutely for Prs above 0.25 MPa, which suggests some level of perturbation to the vascular endothelium and/or exposed

muscle, further indicating that the angiogenic response is, in part, influenced by collapse of UCAs.

US-UCA-induced angiogenesis

The expression of VEGF was demonstrated to occur *in vitro* (Reher et al. 1999) and *in vivo* (Barzelai et al. 2005) after exposure to US which agrees with the findings in this study. One of the proposed mechanisms underlying US exposure and vascular growth relates to the induction of local hypoxia and inducing VEGF expression (Barzelai et al. 2005). This reinforces the possibility of the mechanical effect inducing VEGF. US and UCAs seem to disturb the normal state, and this disturbance caused an increase in VEGF expression both in this study and others (Barzelai et al. 2005, Chappell et al. 2006). This study displayed higher fold changes in VEGF for all pressures explored when compared to previous findings in an ischemic model (Barzelai et al. 2005).

Heating as a possible mechanism

Ultrasound induced heating has also been documented to provide some therapeutic benefit (Draper et al. 2010). The maximum change in temperature can be approximated with $\Delta T_{max} = (\dot{Q}\,\Delta t)/C_v$, where Δt is the exposure duration (for a single pulse, ED is 10 μs), C_v is the medium's heat capacity per unit volume (4.18 J/cm^3-˚C for biological tissue) and $\dot{Q}$ is the rate of heat generation per unit volume (Fry et al. 1953, Cavicchi et al. 1984, O'Brien et al. 2007). For this study, ΔT_{max} was calculated to be 0.95^0C, for the 2.0 MPa exposure. This approximation assumes no heat removal, which is not necessarily the case for a 5 minute exposure. Further, thermal therapy frequently requires repeated exposures of continuous ultrasound (Usuba et al. 2006, Draper et al. 2010), whereas one-time pulsed US was used herein. Thus, it is reasonable to assume that heating is not a significant biophysical mechanism for the results noted herein.

Previously published work conducted in this lab used the same [UCA], but a pressure that was approximately double the maximum Pr used in this study (Johnson et al. 2010). Unlike the damage seen in previous work, this study supports that a mechanical effect elicits the angiogenic response and with the introduction of UCAs there is more variation in such effects. It should be noted that the literature has, to date, reported only effects seen days after treatment, with no investigation of connections between exposure and angiogenesis. If we remove 0 and 3 DPE from this dataset, we find that capillary density and inflammation are statistically different from the control for all measured endpoints. The results of this study raises mechanistic questions for other US-UCA induced angiogenesis studies.

This chapter took a large-scale study to determine if trends could be discerned based upon Pr, DPE, and infusion media. UCAs were determined to affect the induction of the angiogenic response with US exposure, with increased capillary density (combined 3&6 DPE data), acute inflammation and VEGF expression. Because a large amount of comparisons were made for this factorial study, subtle effects did not reach significance. However, based upon inflammation, and macroscopic examination of VEGF expression and capillary density, there exists a relationship between Pr, the biological effect and the angiogenic response. Acute inflammation increases for the UCA group suggests that the presence of UCAs play a role in US-UCA induced bioeffects and therapy but the extent to which UCAs affect the response is unclear from this study. The next chapter uses a smaller scale study to examine the [UCA] in an effort to better understand the role of UCAs.

CHAPTER 7: THE ANGIOGENIC RESPONSE IS DEPENDENT ON ULTRASOUND CONTRAST AGENT CONCENTRATION

There are presently three scenarios for which proangiogenic therapies are used clinically: chronic wounds, peripheral arterial disease and ischemic heart disease (Li et al. 2004, Li et al. 2005), where the goal is to create neovascularization to promote healing. The main drawbacks for current drug, surgical, and cell-based therapies are the diffuse spread of growth factors, invasiveness, or the inability to provide spatially specific treatment. US and UCAs have been shown to provide noninvasive and spatially specific treatment, resulting in an angiogenic response to exposure (Johnson et al. 2010).

Several studies report a reparative response to US and UCA exposure (Chappell et al. 2005, Hwang et al. 2005, Korpanty et al. 2005, Miyake et al. 2007, Song et al. 2008, Bohmer et al. 2010). While there is a body of literature that seems to show efficacy, there is a great deal of conflicting results, perhaps because there is a lack of mechanistic exploration. The previous chapter detailed how UCAs affect the angiogenic response by increasing expressed vascular endothelial growth factor (VEGF), inflammation and capillary density at higher Prs. In that study, however, the difference between the controls and exposed groups were significant, but subtle, possibly due to the relatively low UCA concentration ([UCA]). Current diagnostic recommendations for imaging are up to twenty times lower than concentrations used in therapeutic studies, with a wide range of [UCA]s represented in the literature (Johnson et al. 2011, Zen et al. 2006, Chappell et al. 2008, Miller et al. 2009).

Therefore, to further understand the US and UCA therapy to induce angiogenesis, [UCA] has been explored. [UCA] is of particular interest because, as alluded to previously, increasing the [UCA] increases the number of potential cavitating bodies and the opportunity for bubble-bubble and bubble-vascular interaction. It is, presumably, these interactions that facilitate US

and UCA's therapeutic effects. A major impediment for progress to clinical applicability is the lack of understanding of the mechanisms that connect US and UCA to the angiogenesis response, and bioeffects to subsequent angiogenesis. Therefore, in an effort to understand the mechanism and characterize the angiogenic response, [UCA] was explored in this study both at 0 days post exposure (DPE) and at 5 DPE. This chapter explores the acute effects (0 DPE) in terms of capillary density and Evans blue dye (EBD) as a marker for vascular permeability (as opposed to acute VEGF expression that was used in Chapter 6). EBD was used because it can be instantaneously visualized and VEGF expression for increased permeability is not well documented with this procedure. In addition, this study does not assess inflammation. Though inflammation reached statistical significance in the previous chapter, a 2% increase from the control is not readily extrapolated to biological significance. Instead H&E was used to determine if inflammation had occurred via the presence of inflammatory infiltrates. Damage was also assessed via hemorrhage necrosis and changes in capillary density. For the 5 DPE angiogenic responses, both capillary density and VEGF expression were explored.

Using twenty-eight rats four separate [UCA]s were explored: 0x, 1x, 5x, and 10x [UCA] for both 0 and 5 DPE. At 0 DPE there was an n = 4 per [UCA]; at 5 DPE there was an n = 3 per [UCA]. The 1.5 mL infused solution contained 0, 0.07, 0.25 and 0.75 mL of Definity® for 0x, 1x, 5x, and 10x [UCA] respectively. US exposure parameters were: Pr = 0.7 MPa, f = 1 MHz, PD = 10 μs, PRF = 10 Hz, and ED = 5 min. EBD was used only for acute exposures as it has been documented to interfere with regenerating vasculature (Jackieqciz et al. 1998). Bilateral sites on the lateral sides of the left and right gracilis muscles were exposed and the medial site served as the control.

7.1 Results

Capillary density (CD-31)

Capillary density was normalized to the medial-site control value. Two-way ANOVA determined that DPE was not a significant parameter for capillary density ($p > 0.05$), however, significance was found for [UCA] ($p < 0.05$); suggesting a change in capillary density with increased [UCA] (Figure 7.1). The interaction term, DPE* [UCA] was not significant ($p > 0.05$). Multiple comparisons between 0 DPE and 5 DPE found, the capillary density to be significantly different at 10x [UCA] ($p < 0.05$).

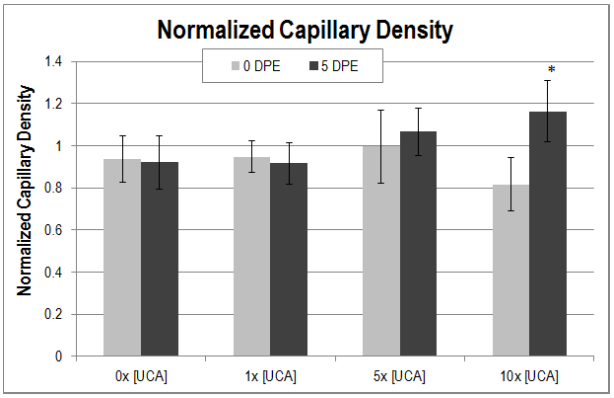

Figure 7.1: Normalized capillary density at various [UCA]s.* $p < 0.05$ with respect to 0 DPE at 10x [UCA]

Histological assessment (H&E and CD-31)

Tissue-level effects for 0 DPE demonstrated signs of capillary engorgement at 10x [UCA]. No tissue damage, inflammatory infiltrate or necrosis was observed at any of the UCA concentrations (Figure 7.2).

Evans blue dye (vascular permeability)

EBD leakage as a measurement of vascular permeability was also normalized to the medial-site control. One-way ANOVA was used to determine that [UCA] was a significant parameter for EBD leakage ($p < 0.001$) (Figure 7.3). The medial-site control samples were not significantly different from the saline-infused (0x [UCA]) rats ($p > 0.05$). EBD leakage demonstrated an increasing trend of permeability as the [UCA] increased, with 1x [UCA] and 5x

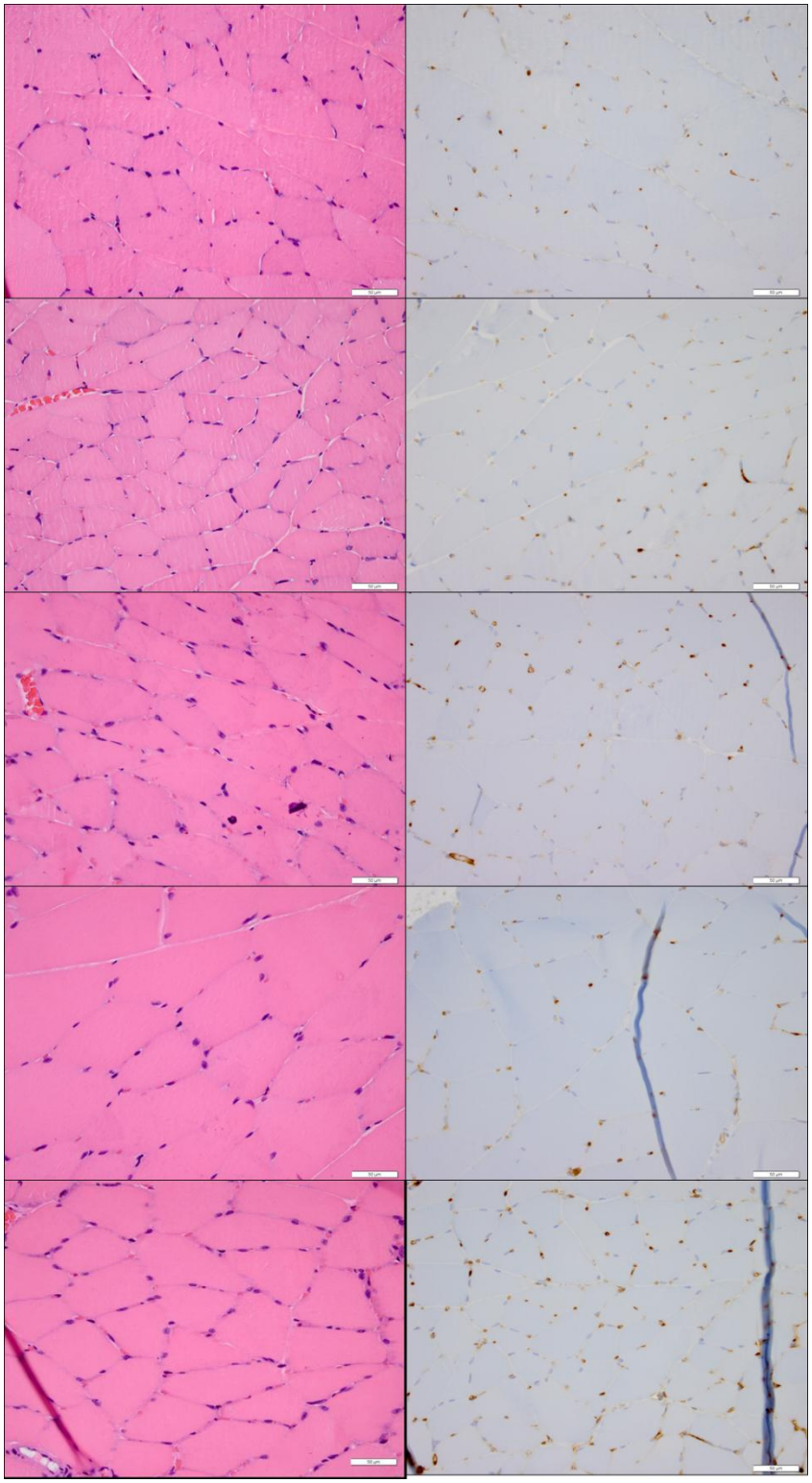

Figure 7.2: Acute histology, H&E (left) and CD31 (right) demonstrating the lack of tissue level effects associated with US-UCA exposure for various [UCA] at 40x magnification. Top to bottom: medial-site control, saline (0x [UCA]), 1x, 5x, and 10x [UCA]. Bar = 50 µm.

[UCA] being near the control value for the assessment (Figure 7.3). Multiple comparisons between UCA concentrations determined that 1x, 5x and 10x [UCA] were significantly different from 0x [UCA] ($p < 0.05$). 10x [UCA] was significantly different from 1x and 5x [UCA] ($p < 0.05$).

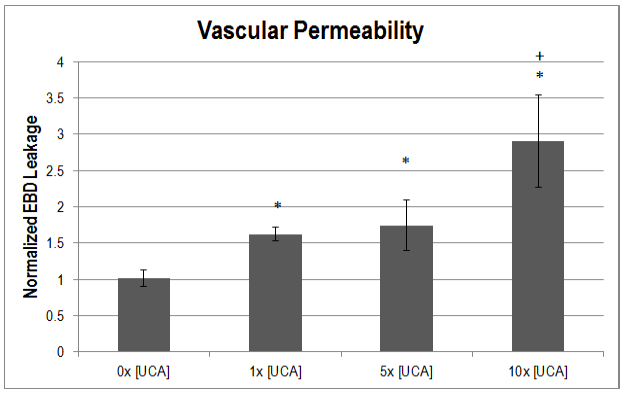

Figure 7.3: Normalized EBD leakage indicating vascular permeability at varying [UCA]. *$p < 0.05$ with respect to the control and 0x, + $p < 0.05$ with respect to 1x. The medial-site control EBD leakage was 8.8 µg/g.

Vascular endothelial growth factor-A (VEGF)

To supplement capillary density, VEGF expression was measured to assess the angiogenic response. One-way ANOVA was used to determine if [UCA] was a significant parameter for VEGF expression ($p < 0.001$). Lower [UCA]s showed less than half the VEGF expression seen at 10x [UCA] (Figure 7.4). Multiple comparisons between [UCA]s indicated that 1x, 5x and 10x [UCA] were significantly different from 0x [UCA] ($p < 0.05$). 10x [UCA] was also significantly different from 1x and 5x [UCA] ($p < 0.05$).

7.2 Discussion

The objective of this study was to determine the effect, if any, of [UCA] on the angiogenic response induced by US and UCA. Further, this study examined the acute bioeffects

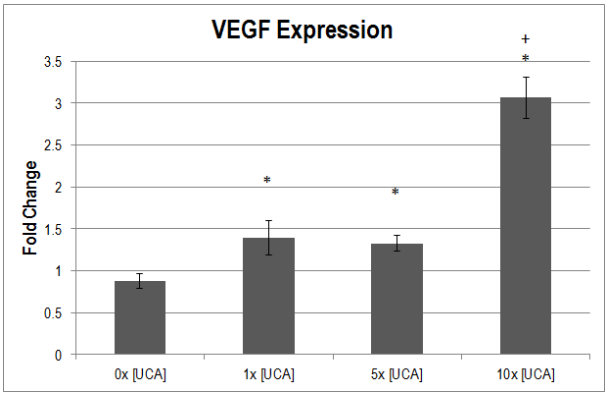

Figure 7.4: Relative VEGF expression (in fold change) at various [UCA]s. * $p < 0.05$ with respect to 0x [UCA], + $p < 0.05$ with respect to 1x, 5x [UCA].

in an effort to provide biological mechanistic clues leading to the angiogenic response. US exposure parameters were chosen to reduce the thermal effects, with an estimated maximal temperature increase of 0.5^{o}C (Fry et al. 1953), assuming no heat removal, which is not necessarily the case for a 5 minute exposure duration. The previous chapter demonstrated that at 5x [UCA] only subtle significant differences existed with respect to the saline control with VEGF expression assessment and up to a 2% increase in inflammation, without inflammatory infiltrate. This study demonstrated that [UCA] is an important determinant of not only bioeffects, but also angiogenic responses.

Understanding the role of [UCA] is important for understanding the mechanism of US and UCA therapeutic applications. In US-induced angiogenic therapy, typically, [UCA]s have exceeded the standard recommendations for imaging (Chappell et al. 2006, 2008, Fuji et al. 2009). US and UCA therapy in the literature use [UCA]s ranging from 0 to 60% UCA by volume of solution (0 to 16x [UCA]) (Chappell et al. 2006, 2008, Bohmer et al. 2010, Zen et al. 2006, Miller et al. 2009). Variability in the dosages (some [UCA]s are not reported) and differing delivery methods (ie. bolus or infusion) make it difficult to extrapolate the results to new applications (Hwang et al. 2005, Bohmer et al. 2010, Zen et al. 2006 Miller et al. 2007). The [UCA] range chosen was scaled to ensure animal survival. Chappell et al. (2006) found that

animal death occurred once the infusion concentration reached 2.5 x 10^7 microbubbles/min in mice (estimated to be 3.3 x 10^9 in rats); this information was used to determine the upper [UCA] limit.

One must note that increasing [UCA] to significantly high doses may also cause excess bioeffects to occur. 'Excess bioeffects' is defined here as a reduction in acute (0 DPE) capillary density or tissue-level changes. One study showed that an estimated dosage of 3.2 x 10^{10} microbubbles/min (an equivalent of 16x [UCA] with the parameters used in this study) injured rat cardiomyocytes but recovery from injury was not explored (Miller et al. 2005). Another study demonstrated that after a 'sufficiently' high dose of UCAs was used in mice, increasing that dose did not change the response (Chappell et al. 2006).

To study the bioeffects of US, EBD is frequently used. Research has shown that US and UCAs cause vessel leakage (Bohmer et al. 2010, Miller et al. 2000, 2007, Zachary et al. 2006, Shang et al. 2011). Microvascular effects have been shown to increase with increasing UCA dosage (Miller et al. 2007), which agrees with the findings herein (Figure 7.3). It has been speculated that US and UCAs increase vascular permeability by destabilizing the tight junctions associated with blood vessels, showing increased permeability up to 9 hours after exposure (Shang et al. 2011). Focused US, along with lipid shelled UCAs has been shown to increase EBD extravasation in muscle with as much as 8% of the total injected dose leaking at the exposed site (Bohmer et al. 2010). It was also noted that microvascular leakage may be reversible (Miller et al. 2007). As such, the role of [UCA] in inducing this acute bioeffect was assessed as a potential motivating factor for an angiogenic response.

VEGF, like US application, is known to play a role in increasing vascular permeability. However, at 10x [UCA], EBD leakage was observed under 1 min after the start of the exposure,

which is insufficient time for increases in VEGF expression (Bates et al. 2003). Typically VEGF peaks 3 to 7 days after injury in wound healing (Bates et al. 2003), though minimal increases may be captured in as little as 10 hours as seen in Chapter 6. US-UCA could acutely increase VEGF through shear stress inducible pathways (via biological signal transduction) and this increase in VEGF could be responsible for increased permeability, it could be purely mechanical (physical effect of UCA motion), or both.

Several studies suggest that therapy is bioeffect driven—as a result of high Prs inducing thermal or mechanical (UCA destruction) perturbations to the vasculature (Gormley et al. 1998, Leong-Poi et al. 2007, Chappell et al. 2008). The angiogenic response did not result from tissue level changes in this study, however. Although UCAs increase the potential for bioeffects by introducing cavitation bodies intravascularly, the Pr used herein was chosen to reduce the incidence of UCA collapse such that excess bioeffects were not caused. The 0 DPE capillary density did not significantly change with [UCA] (Figure 7.1), nor were there any biologically significant signs of hemorrhage, inflammation, or necrosis after exposure (Figure 7.2). The lack of acute effects suggest that the increased vascular permeability was the result of US-UCA mechanical interactions with the vascular ECs which lead to either increased porosity or increased size of pores between ECs.

The assumption is that US-UCA exposure leads to increased microvascular permeability which induces vascular remodeling (Chappell et al. 2006, Bohmer et al. 2010). While locally circulating cells may be damaged, the vessel lumen remains intact as demonstrated by capillary density assessments at 0 DPE (Figure 7.1). Because this study sought to understand the role of [UCA] in the context of angiogenesis, recovery from the perturbed state with signs of benefit

was of importance. Capillary density (at 5 DPE) and VEGF expression were used to assess recovery in the context of an angiogenic response.

Capillary density assessed at 5 DPE showed a significant difference with respect to 0 DPE for the 10x [UCA] (Figure 7.1), supporting the notion that sufficient increases in permeability could motivate an angiogenic response. In agreement with this study, when gene transfer was used with US and UCA exposure, the therapy caused an increase in capillary density (Taniyama et al. 2002). Others have measured significant increases in angiogenic related events such as: vascular density, arteriogenesis, or tissue perfusion (Chappell et al. 2006, 2008, Miyake et al. 2007, Song et al. 2004).

VEGF is known to have a vital role in angiogenesis, thus was measured in this study (Bates et al. 2003, Mariotti et al. 2006, Medinger et al. 2010). There has been very limited research on the induction of VEGF with US and UCAs; the expression of VEGF was demonstrated to occur *in vitro* (Reher et al. 1999, Doan et al. 1999) and *in vivo* (Barzelai et al. 2006) after exposure to US which agrees with the findings in this study. This reinforces the possibility of the acute mechanical effect inducing VEGF and causing an increase in the angiogenic response seen in Figures 7.1 and 7.4. In normal wound healing associated angiogenesis, changes in vascular permeability occur prior to increased VEGF expression (Song et al. 2004, Mariotti et al. 2006). Under normal conditions, blood vessels are at steady state, where vascular endothelial cell proliferation equals that of cell death and VEGF levels remain nominal (Cherwek et al. 2000). This study demonstrates an offset of that balance owing to increased VEGF and, as mentioned earlier, a higher capillary densities for 10x [UCA] at 5 DPE (Figures 7.1 and 7.4). This further suggests a mechanical dependence of VEGF stimulation through permeability perturbation, not by tissue damage (Figure 7.2).

Chapter 6 used a 5x [UCA] to study the angiogenic effect and that study supported that a mechanical effect elicits the angiogenic response and that the introduction of UCAs disturbs the effects. Using the same experimental setup, this study extended previous work by examining the concentration. The findings in this chapter at 5x [UCA] are in agreement with those seen in the previous chapter. In Chapter 6, VEGF acutely peaked, which was indicative of increased vascular permeability. This chapter also found increases in vascular permeability at 5x [UCA]. Both studies showed no change in capillary density at 0 DPE or 5 DPE, but this chapter demonstrated that [UCA] may have been the reason why significance was not reached in Chapter 6. VEGF levels peaked at 5 DPE for this study which agrees with the progression for wound healing. So, [UCA] determines the angiogenic pathway utilized—where no or low [UCA]s stimulates VEGF acutely and high [UCA] causes it to peak later (at 5 DPE). This peak at 5 DPE is possibly because it uses shear stress factor activation to increase VEGF expression as shown in Figure 4.1. Also this study found VEGF expression to be about the same as in Figure 6.8 for the low Pr group at the angiogenic response day of assessment.

This chapter demonstrated that [UCA] has a significant effect not only in the acute bioeffects, but also in the subsequent angiogenic response. The response for both acute bioeffects and angiogenic response are positively correlated with the infused [UCA]. Beginning with a suggested mechanically induced increase in permeability, up to a 20% increase in capillary density and a 3 fold change in VEGF expression was found. Because the [UCA] was strongly correlated with the acute bioeffects and the angiogenic response, and [UCA]s less than 10x [UCA] demonstrated only subtle effects with respect to the control, Pr should be reinvestigated at higher [UCA].

Mechanistically, the data from Chapter 6 and this study suggest that UCAs enhance bioeffects and that increasing the [UCA] enhances the angiogenic response. Because Chapter 6 demonstrated an increase in capillary density (5 DPE) and VEGF expression with higher Prs at relatively low [UCA], and this chapter showed that at relatively low Pr, higher [UCA] yielded increases in capillary density (5 DPE) and VEGF expression, there appears to be a trade off with respect to US-UCA induced angiogenesis. The next chapter details the reinvestigation of Pr at 10x [UCA] and comments on the differences between 1x, 5x, and 10x [UCA] for a Pr range representative of linear oscillation, nonlinear oscillation and collapse.

CHAPTER 8: THE ULTRASOUND AND ULTRASOUND CONTRAST AGENT CONCENTRATION'S INDUCED ANGIOGENIC RESPONSE IS PRESSURE DEPENDENT

Though the concept of US and UCA induced wound-healing has existed for over three decades (Dyson et al. 1968, Hogan et al. 1982), there has been no established protocol for the usage of US-UCA induced angiogenesis.

Chapters 6 and 7 showed that UCAs affect the angiogenic response, and that UCA concentration ([UCA]) influence both the bioeffects and subsequent therapy associated with US-UCA induced angiogenesis, which agrees with other literature (Miller et al. 1998c, 2007, Chappell et al. 2006, Johnson et al. 2011, in press (Chapter 6), Johnson et al. 2011, submitted (Chapter 7)). In addition, Pr seems to be related to the angiogenic response from the range of pressures used and the consequent variation in effects. US Prs have ranged from 0.18 to 4.5 MPa in the effort to treat ischemia with UCAs (Zen et al. 2006, Chappell et al. 2006, Fuji et al. 2009, Johnson et al. 2010).

Because UCAs behavior varies with the applied Pr, understanding how the microbubbles interact with US (and the vasculature) to produce an effect is of particular interest. While Pr was varied in previous studies (Dalecki et al. 2000, Song et al. 2002, Johnson et al. 2011, in press (Chapter 6)), this study seeks to revisit the angiogenic response with Prs that range from atmospheric pressure (ie. 100 kPa) to a Pr that fits within the FDA-regulated mechanical index of 1.9 (AIUM/NEMA 1998, ODS 1998, NEMA 2009a, 2009b). In addition, since previous findings demonstrated that low [UCA] produces an angiogenic response within the noise range of detection, this study sought to reinvestigate Pr using a higher [UCA]. After 10x [UCA] was explored, the [UCA] was reduced to 1x and 5x, and Pr reassessed for the angiogenic responses at 5 DPE.

Using forty female Sprague Dawley rats, Pr was explored at 10x [UCA]. For both 0 and 5 DPE there was an n = 4 rats per Pr. The infused solution contained 0.75 mL Definity® brought up to 1.5 mL with saline. US parameters included Pr = 0.1, 0.7, 1.3 and 1.9 MPa, f = 1 MHz, PRF = 10 Hz, PD = 10 μs, and ED = 5 min. Following the 10 x [UCA] study, 1x and 5x [UCA] was investigated for the angiogenic response to determine the significance of the interaction term Pr X [UCA]. This follow up study used nineteen rats to assess 0.7, 1.3 and 1.9 MPa for VEGF expression and capillary density at 5 DPE. For both studies bilateral sites on the lateral side of the left and right gracilis muscles was exposed and the medial site served as the control.

8.1 Results

Capillary density

Capillary density was measured as capillaries per square millimeter; the values were normalized and results are presented in Figure 8.1. Two-way ANOVA determined that DPE, Pr and DPR*Pr were significant parameters for capillary density ($p < 0.01$) (Figure 8.1). Multiple comparisons showed that 0.1 MPa was not significantly different from the control ($p < 0.001$), but 0.7, 1.3, and 1.9 MPa were significantly different from 0.1 MPa ($p < 0.001$) at 5 DPE.

A trend was noticed at 10x [UCA] with Pr at 5 DPE, therefore the [UCA] was lowered to 1x and 5x [UCA] to further explore the relationship between Pr, [UCA] and the angiogenic response (Table 8.1). Because no effect was seen at 0.1 MPa for the highest concentration (10x [UCA]), this Pr was excluded from the assessment.

Table 8.1 shows the 5 DPE normalized capillary density $\pm$ SEM. The table shows that the 5 DPE capillary density tends to increase with increasing pressure at 1x [UCA], however, as the [UCA] increases the capillary density first increases with respect to the control, but then decreases at high Pr. Multiple comparisons showed that at 5x [UCA] capillary density was not

significant across Pr. When Pr is low, an increase in capillary density with increasing [UCA] is noted, however increasing Pr to 1.3 MPa does not impact the capillary density with varying [UCA]. At the highest Pr setting, there is a distinct separation in capillary density with [UCA].

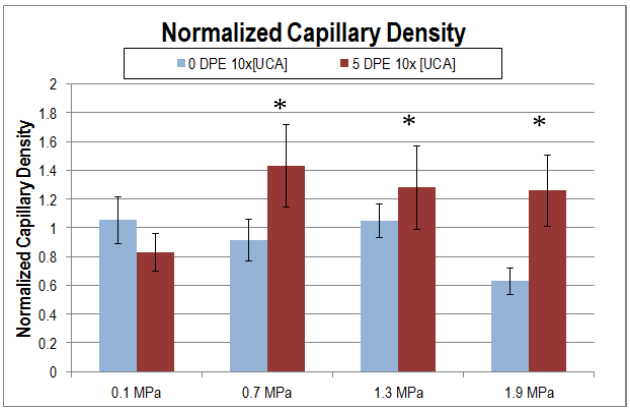

Figure 8.1: Normalized capillary density at 0 DPE (blue) and 5 DPE (red) across Pr. *p < 0.001 with respect to 0.1 MPa at 5 DPE.

Table 8.1: 5 DPE Normalized capillary density for Pr X [UCA]

Pressure (MPa)	1x	5x	10x
0.1	--	--	0.8 ± 0.1
0.7	1.0 ± 0.1	1.2 ± 0.1	1.4 ± 0.3
1.3	1.1 ± 0.2	1.2 ± 0.3	1.3 ± 0.3
1.9	1.6 ± 0.2	0.9 ± 0.1	1.3 ± 0.2

Also of note is that as [UCA] increases, so does SEM of the capillary density measurement, which was also seen in a [UCA] bioeffect studies completed by Miller et al. (1998, 2007, 2008). N-way ANOVA determined that the interaction of Pr and [UCA] was significant for 5 DPE capillary density with $p < 0.05$.

Evans blue dye (vascular permeability)

One-way ANOVA was used to determine that Pr was a significant parameter for vascular permeability ($p < 0.001$). EBD leakage demonstrated an increasing trend of permeability as the Pr increased (Figure 8.2 and 8.3). Multiple comparisons showed that the 0.1 MPa group was not significantly different from the control, but 0.7, 1.3, and 1.9 MPa was significantly different from

0.1 MPa ($p < 0.001$). Further, vascular permeability at Prs > 0.1 MPa was significantly different from the lower pressure groups ($p < 0.001$) (ie. 0.7 MPa < 1.3 MPa < 1.9 MPa).

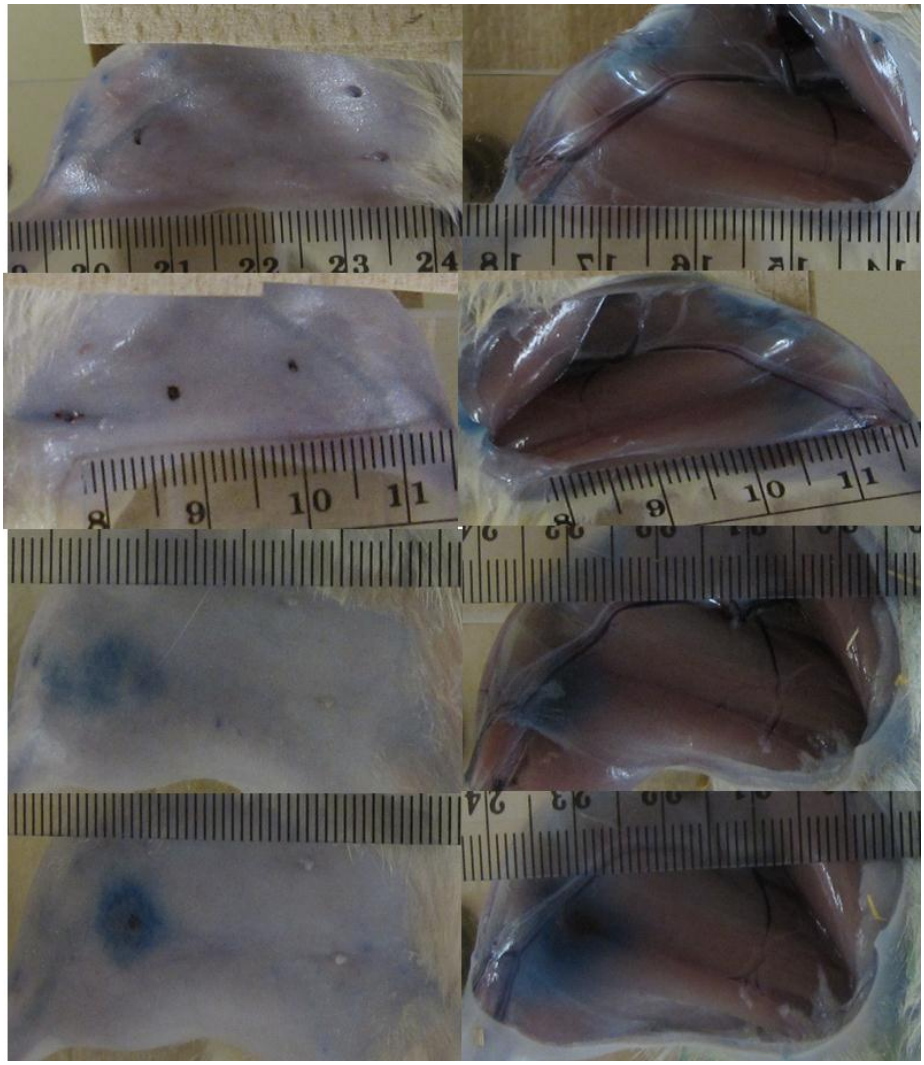

Figure 8.2: Photographic log of Evans blue dye leakage. Left photo is skin, right is muscle. Top to Bottom: 0.1 MPa, 0.7 MPa, 1.3 MPa, 1.9 MPa exposures.

Vascular endothelial growth factor-A (VEGF)

VEGF expression was significant across Pr ($p < 0.001$) with one-way ANOVA. The 0.7 MPa pressure displayed the greatest amount of VEGF expression, whereas the lowest and highest Prs demonstrated relatively low VEGF expression (Figure 8.3).

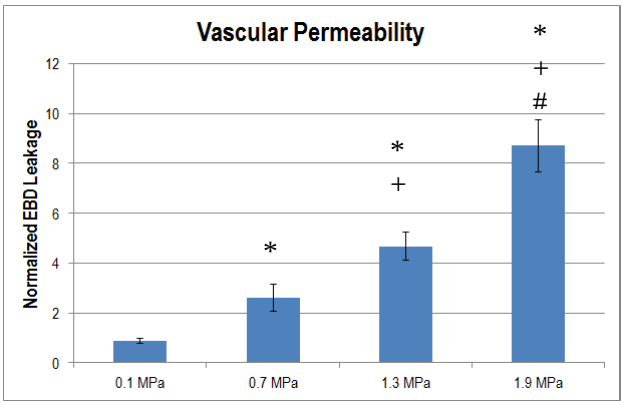

Figure 8.3: Normalized EBD as a marker for permeability at 0 DPE across Pr. *p < 0.001 with respect to 0.1 MPa, +p < 0.001 with respect to 0.7 MPa, and #p < 0.001 with respect to 1.3 MPa.

Multiple comparisons between Prs showed that 0.7 MPa and 1.3 MPa were significantly different from 0.1 and 1.9 MPa ($p < 0.001$).

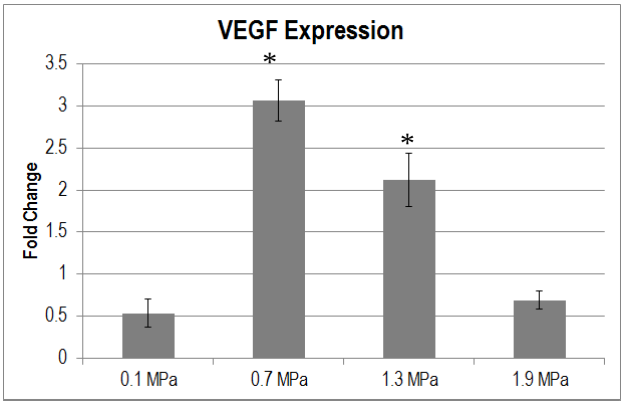

Figure 8.4: Relative VEGF expression at 5 DPE across Pr. *p < 0.001 with respect to 0.1 MPa.

Similar to capillary density at 5 DPE, VEGF expression demonstrated a trend with Pr at 10x [UCA]. To support capillary density and explore the angiogenic response with respect to Pr and [UCA], the [UCA] was reduced and VEGF expression quantified. The analysis neglected 0.1 MPa due to the lack of effect at 10x [UCA] (Table 8.2).

Table 8.2: 5 DPE VEGF expression (in fold change) for Pr X [UCA]

Pressure (MPa)	1x	5x	10x
0.1	--	--	0.5 ± 0.2
0.7	1.5 ± 0.3	1.3 ± 0.1	3.1 ± 0.3
1.3	1.9 ± 0.3	1.3 ± 0.2	2.1 ± 0.3
1.9	1.2 ± 0.6	2.0 ± 0.1	0.7 ± 0.1

Table 8.2 shows the relative VEGF expression (in fold change) ± SEM at 5 DPE. VEGF expression tends to decrease with 5x [UCA] except in the 1.9 MPa case. There appears to be an optimal Pr window of VEGF expression that varies with [UCA]. Lower concentrations require higher Pr to create larger increases in VEGF. N-way ANOVA determined that the interaction of Pr and [UCA] was significant for VEGF with $p < 0.01$.

8.2 Discussion

Previous work conducted in this lab sought to reduce the amount of acute damage to vasculature and surrounding tissue by keeping the [UCA] relatively low (Johnson et al. 2011, in press (Chapter 6)). However, subsequent work suggested that the angiogenic response is highly dependent upon [UCA], and that using a comparatively high [UCA] affords more of a response as measured by VEGF and changes in capillary density (Chappell et al. 2006, Johnson et al. 2011, submitted). "High [UCA]" is with respect to imaging concentrations because standards for therapeutic applications have not been assessed. Therefore it does not make sense to apply therapeutic limitations based upon established (imaging) standards—especially if angiogenesis is, in fact, damage induced. Using EBD, capillary density and VEGF, this study sought to address angiogenesis across a functional range of Pr with a high [UCA] at both 0 DPE and 5 DPE, such that mechanistic motivation could be elucidated.

This study supported the original finding that UCAs affect the angiogenic response and that [UCA] is an important parameter for determining this response. Again, no acute changes in capillary density occurred (Figure 8.1), which is in agreement with previously reported findings (Chappell et al. 2006, Korpisalo et al. 2010, Johnson et al. 2011, in press (Chapter 6)). No tissue-level damage was seen in histological section acutely, either. It should be noted that the initial signs of tissue damage do not appear until approximately 8 hours after damage (Robbins

& Kotran, Tiidus et al. 2008). Korpisalo et al. (2010) suggests that capillary enlargement precedes angiogenesis for therapy driven applications. The capillaries could either be dilating or there could be a physical stretching of capillaries from the US and UCA exposure that leads to increased pore size between endothelial cells. This increased pore size would allow EBD to leak. In accordance, acute measurements of EBD were shown to increase with increasing Pr (Figure 8.2 & 8.3). Bioeffects studies using EBD support that permeability increases with increasing Pr (Miller et al. 2007, Miller et al. 2009, Shang et al. 2010, Bohmer et al. 2010), but this is the first time it has been explored as a mechanism to potentiate the angiogenic response.

Capillary density at 5 DPE did change across Pr (Figure 8.1). A change in capillary (or vessel) density agrees with other US-induced angiogenesis studies (Barzelai et al. 2006, Chappell et al. 2006, Song et al. 2008, Bohmer et al. 2010). Also VEGF expression changes have been measured in ischemic studies conducted on skeletal and cardiac muscle (Reher et al. 1999, Wang et al. 2004, Nakajima et al. 2004, Barzelai et al. 2005). The co-occurrence of increased VEGF expression and increased capillary density was found at 0.7 MPa in this study, which disagrees with the notion put forth by Barzelai et al. (2005) that very low intensity US can be used to induce an angiogenic response. The data herein shows strong agreement with different studies that used Pr ≈ 0.8 MPa, and showed increases in capillary density, however (Song et al. 2004, Chappell et al. 2006, 2008).

As Pr increases UCAs undergo a dynamic range of events ranging from oscillation to collapse (Holland et al. 1996). Oscillation and collapse produce secondary effects including microstreaming, hemodynamic disturbances, and brief duration high temperatures and pressures in the surrounding media (Didenko et al. 1999, Suslick et al. 2001). The range of Prs was chosen because it encompasses the entire range of microbubble effects. Also, it includes only Pr

quantities that are FDA regulated (mechanical index = 1.9) (ODS 1998, Holland & Apfel 1989, Apfel & Holland 1991, NEMA 2009). With US exposure to low Pr, UCAs oscillate, therefore with Pr = 0.1 MPa, virtually no bubbles undergo collapse. By 0.7 MPa, however, approximately 60% of exposed UCAs undergo collapse with oscillation co-occurrence; this percentage rises to 100% by 1.9 MPa (King et al. 2010, Figure 3.6). Because this study demonstrated an angiogenic response onset at 0.7 MPa, it suggests that UCA collapse is necessary for an angiogenic response. Chapter 6 and 7 show agreement with the findings in this chapter showing increased bioeffect and angiogenic responses when collapse occurs and increased VEGF expression at 10x [UCA] when 0.7 MPa is used, respectively.

This study and Chapter 6 determined Pr was significant at 10x and 5x [UCA] respectively. Chapter 7 assessed [UCA] and found significance at a set Pr. Pr X [UCA] was expanded in terms of the angiogenic response (5 DPE) to determine if the interaction term was significant (Table 8.1 and 8.2). Not only was significance found, but higher VEGF expression also corresponded relatively well to higher capillary density, particularly in the 10x [UCA] case.

Thus far, Pr, [UCA], and Pr X [UCA] have been explored with respect to the induction of bioeffects that lead to an angiogenic response. These studies found that the presence of UCAs increases both acute and 5 DPE responses, Pr was significant for determining the extent of the responses, and that there was an interaction between Pr and [UCA] to elicit the responses. These findings suggest that collapse, or inertial cavitation is necessary for the optimal response because the oscillation regime (at 0.1 MPa) did not show significance for biological effects nor the angiogenic response when compared to the control. The biophysics of the UCA is further explored with respect to bioeffects and the angiogenic response in the next chapter by narrowing the Pr range to observe responses and discuss UCA radial expansion and collapse trends.

CHAPTER 9: ULTRASOUND CONTRAST AGENT COLLAPSE POTENTIATES ANGIOGENIC RESPONSE

The findings from the previous studies include both a [UCA] and Pr dependency of the angiogenic response, which agrees with results from other literature that use a range of [UCAs] and Prs in ischemia related US-UCA therapy. Concentrations ranging from no UCAs to bolus, and Prs ranging from 40 kPa to 4.5 MPa have all been used and demonstrated some effectiveness (Song et al. 2002, Barzelai et al. 2005, Chappell et al. 2006, Chappell et al. 2008, Zen et al. 2006, Song et al. 2004, Korpanty et al. 2005, Fuji et al. 2009, Johnson et al. 2010, Bohmer et al. 2010, Johnson et al. 2011, in press). Numerous researchers have documented Pr's effect on UCAs (Atchley et al. 1988, Stride et al. 2003, Sboros et al. 2008, Santin et al. 2010), which makes broad ranges of Pr and [UCA] curious. There is a well-established body of literature detailing the progression of UCAs from oscillation (stable cavitation) to collapse (inertial cavitation) with increasing Pr and the effects that this perturbation has on the surrounding media (Wu et al. 1997, Stride et al. 2003, Marmottant et al. 2005, Sboros et al. 2008, King et al. 2010). Both oscillation and collapse have been observed with *in vitro* single bubble experiments in this lab (Ammi et al. 2006b, Haak et al. 2007, King et al. 2010) and theoretically modeled (Lauterborn et al. 1976, Marmottant et al. 2005, King et al. 2010, 2011). More sophisticated models have been attempted to address the complexity of *in vivo* models, but *in vivo* variability slows the adaptation of a model robust enough to be applicable in all scenarios (Qin et al. 2010).

Bioeffect studies have attempted to address the effects of US-UCA from a biological standpoint. Hemorrhage, premature ventricular contractions, lesions, and microvascular disruptions have all been noted to occur with US-UCA exposure (Skyba et al. 1999, Dalecki et al. 1995, Chappell et al. 2006, Zachary et al. 2006, Miller et al. 2008). However, the correlation

to bubble dynamics is rarely, if at all, studied with respect to bioeffects or therapy. Therefore, the question that plagues most bioeffect and therapeutic studies is: "Is collapse necessary for a response, and if so, is there a particular level of collapse that will optimize this response?" The intent herein is to address this question for the specific case of US-UCA-induced angiogenesis.

Because the collapse incidence of the UCA used in this study, Definity®, has been extensively examined *in vitro* in this lab (Ammi et al. 2006b, Haak et al. 2007, King et al. 2010), of particular interest is to understand how the bubble dynamics related to both acute bioeffects and subsequent angiogenesis. Therefore, a narrow range of Pr was used to assess the acute bioeffects and subsequent angiogenic response via a theoretical correlation of bubble dynamics to *in vivo* experiments. Using thirty-six rats 5 different Pr were explored: 0.1, 0.3, 0.5, 0.7, and 0.9 MPa. There were 3 control rats and an n = 3 for each Pr. US exposure settings were: f = 1 MHz, PRF = 10 Hz, PD = 10 μs, ED = 5 min, and a 10x [UCA]. Capillary density, vascular permeability and VEGF expression were used to assess bioeffects and the angiogenic response. All assessments were normalized to the control. Bilateral exposures on lateral sites were exposed and the medial site served as the control.

9.1 Results

Capillary density

Two-way ANOVA demonstrated that DPE and Pr, but not DPE*Pr were significant for capillary density ($p < 0.05$, $p < 0.001$ and $p > 0.05$, respectively) (Figures 9.1). Multiple comparisons showed that 0.1 MPa was not significantly different from the control ($p > 0.05$), but 0.7 MPa was significantly different from the control and 0.1 MPa ($p < 0.001$), and 0.9 MPa was significantly different from 0.1 MPa at 5 DPE.

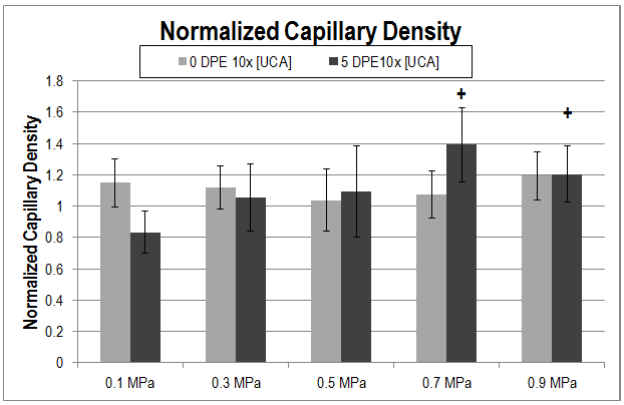

Figure 9.1: Normalized capillary density at 0 DPE (light grey) and 5 DPE (dark grey) across Pr. *p < 0.001 with respect to 0.1 MPa.

Evans blue dye (vascular permeability)

One-way ANOVA showed that EBD leakage was significant with Pr ($p < 0.001$). EBD leakage demonstrated an increasing trend of permeability as the Pr increased (Figure 9.2). Multiple comparisons showed that the control was not significantly different from the 0.1 MPa group, but 0.3, 0.5, and 0.7 MPa were significantly different from the control and 0.1 MPa ($p < 0.001$). Further, 0.7 MPa was significantly different from 0.3 MPa ($p < 0.01$), and 0.9 was significantly greater than the other pressure groups ($p < 0.001$).

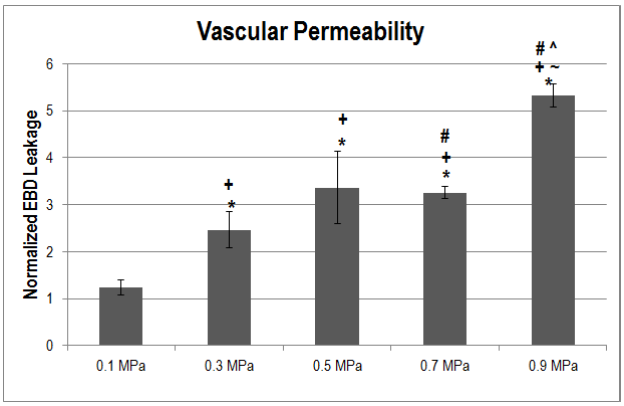

Figure 9.2: Normalized Evans blue dye as a marker for permeability at 0 DPE across Pr. *p < 0.001 with respect to the control, +p < 0.001 with respect to 0.1 MPa, #p < 0.001 with respect to 0.3 MPa, and ^p < 0.001 with respect to 0.5 MPa, ~p < 0.001 with respect to 0.7 MPa.

Maximal radial expansion (MRE)

The maximal radial expansion (MRE) was calculated using the Marmottant equation (Eq. 3.35), (Figure 9.3) with the parameters listed in Table 9.1. According to the Marmottant theory, bubbles collapse when R/Ro reaches approximately 1.5 (or less) (Marmottant et al. 2005, King et al. 2010, 2011). At Pr = 0.9 MPa the MRE ~ 9, suggesting that a large percentage of these UCAs undergo collapse.

Table 9.1: Summary of values used in the Marmottant equation simulation.

F	0.93 MHz	ρ_{blood}	1060 kg/m^3
R_o	1 µm	P_o	101.3 x 10^3 Pa
Pr	0.1, 0.3, 0.5, 0.7, 0.9 MPa	σ_{bubble}	0 N/m
No. of cycles	10	σ_{blood}	0.046 N/m
c	1500 m/s	χ	0.38 N/m
κ	1.06	$R_{buckling}$	0.99R$_o$
μ_{blood}	0.005 Pa*s	$R_{breakup}$	1.5R$_o$
k_s	0.5 x 10^{-9} N	$R_{rupture}$	1.08R$_o$

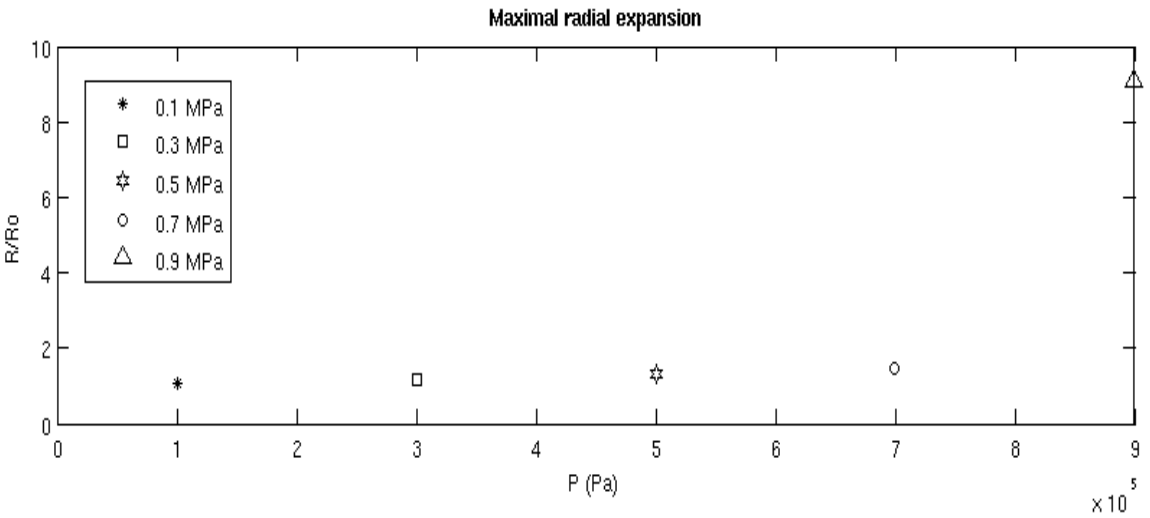

Figure 9.3: Maximal radial expansion of UCAs at varied Pr.

According to King et al. 2010, Definity® exhibits increasing percentage collapse with increasing Pr, where at 0.9 MPa approximately 85% of UCAs collapse at f = 1 MHz. If the percent collapse is compared to the EBD leakage, we see that the trends are similar (Figure 9.4).

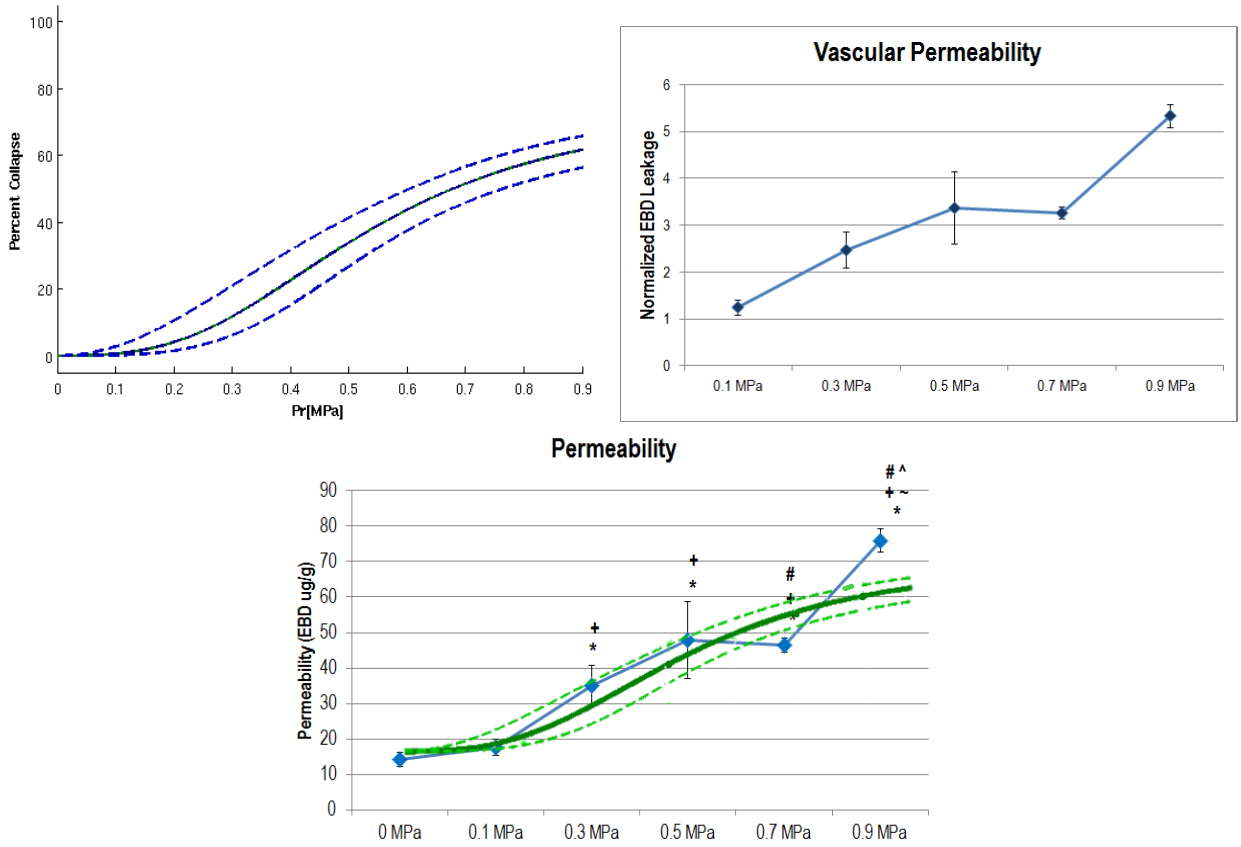

Figure 9.4: A trend comparison of relevant portion of percent collapse (left, King et al. 2010) and normalized vascular permeability (right). An overlay of percent collapse and absolute vascular permeability (bottom, also in Figure 9.2) the collapse curve was shifted.

Vascular endothelial growth factor-A (VEGF)

Pr was a significant parameter for VEGF expression ($p < 0.01$) as determined by one-way ANOVA. The greatest level of VEGF expression occurred at 0.7 MPa, rising to significance when compared to 0.1, 0.3 and 0.5 MPa ($p < 0.01$). The VEGF expression decreased at 0.9 MPa. Where there is oscillation only, 0.1 MPa, demonstrated the lowest amount of VEGF expression. (Figure 9.5).

9.2 Discussion

This study found that an increase in vascular permeability (EBD leakage, Figure 9.2) coincides with the occurrence of increased VEGF expression and capillary density at 0.7 MPa

(Figures 9.1 and 9.5) which agrees with the findings in Chapter 8. Previous *in vitro* experiments concluded that Definity®'s collapse threshold (5% occurrence rate) was approximately ~ 0.2 MPa—Definity® reaches 100% collapse by ~ 1.0 MPa (King et al. 2010). Therefore collapse co-occurs with US-UCA induced angiogenesis.

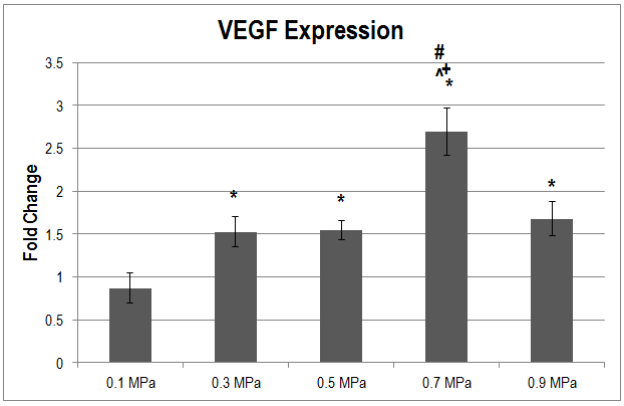

Figure 9.5: Relative VEGF expression at 5 DPE across Pr. *p < 0.01 with respect to 0.1 MPa, +p < 0.01 with respect to 0.3 MPa, #p < 0.01 with respect to 0.5 MPa, ^p < 0.01 with respect to 0.9 MPa.

UCAs have a resonant frequency at which they oscillate most efficiently that is dependent on bubble size. An activated vial of Definity has a range of bubble sizes with the following descriptors for its profile: a mean diameter range of 1.1 to 3.3 µm, 98% of bubbles are less than 10 µm, but the maximum diameter is 20 µm (Definity package insert). Because of the presence of larger bubbles, the resonant frequency of Definity® is on the order of f_o = 1 MHz, which is comparable to the frequency used in this study (and other therapeutic applications). Therefore, when sonicating at the approximate resonant frequency of the UCA, we can assume that there is a predictable pattern of behavior for the oscillation regime (0.1 MPa, in this study).

Chapter 3 discussed the fitting of theoretical equations to single bubble experiments. Further, Chapter 5 estimated a volume fraction that suggested that the theoretical constructs could be used as an approximation. With this trail of evidence, we can link the theory to the

bioeffects noted in this study. Changes in vascular permeability did not occur until the 5% collapse threshold, determined by *in vitro* experiments, was exceeded, signifying that collapse is required to elicit the acute bioeffect. As in previous chapters, capillary density at 0 DPE remained constant.

The literature proposes that collapse is necessary for angiogenesis to occur. However, reports that microbubble destruction leads to an angiogenic response was not supported by bubble characterization or theoretical simulations (Chappell et al. 2006, Chappell et al. 2008, Song et al. 2008, Geis et al. 2009). Herein we saw that the angiogenic response is not initiated (ie. does not reach significance) until after Definity reaches an approximate 60% collapse occurrence. Figure 9.1 and 9.5 demonstrated increases in both 5 DPE capillary density and VEGF expression. Thus the notion of collapse being required for both the bioeffect and the subsequent angiogenic response is supported. In general, the work herein shows agreement with theoretical models demonstrated by Miao et al. (2008) with vessel perturbation (where wall stress exceeds the capillary strength) being analogous to increased permeability eventually leading to probably rupture at Pr = 0.2 MPa (see more detail in Chapter 3.4).

To extend the findings thus far, the Marmottant model can be used to predict the Pr at which UCAs collapse. Up to now, the biological findings for increases in vascular permeability have been observed with increasing Pr. This chapter demonstrated that the *in vitro* trend for UCA collapse is similar to that of the induction of increased vascular permeability up to 0.9 MPa even though in vitro experiments used a single bubble setup. The next chapter examines the following: if the Marmottant equation can be used to explain the cause of bioeffects and the subsequent angiogenic response for all Prs in Chapters 7 to 9, if the theoretical simulation aligns

with the in vitro data from King et al. 2010, and finally if both can be connected to the *in vivo* data presented in this thesis.

CHAPTER 10: UCA BIOPHYSICAL EXPLORATION: OSCILLATION OR COLLAPSE?

Based upon previous concentration and volume fraction calculations the single bubble model is appropriate for describing UCA dynamics *in vivo* with the [UCA]s used herein. This chapter focuses on the biophysics of the bubbles and their associated biological implications in an effort to further explore the cause of acute bioeffects. Chapter 9 demonstrated a trend similarity between the collapse of UCAs and increases in vascular permeability. This chapter will expand upon the findings in Chapter 6 through 9 and discuss what is presumed to be occurring to the UCAs in the beam of the transducer during exposures.

Table 10.1: Summary of values used in simulations.

f	0.93 MHz	ρ_{blood}	1060 kg/m^3
R_o	1 µm	P_o	101.3 x 10^3 Pa
Pr	0.1, 0.3, 0.5, 0.7, 0.9, 1.3, 1.9 MPa	σ_{bubble}	0 N/m
No. of cycles	10	σ_{blood}	0.046 N/m
c	1500 m/s	χ	0.38 N/m
κ	1.06	$R_{buckling}$	0.99R$_o$
μ_{blood}	0.005 Pa*s	$R_{breakup}$	1.5R$_o$
k_s	0.5 x 10^{-9} N	$R_{rupture}$	1.08R$_o$

Up to now, a range of Prs have been explored (0.1 to 1.9 MPa). Table 10.1 lists the constants used for the Marmottant equation modeling bubble radius and driving pressure as a function of time. Figure 10.1 shows pressure and radius as a function of time for "low Pr": 0.1, 0.3, 0.5 and 0.7 MPa. When the bubble is oscillating, there are low amplitude decreases and increases in bubble radius, involving equal contraction than expansion. Even at relatively low Pr the bubble expansion may be non-uniform due to the density, surface tension and viscosity of blood. In addition, the value of the surface dilation viscosity slightly alters curve, and has been reported to be anywhere from 0.5 x 10^{-9} to 12 x 10^{-9} N (Marmottant et al. 2005, Goertz et al.

2007, Santin et al. 2010). From this simulated bubble reaction to US, we note that the UCA becomes more susceptible to slow large amplitude expansions followed by rapid contractions as Pr increases eventually leading to UCA collapse (Figure 10.1 and 10.2).

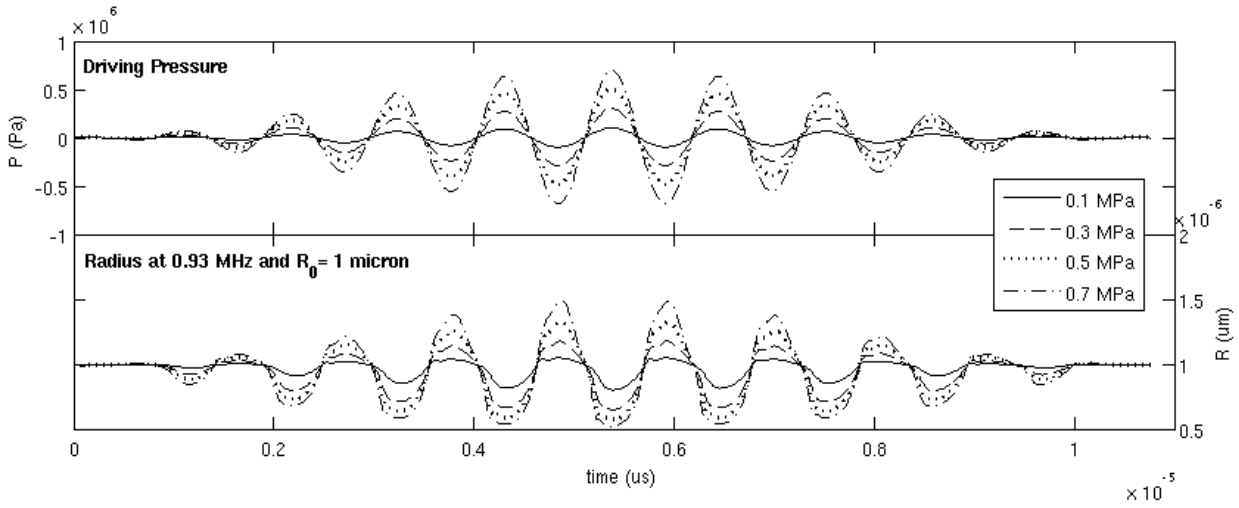

Figure 10.1: Radial displacement and driving pressure for low Pr.

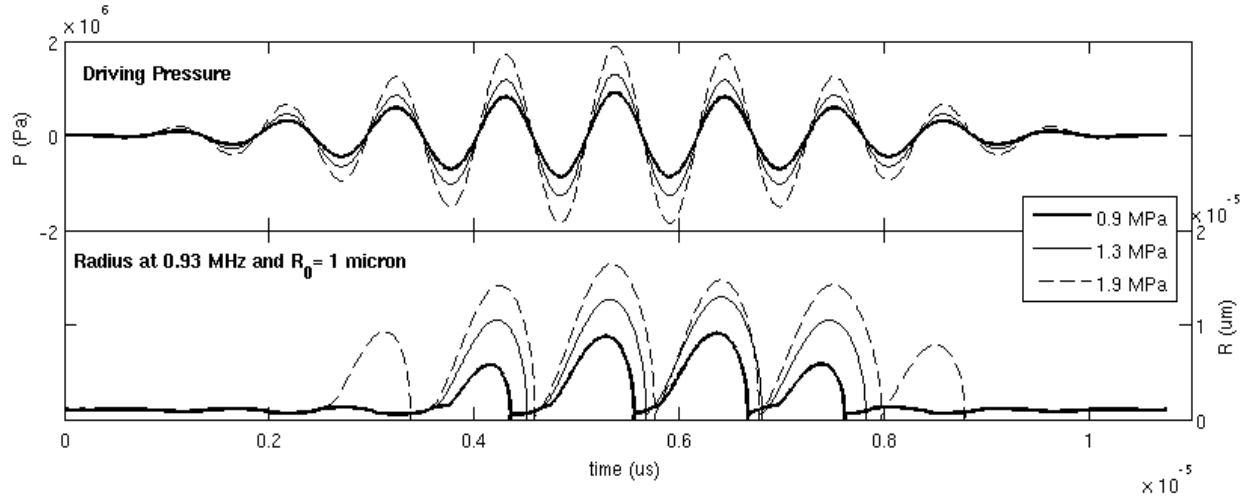

Figure 10.2: Radial displacement and driving pressures for high Pr. Note that the initial radius of the UCA is 1 x 10^{-6} m (or 1 µm); the scale of the radius on the right is of the 10^{-5} order.

Figure 10.3 shows the maximal radial expansion (MRE) of the Definity bubbles at various Prs. The MRE ranges from 1.03 at 0.1 MPa to 16.58 at 1.9 MPa. The general acceptance for when a bubble will collapse is when $R/R_o \geq 2$, though recent studies suggest that collapse

occurs at MREs $\geq$ 1.1 (King et al. 2011). Thus the MRE from the Marmottant model approximates the Pr at which 100% of UCAs collapse.

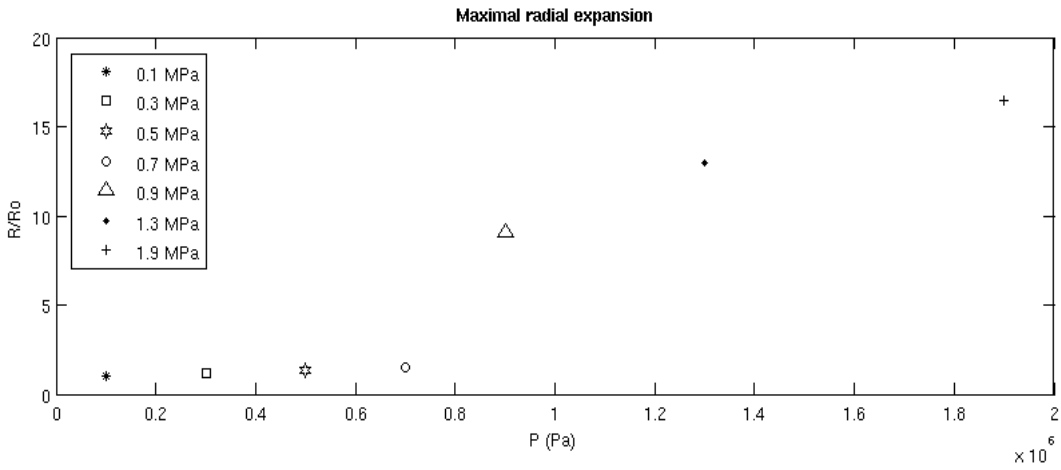

Figure 10.3: Maximal radial expansion for all experimental Pr, where a value of 1 means that maximal expansion is equal to the initial radius, ie. no expansion.

Once the Pr reaches 0.9 MPa there is a much slower and considerably larger expansion that is questionably beyond the confines of a lipid-shelled bubble. This is followed by a rapid contraction depicted in Figure 10.2 as an infinite radius slope, therefore the fact that collapse has occurred can be derived. From separate *in vitro* experiments it was found that the onset of collapse is not finite, but rather collapse occurs with greater frequency as Pr increases (King et al. 2010). This is possibly due to the range of bubble sizes present in a vial of Definity®, so bubbles respond slightly different depending upon how close to resonance the UCA is. Therefore microstreaming co-occurs with collapse at Prs less than about 1.0 MPa, at which point 100% of UCAs collapse (Figure 3.6) (King et al. 2010).

Microstreaming is of particular interest because of its ability to alter the normal shear stresses present intravascularly. As mentioned in Chapter 4, as little as 0.075 Pa is linked to increased permeability and enhanced endothelial cell biosynthetic capabilities. Because shear

stress is directly proportional to bubble radius, and radius is proportional to Pr, as Pr increases, shear stress increases. Figure 10.4 shows the shear stress as a function of radius for a Pr up to 1.9 MPa. From Eq 3.43 to 3.45 we find that a radius change of $\pm$ 0.002 nm is where the vascular shear stress exceeds 0.075 Pa, which suggests that US induced microstreaming via bubble oscillation affects the vascular endothelium at even very low Pr, *excluding* any US radiation force effects. From the data gathered thus far, though 0.1 MPa can induce changes in shear stress, the changes are insufficient to elicit changes in vascular permeability or the angiogenic response with one exposure.

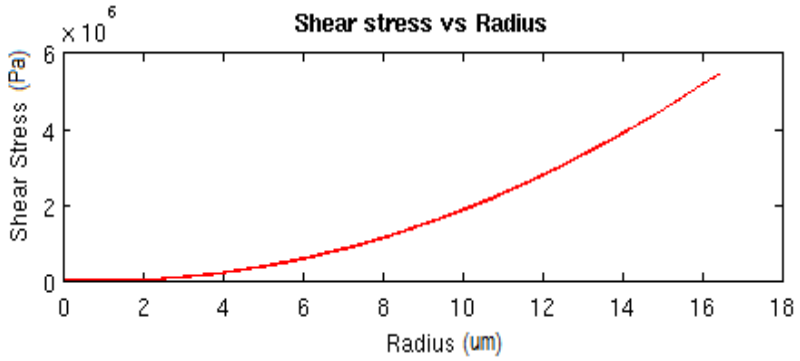

Figure 10.4: Shear stress as a function of radius. When Pr = 1.9 MPa a range of shear stresses are produced as the UCA grows and undergoes IC.

For a microbubble to produce double the shear stress naturally occurring intravascularly, a radial expansion of only 0.01 nm is needed. In Figure 10.1 the oscillation regime produced high enough radial oscillations to locally increase the shear stress experienced by endothelial cells. Shear stresses produced with radial expansions of 0.5µm are on the order of several hundred Pa. Combining the physical effect of microstreaming-induced shear stresses and collapse to the acute bioeffects presented in previous chapters, the trend of vascular permeability agrees with the trend for collapse as seen in Figure 10.5 and in Chapter 9, Figure 9.4. For Figure 10.5, the absolute values for vascular permeability were in µg of dye/g of tissue. The EBD

leakage values were shifted down by 10 µg/g (ie. 10 ug/g was subtracted from the absolute permeability value such that the curve intersected (0, 0) and so that the curves could be plotted on top of one another. Noting that the percentage of collapse increases with increasing Pr, it can be inferred that the percentage of oscillating bubbles decreases (from the total number of bubbles at t = 0) as we increase Pr. It should be noted that this graph does not show a one-to-one correspondence with percentage leakage and percentage collapse, but rather that the trends are comparable. The pressure at which moderate leakage and maximal angiogenesis occurred for the studies presented is at Pr = 0.7 MPa—the pressure where approximately 60% of UCAs collapse.

Further, if we assess the angiogenic responses presented in previous chapters, we find that 0.9 MPa is not only the point at which the VEGF expression declines (from the peak VEGF expression value at 0.7 MPa), but it is also the approximate onset point of inertial cavitation of the UCAs (Figure 10.2).

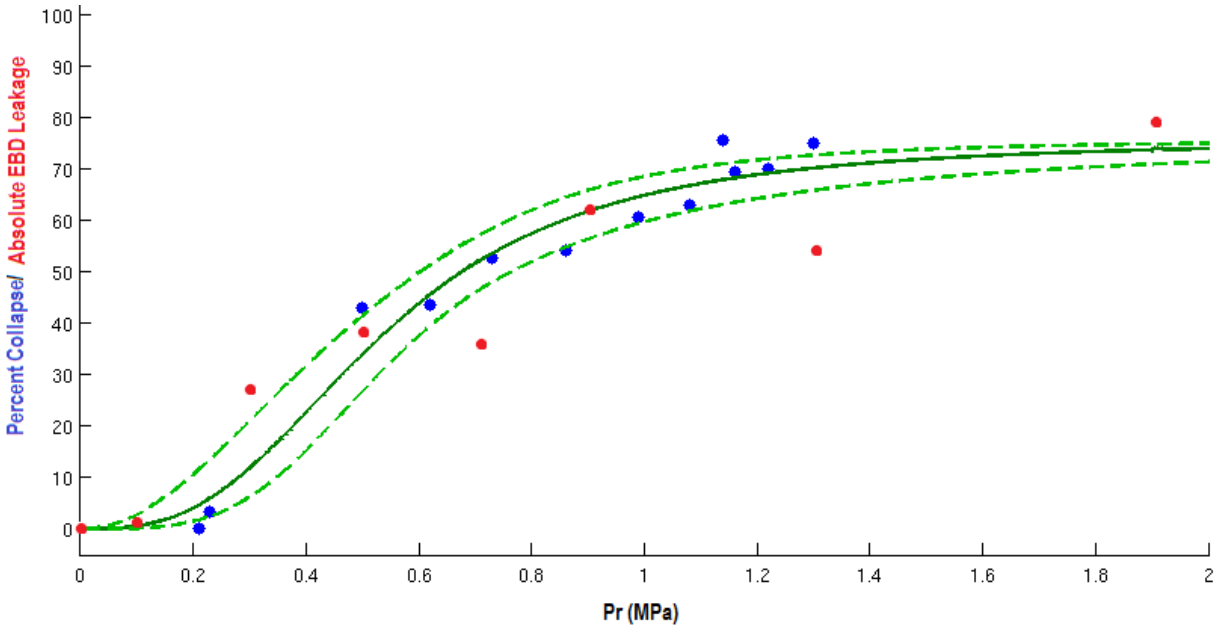

Figure 10.5: Overlay of experimental Pr-associated changes in vascular permeability with the percentage collapse of Definity®. Blue dots represent the average *in vitro* collapse data and fitting of the collapse data with a logistic regression curve (solid green) with a 95% confidence interval (dashed green). Red dots indicate the average absolute vascular permeability from Chapter 7 to 9.

Ultimately, acute bioeffects should be evaluated with a risk/benefit measurement for therapeutic applications. In an effort to develop an understanding of the path from acute bioeffects to the end goal of therapy, examining the tissue at several time points after exposure will provide information regarding of the risk of US-UCA therapy. This investigation will specifically further the understanding of not only the connection of biophysical events to tissue-level effects, but also the nature of the damage that is induced for the therapy. The next chapter explores the tissue-level damage from US-UCA exposure with respect to collapse and the induction of angiogenesis.

CHAPTER 11: TISSUE EFFECTS OF US-UCA-INDUCED ANGIOGENESIS

Inflammation, vascular permeability and capillary density have been assessed at 0 DPE for acute damage, where a reduction in capillary density was indicative of lumen disruption. This chapter focuses on the tissue effects, which are not seen until a minimum of 8 hours after exposure to ultrasound. Studying the histological progression of the bioeffect leading to the angiogenic response adds value to the risk/benefit notion that is implied with therapeutic applications.

In wound healing, the general progression is as follows: homeostasis, inflammation, proliferation, and remodeling. Only minutes pass prior to the formation of platelet aggregates once a vessel lumen is disrupted. This effect may appear as hemorrhage on cross section of the muscle. The first signs of tissue damage are nonuniformity in the Z-lines and A-lines at approximately 8 hours after the damage occurs. Several hours later, signs of coagulative necrosis, demonstrated as blurry nuclei and overall lighter pigmentation appear. There also may be silhouettes of cells without definite form that appears with damage. Then, neutrophils and macrophages appear at the site to phagocytose debris (inflammatory infiltrate). These cell types release several factors for angiogenesis, including VEGF. VEGF begins the proliferative phase of angiogenesis by approximately 48 hours after injury as discussed in Chapter 2. After which, in wound healing, there is maturation and remodeling phase.

To examine the effect of US and UCA on the skeletal muscle, a histological assessment was completed. This study used 12 animals to test 4 Prs (Pr = 0.1, 0.7, 1.3 and 1.9 MPa) at 4 time points 0, 8, 16, and 24 hours post exposure (HPE). Two sites on each gracilis muscle were exposed for a total of 4 exposure sites per animal (N = 3/HPE group). This tissue effect study was carried out to assess whether the cause of the angiogenic response was ‘frank damage’ (as in

myocyte damage) or if it was solely a permeability effect (ie. minor vascular endothelial cell perturbation). H&E was used to observe tissue level effects for all time points.

11.1 Results

The 0 HPE myocytes show no difference from normal skeletal muscle for all Pr groups. However, hemorrhage was inconsistently present at higher Prs (Figure 11.1).

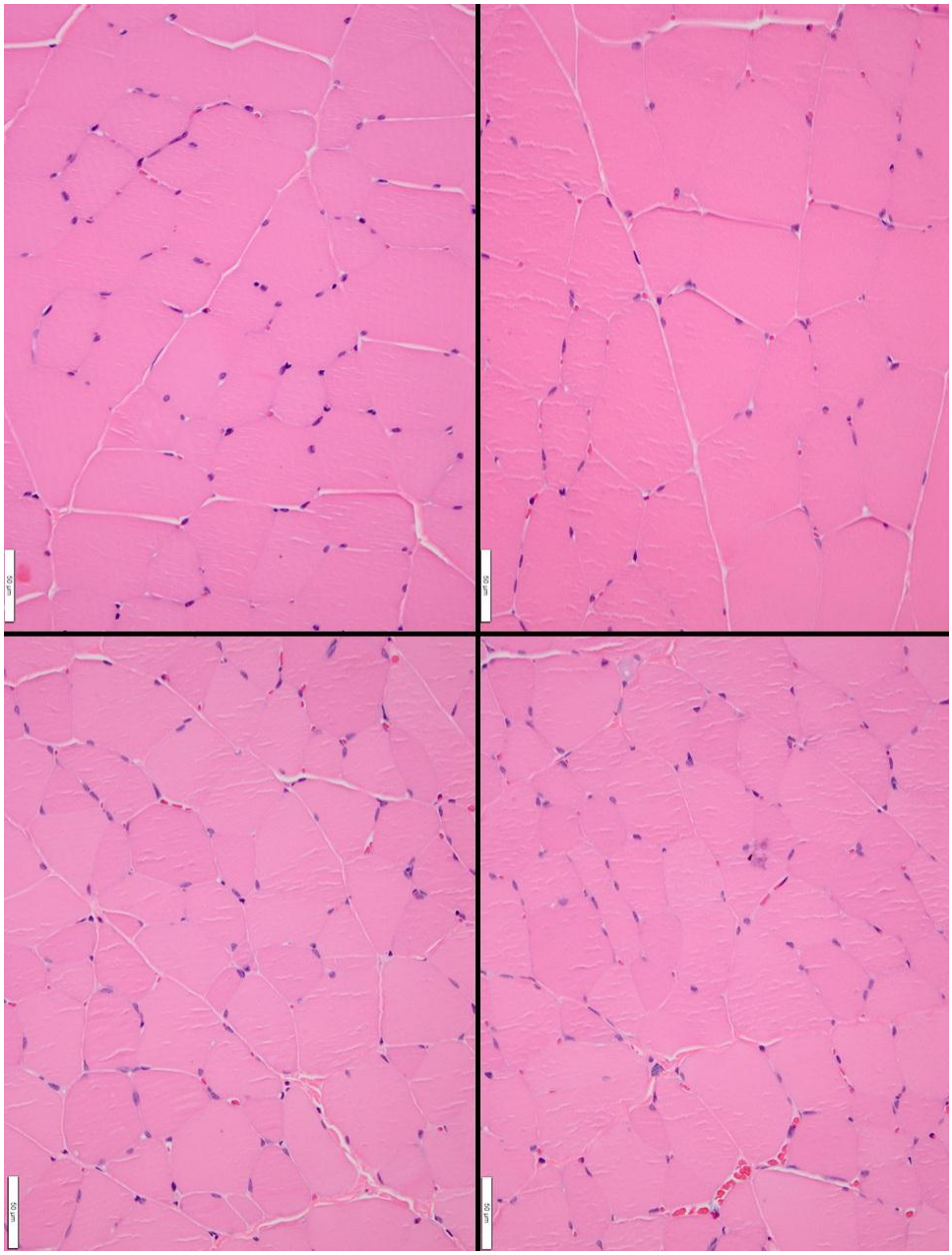

Figure 11.1: 0 HPE Histological images. Top left: 0.1 MPa, Top right: 0.7 MPa, Bottom left: 1.3 MPa, Bottom right: 1.9 MPa White bar = 50 µm.

The 8 HPE myocytes demonstrated some nucleus internalization and hemorrhage at 1.3 and 1.9 MPa, but were normal at 0.1 and 0.7 MPa (Figure 11.2). Because the muscle was sliced to be 3 µm thick, some artifacts like tissue folds appear in section.

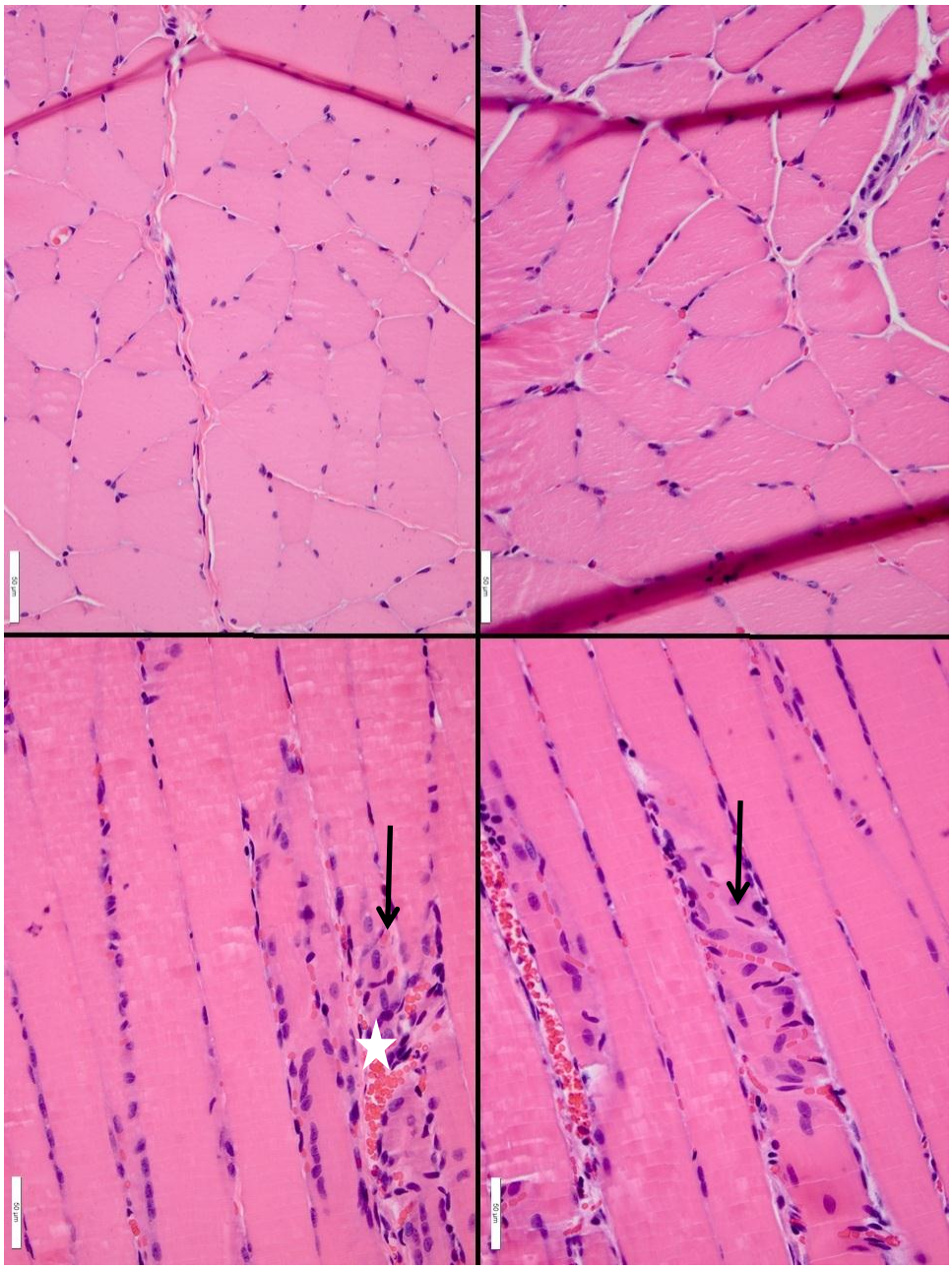

Figure 11.2: 8 HPE Histological images. Top left: 0.1 MPa, Top right: 0.7 MPa, Bottom left: 1.3 MPa, Bottom right: 1.9 MPa Arrow shows nucleus internalization, white star shows hemorrhage. White bar = 50 µm.

By 16 HPE, the skeletal muscle began to show signs of coagulative necrosis along with hemorrhage, nucleus blurring, and A- and Z-line disruption when exposed to Pr greater or equal to 1.3 MPa. While the myocytes were normal at 0.7 MPa, there is notable capillary engorgement and possible arteriogenesis. The 0.1 MPa group was normal (Figure 11.3).

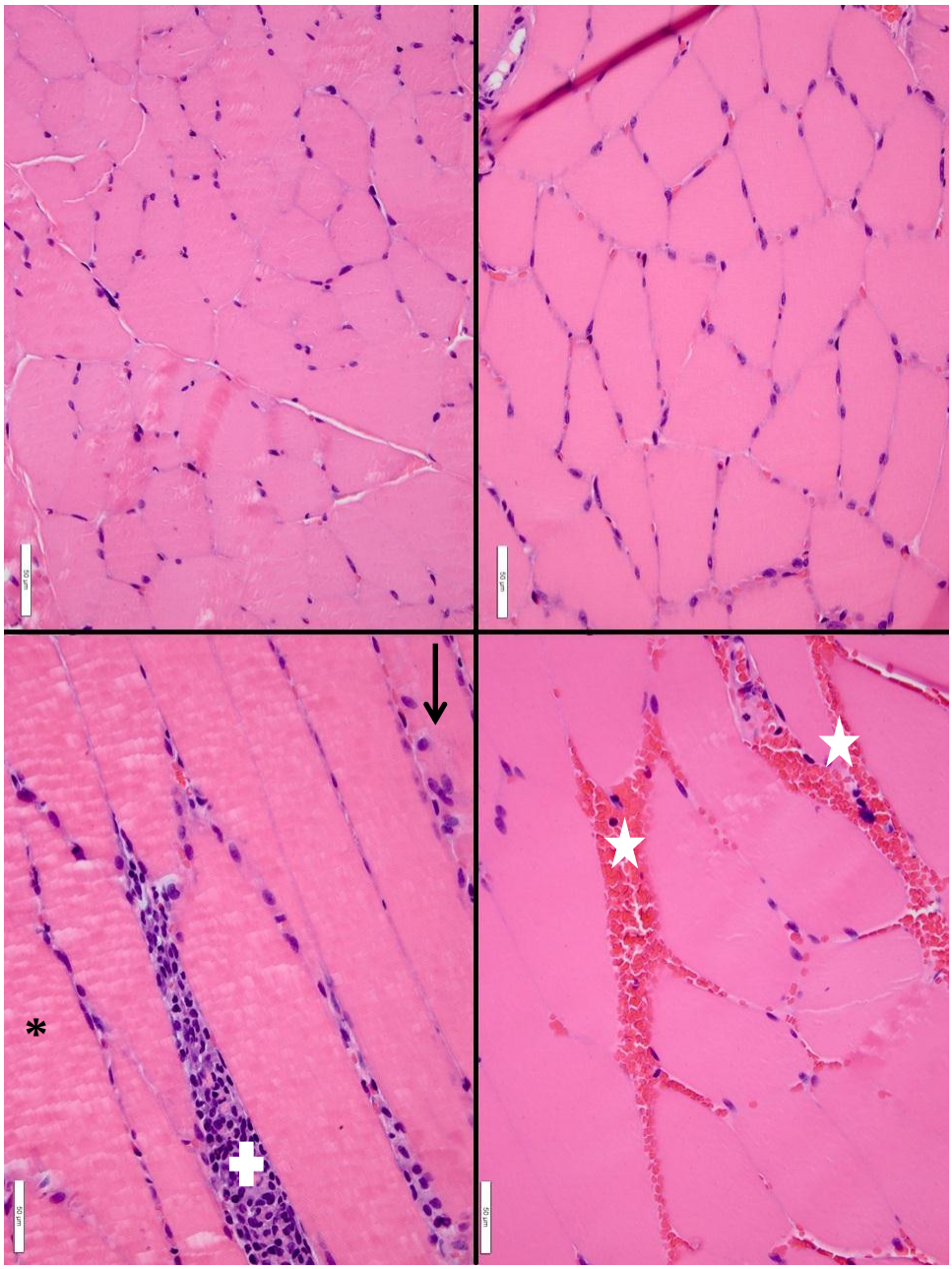

Figure 11.3: 16 HPE Histological images. Top left: 0.1 MPa, Top right: 0.7 MPa, Bottom left: 1.3 MPa, Bottom right 1.9 MPa. The white star shows hemorrhage, the arrow shows nucleus internalization, and the plus sign shows inflammatory infiltrate. The asterisk shows contraction bands. White bar = 50 µm.

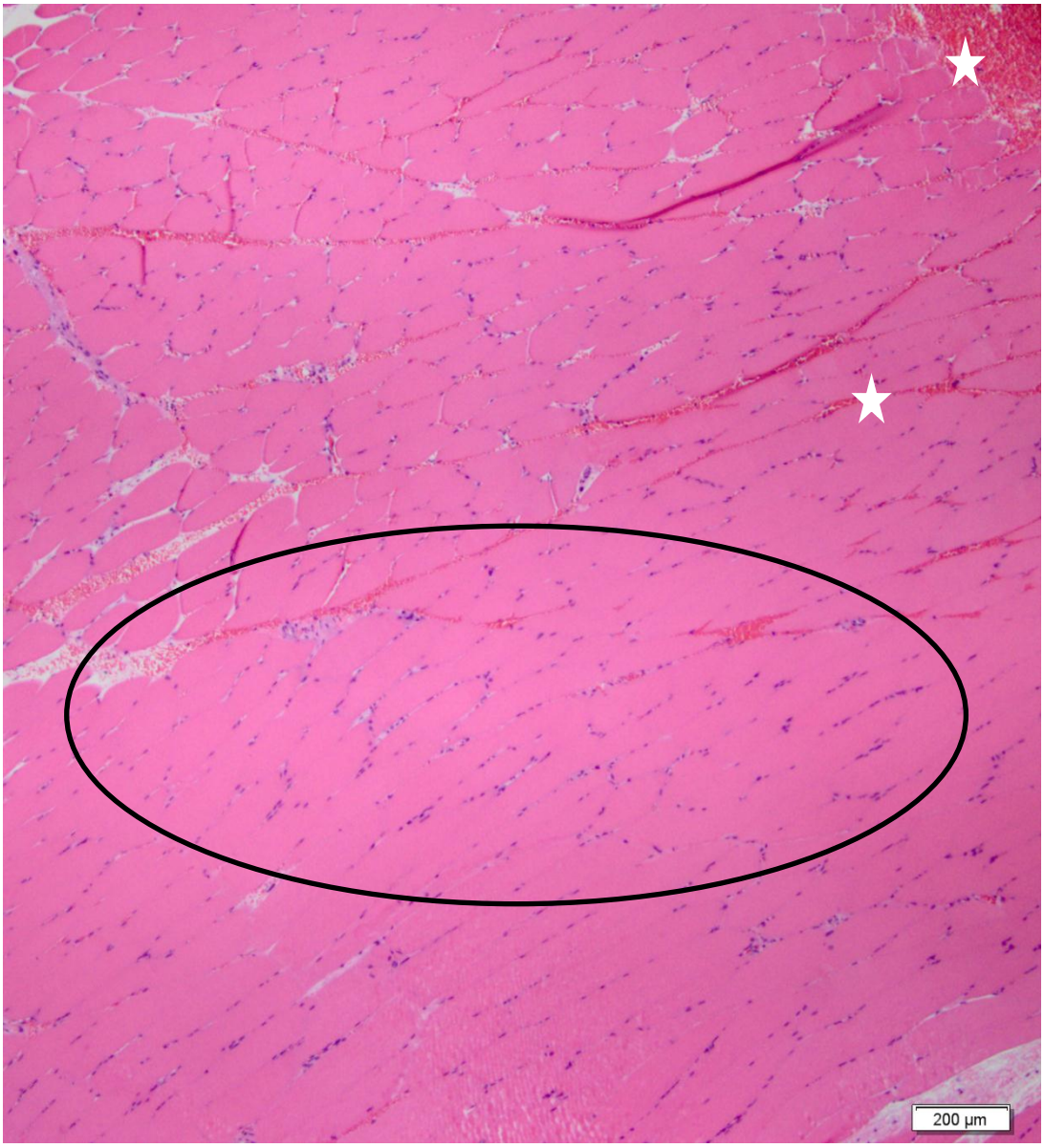

Figure 11.4: 16 HPE Histological image showing ligher area where coagulative necrosis (inside black circle) occurred. The white star shows hemorrhage. 1.9 MPa White bar = 200 µm.

The 16 HPE group also demonstrated observable changes in pigmentation indicative of coagulative necrosis (Figure 11.4). The lighter pigmentation is the result of loss of intracellular structures and cytoplasm dominance. The necrosis occurs downstream of hemorrhage, suggesting that the tissue is no longer receiving oxygen and/or nutrients.

At 24 HPE, there were definite signs of coagulative necrosis for all animals exposed at 1.3 and 1.9 MPa. No damage was observed at 0.1 or 0.7 MPa (Figure 11.5).

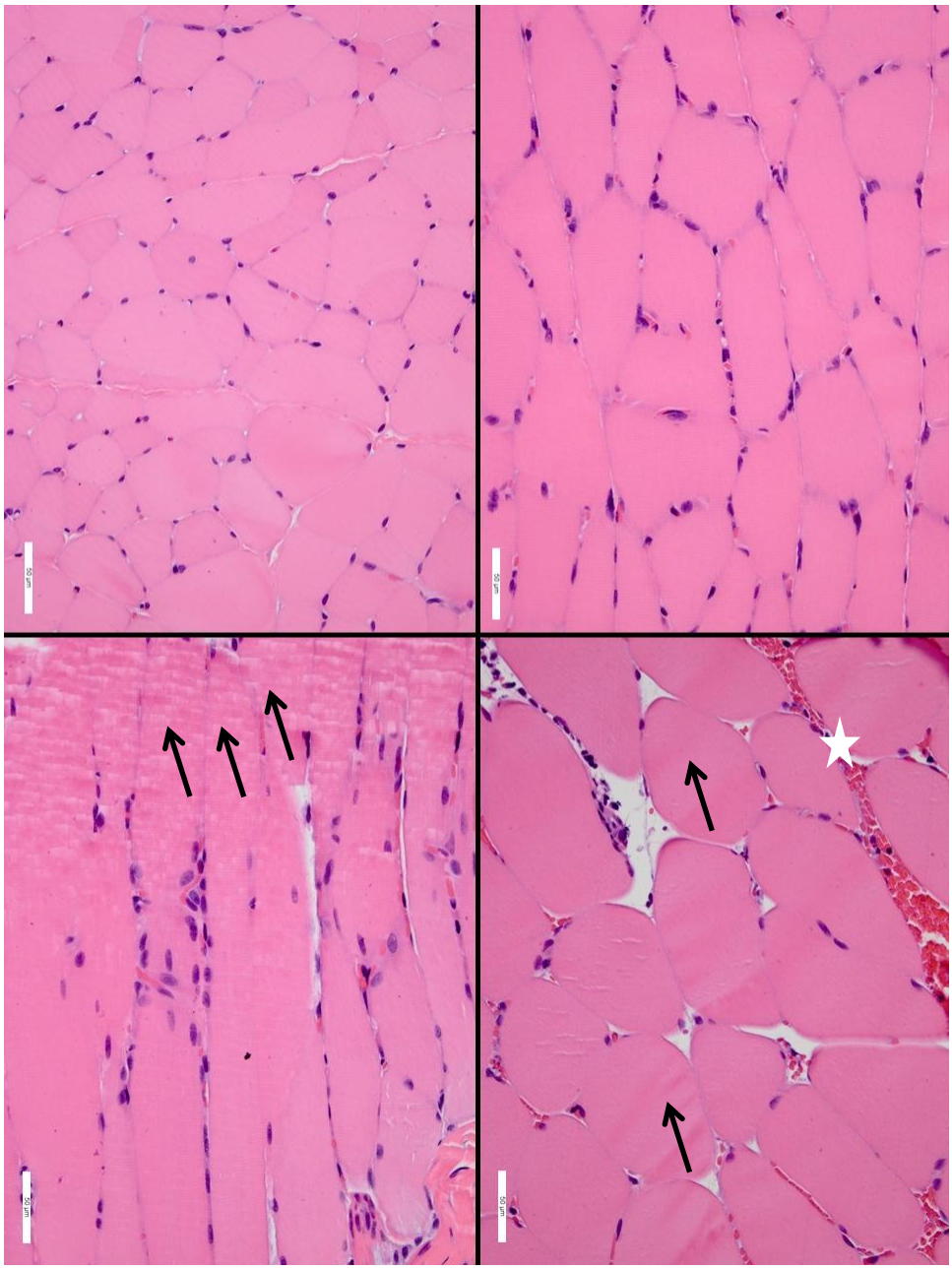

Figure 11.5: 24 HPE Histological images. Top left: 0.1 MPa, Top right: 0.7 MPa, Bottom left: 1.3 MPa, Bottom right: 1.9 MPa The white star shows hemorrhage, and black arrows show contraction bands. White bar = 50 µm.

11.2 Discussion

This is the first study to assess what happens histologically at various time points following US-UCA exposure. The assumption for the mechanistic motivation of US-UCA-induced angiogenesis is that it is damage driven. This study shows that it is not damage, but rather an increase in permeability, caused by the dynamic motions of the UCAs, that potentiate the increases in VEGF expression (and capillary density) noted in previous chapters.

This study showed that mere UCA oscillation (0.1 MPa) did not cause any measurable amount of damage to the muscle. Previous chapters also demonstrated that there was no increase in EBD leakage acutely and thus no angiogenic response at oscillatory pressures. However, measurable differences occur between 0.1 and 0.7 MPa, as shown histologically here, and also in Chapter 9. Along with increases in acute permeability a dramatic increase in VEGF expression presented at 0.7 MPa. Histologically, at 0.7 MPa there is no change to the muscle at 0 and 8 HPE, but by 16 HPE there are capillaries that are possibly engorged. This observation supports the notion that US-UCA induced angiogenesis is a vascular event—where the vascular endothelial cells sense the mechanical disturbance and activate increases in permeability. Chapter 9 and 10 expounded upon the regime of collapse, so it is known that about 60% of microbubbles exposed to 0.7 MPa undergo inertial cavitation (with oscillation co-occurrence). Collapse may very well enhance the mechanical disturbance that US alone provides. Heating (maximal temperature increase) at 0.7 MPa is an estimated 0.47^{o}C, and thus is insufficient to explain the difference. Related studies have assessed US and UCA induced arteriogenesis and have noted engorged capillaries (Song et al. 2004, Chappell et al. 2008), which supports the histological findings herein.

Increasing the Pr to 1.3 MPa (where there is 100% collapse) causes a paradigm shift toward damage for all time points. Multiple slides demonstrated nuclei internalization (Figure

11.2). Internalization is a nonspecific finding, but the occurrence of this event was found to increase with the Prs greater than 0.7 MPa. Also, signs of coagulative necrosis with pale pigmentation appeared at 1.3 and 1.9 MPa (Figure 11.4). Chapter 4 briefly discussed the concept of a risk/benefit for using US and UCAs to induce angiogenesis under the assumption that the therapy was driven by frank damage. However, what this chapter indicates is when damage becomes obvious histologically, the therapy is no longer beneficial. Previous chapters insinuated this by demonstrating high increases in permeability acutely that corresponded to lower VEGF expression at 5 DPE. A further increase to 1.9 MPa displays even more damage markers (Figure 11.1, 11.2, 11.3, 11.4, 11.5). The curious thing is that all of the Prs used in this study fall at or below an MI of 1.9 (AIUM/NEMA 1998, ODS 1998, NEMA 2009). Because a 1 MHz transducer was used, mechanical indices of 0.1, 0.7, 1.3 and 1.9 correspond to the 0.1, 0.7, 1.3 and 1.9 MPa Prs used respectfully. Therefore, therapeutically speaking, the MI is not necessarily a useful parameter—particularly when UCAs are involved. One study used a Pr above 0.7 MPa and confirmed therapeutic effects (Fuji et al. 2009). However, that study used a higher frequency transducer, where the collapse threshold (Pr) was greater (Ammi et al. 2006b, King et al. 2010).

The questions remain, though, if UCA collapse occurs intravascularly, why are effects seen in the tissue, and why is there no reduction in capillary density in previous chapters? Tissue level effects are seen due to US and UCA induced ischemia, resulting from damaged vasculature (Figure 11.6). Because homeostasis is the first stage in wound healing, the clotted vessel is no longer providing nutrients or oxygen to the surrounding tissue. Biologically speaking, the distance between two capillaries can be no greater than the diffusion area of oxygen for a given time frame to prevent hypoxia from developing. What is shown in this chapter is that the

myocytes are displaying damage due to lack of blood supply (Figure 11.4), and possibly high Pr and temperature generated by mass concurrent collapsing. So why is there not a corresponding decrease in acute capillary density?

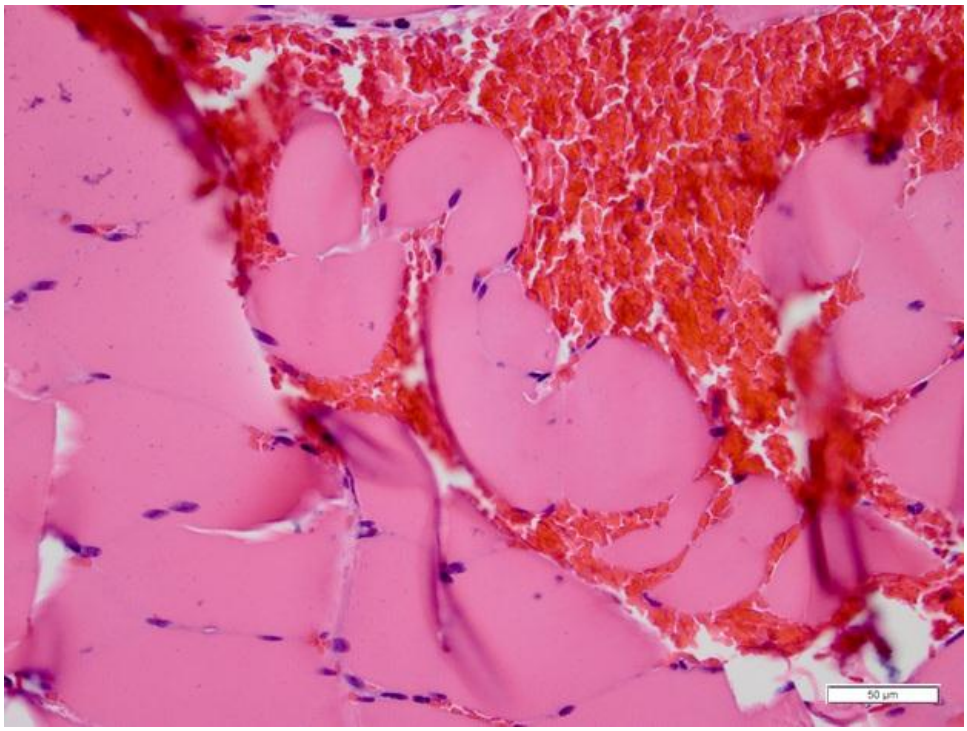

Figure 11.6: Marked hemorrhage at 8 HPE with a 1.9 MPa exposure. White bar = 50 µm.

Capillaries comprise only a portion of the conduits that carry blood and oxygen to tissues. Capillaries were assessed herein because angiogenesis begins from capillary sprouting, by their endothelial cells migrating toward regions of hypoxia, and because it is used by other similar studies. The tissue level effects could be due to damage caused to arterioles. Also, capillary density is a 2-D measurement and does not take into account the complex entanglement that is found in situ. In addition, capillary density may vary from one batch of animals to the next, and that the 0 DPE groups and 5 DPE groups were comprised of different animals. These are the reasons why VEGF expression was chosen to support angiogenesis elicitation.

Up to now, several factors for US-UCA induced angiogenesis have been investigated in terms of bioeffects leading to therapy: [UCA] , Pr, UCA collapse (Johnson et al. 2010, Johnson et al. 2011 in press, Chapter 6)), UCA biophysics, and tissue-level manifestations of exposure. From these studies it was found that: UCAs enhance US-induced angiogenesis, vascular permeability changes precede (possibly potentiate) the angiogenic response, there is a Pr-dependency, and thus collapse–dependency of the bioeffect and therapy, and that Prs > 1.3 MPa cause deleterious effects.

Even though some insight to mechanisms has been gained, US has several other parameters that have been implicated with bioeffects and therapeutic applications, such as PRF and ED. These "non-UCA" US parameters have the potential to influence angiogenesis by affecting the acute response. Therefore, the next few chapters assess PRF, ED, and total number of pulse's (NP) roles in the angiogenic response, including acute bioeffects. These chapters not only add to the understanding of US-UCA induced angiogenesis, but potentially provide optimization criteria.

CHAPTER 12: THE ANGIOGENIC RESPONSE IS INFLUENCED BY PULSE REPETITION FREQUENCY

While literature states that bioeffects have been negatively correlated to PRF and positively correlated to Pr, separate experiments confirmed that UCA collapse, which is Pr dependent, is independent of PRF (Ammi et al. 2006b, Haak et al. 2007). With that stated, a few *in vitro* studies have explored the role that PRF plays in the induction of bioeffects when UCAs are used. Buldakov (2008) reported increased cell lysis, necrosis, apoptosis, and cellular death with lower PRFs. Other detrimental bioeffects have been suggested to occur are negatively correlated to PRF (Apfel and Holland 1991, Miller and Thomas 1995; NCRP 2002, Yeh et al. 2008). In addition, studies have found nephron injury, hemolysis, extravasation, and cell sonoporation with PRFs ranging from 3.6 to 40 kHz (Skyba et al. 1998, Miller et al. 2001, 2007, Miller and Quddus 2000, Williams et al. 2007). While *in vitro* studies allowed some insight to be gleaned about the relationship between PRF and bioeffects, this insight applies only to the analogous *in vivo* case of bolus injection.

One study used an *in vivo* model with a bolus injection and gathered similar results to the in vivo studies: lower PRFs caused more of a bioeffect (extravastion) (Song et al. 2002). Another study using an *ex vivo* model found PRF to be negatively correlated with cell death and subsequent extravasation of red blood cells with UCAs being infused (Samuel et al. 2006, 2009). A logical deduction, therefore, is that *in vivo* bioeffects with infused UCAs will display similar PRF dependency.

The literature postulates that therapeutic applications of ultrasound rely on the induction of bioeffects via UCA destruction (Song et al. 2008, Chappell et al. 2008, Fuji et al. 2009). Thus far, this thesis agrees, suggesting that the anigogenic response is contingent upon acute bioeffects

and these bioeffects require collapse (Chappell et al. 2006, Johnson et al. 2010, Johnson et al. 2011 in press (Chapter 6)). The exploration of PRFs relationship to bioeffects has, for the most part, been investigated *in vitro* or *ex vivo*. No work has been done to assess the effect of PRF on subsequent therapy, however. Therefore there remains some uncertainty about the response *in vivo* and if/how it specifically relates to an angiogenic response. To address this uncertainty, this study sought to explore the effect of PRF in US-UCA induced angiogenesis both acutely (0 DPE) and at 5 DPE. Using twenty-four rats, four separate PRFs were assessed: 5, 10, 20 and 40 Hz. US exposure parameters were: Pr = 0.7 MPa, f = 1 MHz, PRF = 5, 10, 20, 40 Hz, PD = 10 μs, ED = 5 min, and 10x [UCA]. As before, bilateral sites were exposed and capillary density, vascular permeability and VEGF expression were used to characterize the responses.

12.1 Results

Capillary density

Capillary density was normalized to the control and results are displayed in Figure 12.1. Two-way ANOVA determined that DPE and DPE*PRF were not significant parameters for capillary density. However, PRF was found to be significantly different for capillary density ($p < 0.05$) (Figure 12.1). Multiple comparisons demonstrated that the 10 Hz exposure was significantly different from 40 Hz at 0 DPE ($p < 0.05$) and that 40 Hz at 0 DPE was significantly different from 40 Hz at 5 DPE ($p < 0.05$).

Evans blue dye (vascular permeability)

One-way ANOVA was used to test for significance for vascular permeability with PRF. EBD leakage was normalized to the control and is shown in Figure 12.2. PRF was a significant parameter for vascular permeability ($p < 0.001$). EBD leakage demonstrated a decreasing trend of permeability as the PRF increased (Figure 12.2). Multiple comparisons revealed that the 5 Hz

group was significantly different from the 10, 20 or 40 Hz groups, and that 20 Hz was significantly greater than 40 Hz ($p < 0.001$).

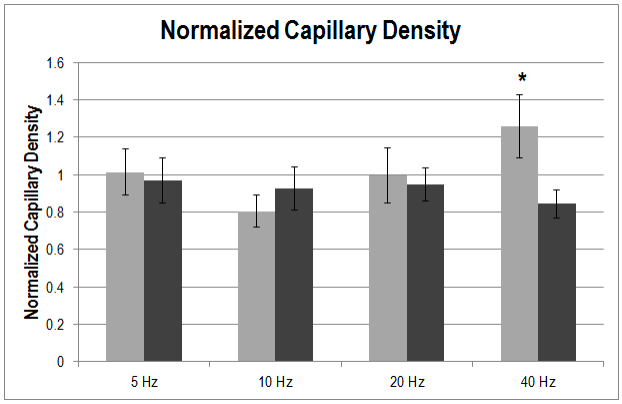

Figure 12.1: Normalized capillary density at 0 DPE (light grey) and 5 DPE (dark grey) across PRF. *$p < 0.05$ with respect to 10 Hz.

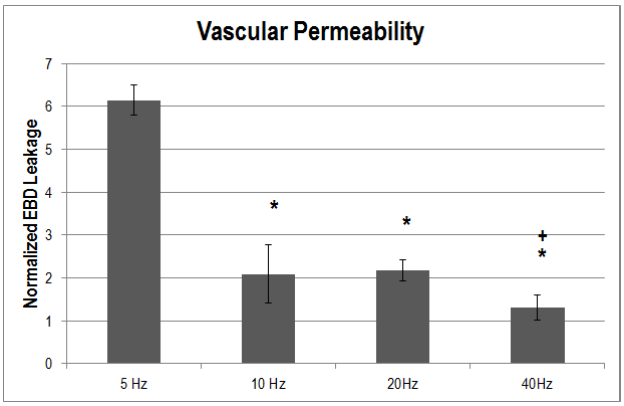

Figure 12.2: Normalized Evans blue dye as a marker for permeability at 0 DPE across PRF. *$p < 0.001$ with respect to 5 Hz, +$p < 0.001$ with respect to 20 Hz.

Vascular endothelial growth factor-A (VEGF)

VEGF expression in fold change was significant across PRF ($p < 0.05$) as determined by one-way ANOVA. The 10 Hz group had the greatest amount of VEGF expression. The VEGF expression decreased at 20 Hz and remained low at 40 Hz (Figure 12.3).

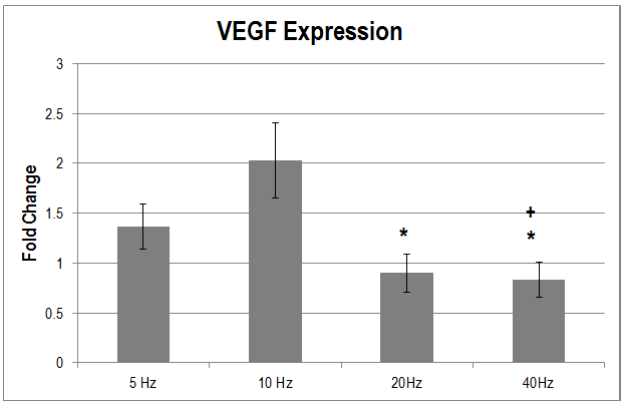

Figure 12.3: Relative VEGF expression at 5 DPE across PRF. *p < 0.01 with respect to 10 Hz, +p < 0.01 with respect to 5 Hz.

12.2 Discussion

Damage, as measured by a reduction in capillary density, was expected to occur with decreasing PRF, because vasculature refill is allowed at lower PRFs. The data agree with this notion showing that acutely as PRF decreases so does capillary density (Figure 12.1). The 40 Hz demonstrated an acute increase in capillary density, which was unexpected. EBD leakage confirms trends seen in previously published literature with higher extravasation of dye resulting from lower PRFs (Figure 12.2) (Miller and Quddus 2000). Typically, lower PRFs (~ 10 Hz) are used when UCAs are infused to allow refill of the vasculature at the site of exposure. If pulsing occurs too often, the [UCA] effectively decreases. Studies have shown that PRFs $\leq$ 100 Hz, over time does not afford sufficient refill, and thus effects dwindle to noise levels with exposure durations in excess of 20 ms (Samuel et al. 2009).

Though the 5 DPE capillary densities remained constant across PRF, VEGF displayed a trend that suggests there is an optimal PRF window at ~ 10 Hz for angiogenesis induction (Figure 12.1 and 12.3). Capillary density was chosen as a marker for angiogenesis because it has repeatedly been used in similar literature and confirmed to be positively correlated with tissue perfusion (Korpanty et al. 2005,Chappell et al. 2006, Barzelai et al. 2006, Chappell et al. 2008).

However, as previously mentioned, capillaries form complex networks, and histological assessment only provides a two-dimensional account, VEGF expression was also used.

VEGF is a well-known pivotal player in angiogenesis. VEGF is present throughout the process of the angiogenic response, peaking at about 4-7 days in first intention wound healing (Bates et al. 2002, Mariotti et al. 2006, Barrientos et al. 2008). The data herein show that VEGF levels did reach significance, which has been shown to occur with exposure to ultrasound (Reher et al. 1999, Korpanty et al. 2005, Barzelai et al. 2006). Because higher levels of VEGF were expressed at lower PRF values and lower PRFs are associated with increased bioeffects, this supports that therapy is motivated by vascular permeability changes.

Like PRF, exposure parameters like exposure duration (ED) may also influence the response. In an effort to optimize the therapy and assess the risk/benefit of long vs. short exposures, the next chapter examines ED.

CHAPTER 13: EXPOSURE DURATION IMPACTS ACUTE PERMEABILITY BUT NOT THE ANGIOGENIC RESPONSE

One of the main considerations for therapeutic application of US and UCA is time. US therapy includes two time properties: pulse duration (PD) and exposure duration (ED). It is a well-known fact that as PD and ED increase so does the temperature at the site of exposure (Fry and Fry 1953, Nyborg et al. 1981, Cavicchi and O'Brien 1984). As PD is raised, it approaches continuous wave US, and could cause burning, ablation, or necrosis of tissue. Though PD has not directly been explored for US-UCA induced angiogenesis, it has been explored via various bioeffects studies and has been shown to be positively correlated with pressure in both theoretical calculations, *in vitro* assessments and *in vivo* studies (Vykhodtseva et al. 1994, Kinsler et al. 2002). The therapeutic range of PDs therefore is typically on the millisecond or even microseconds range when UCAs are used (Song et al. 2004, Chappell et al. 2006). While PDs are relatively consistent, EDs vary significantly ranging from 1 second to 20 minutes (Reher 1999, Miller 2005, Chappell et al. 2008, Kruse et al. 2008, Vancraeynest et al. 2009).

ED is of particular interest because not only is the length of exposure correlated to an increase in bioeffects and temperature (Vykhodtseva et al. 1994), but therapeutically speaking shorter treatments are more favorable for both the patient and provider. Longer EDs allow for more UCA-vessel interaction. This increased interaction owing to increased time can potentially cause more damage after a sufficient amount of time has lapsed. Miller et al. (2008) reported that for increments of ED below 3 minutes, there is no correlation with bioeffects but a positive correlation appears as the duration exceeds this value. Another study suggested that in cardiac tissue, EDs of 9 minutes resulted in an approximate 10% mortality of rats and that EDs in excess of 30 minutes resulted in an 80% mortality rate (Vancraeynest et al. 2009). However, 1 second

exposures were reported to cause bioeffects in a transgenic mouse model (Kruse et al. 2008), and 90 seconds was required to induce angiogenesis in a cardiac model (Zen et al. 2006). Therapeutic applications typically use EDs $\leq$ 5 minutes (Chappell et al. 2006, Zen et al. 2006, Miyake et al. 2007). From the mentioned studies, one can observe the discrepancy with the ED required for bioeffect induction and therapy.

Therefore, in an effort to extend the exploration of US and UCA induced angiogenesis, this study sought to examine the effect of reducing the ED on both bioeffects and the angiogenic response. Using twenty-four rats, four EDs were explored: 30 seconds, 1, 2, and 4 minutes. This range was chosen as to minimize the effects of heating. Bilateral sites were exposed; medial sites served as the control. Capillary density, EBD and VEGF expression were used to quantify the responses. US exposure parameters were: Pr = 0.7 MPa, PRF = 10 Hz, PD = 10 μs, ED = 30s, 1, 2, or 4 min, and 10x [UCA]. The 5 min data from previous studies with the same exposure conditions was added to the graphs, but was not included in statistical analyses.

13.1 Results

Capillary density

Capillary density was normalized to the control and is shown in Figure 13.1. DPE nor ED was found to be significant for capillary density ($p = 0.05$ and $p > 0.05$, respectively) with two-way ANOVA (Figures 13.1).

Evans blue dye (vascular permeability)

EBD leakage was normalized to the control value and is shown in Figure 13.2. One-way ANOVA determined EBD leakage to be significant across ED ($p < 0.01$). EBD demonstrated a decreasing trend of vascular permeability as the ED increased up to 2 minutes (Figure 13.2).

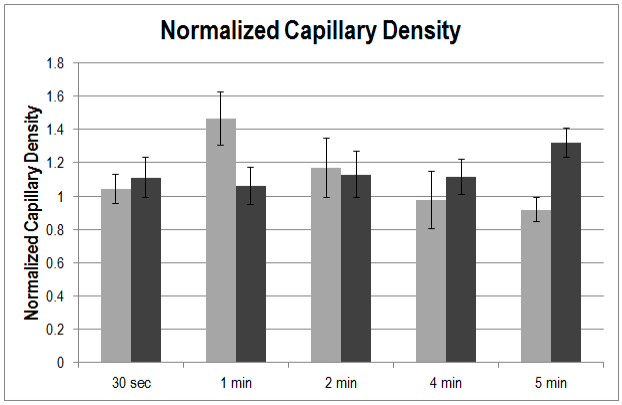

Figure 13.1: Normalized capillary density at 0 DPE (light grey) and 5 DPE (dark grey) across ED.

Multiple comparisons showed that the 2 min ED was significantly different from the 30 seconds or 1 minute group ($p < 0.01$) for vascular permeability.

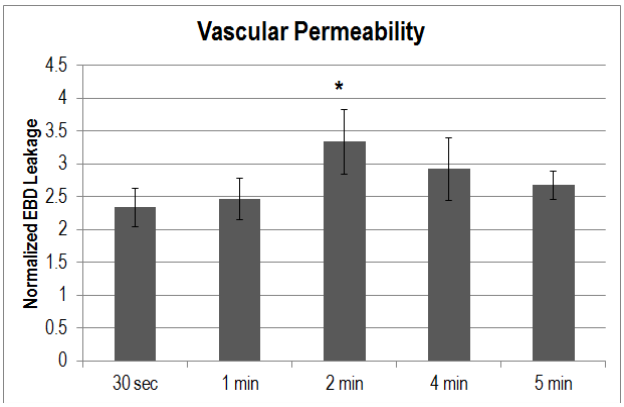

Figure 13.2: Normalized Evans blue dye as a marker for permeability at 0 DPE across ED. *$p < 0.01$ with respect to 30s and 1 minute.

Vascular endothelial growth factor-A (VEGF)

VEGF expression was not significant across ED ($p > 0.05$) when tested using one-way ANOVA (Figure 13.3).

13.2 Discussion

This study examined four separate EDs to determine if the angiogenic response depended on length of exposure. Of the assessments only vascular permeability was found to be significant.

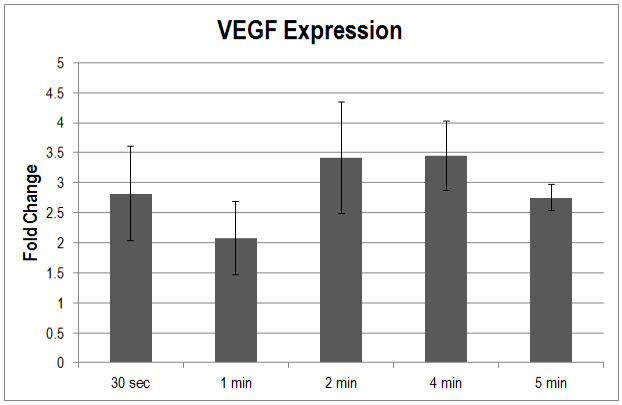

Figure 13.3: Relative VEGF expression at 5 DPE across ED.

The introduction mentioned PD as a significant time factor for US, however numerous studies that observe PDs correlation to UCA collapse show no or weak influence (Ammi et al. 2006b, Haak et al. 2007, Church et al. 2005). Because collapse is the suggested cause of the induction of bioeffects and, by extension, the angiogenic response, PD, by itself presumably has no influence on angiogenesis. In addition, PD is mathematically proportional to the acoustic pressure at which exposures occurs by:

$$I_{TA} = I_{PA} * \tau = p^2 \tau / (2\rho c) \quad (13.1)$$

$$\tau = PD * PRF \quad (13.2)$$

$$p^2 = (2\rho c) * (PD * PRF) * I_{PA}, \quad (13.3)$$

$$p^2 \; \alpha \; PD \quad (13.4)$$

where I_{TA} is the temporal average intensity, I_{PA} is the pulse average intensity, τ is the duty factor, p is the acoustic pressure, ρ is the density of the medium and c is the speed of sound in the medium, PD is pulse duration, and PRF is pulse repetition frequency. It has previously been determined that pressure and bioeffects and (UCA collapse) are positively correlated quantities (Johnson et al. 2011 in press (Chapter 6), Chapters 7-9).

While ED has no direct impact upon UCA collapse thresholds, it does increase the amount of time that vasculature and tissue is exposed to collapsing microbubbles, presumably allowing more time to induce bioeffects. US-UCA induced angiogenesis has been linked to both UCA collapse and bioeffects. Therefore, it was hypothesized that ED would be positively correlated to bioeffects and that effect would be propagated through to the therapeutic end goal.

The 5 min ED from previous studies demonstrates agreement with the findings hereing The 4 min ED begins to show an increase in capillary density at 5 DPE (with respect to 0 DPE), but it is not significant. The separation is more apparent at 5 min because this data is averaged from all previous experiments, thus has a larger N and smaller standard error. Likewise the 5 min ED's VEGF expression overlaps with the 4 min ED.

To keep temperature increases from confounding the results, the range of EDs used with the other parameters chosen in this study was 0 to 4 minutes. Previous studies suggest that the angiogenic effect is provoked by bioeffects and an increase in permeability (bioeffect) was seen, but we do not see this translating to an angiogenic response for 5 DPE capillary density or VEGF expression. The relatively small window of EDs chosen for this study might have been a reason for low significance.

ED has not been investigated with respect to US-UCA induced angiogenesis; therefore it is difficult to compare results gathered herein to other studies. This study does not agree with the finding that EDs below 3 minutes do not show correlation to bioeffects, with a 2 min ED showing the most EBD leakage. This study does, however agree with other US-UCA therapeutic studies in that the 'therapeutic range' falls somewhere between 2 and 5 minutes (Chappell et al. 2006, Zen et al. 2005) (Figure 13.1 and 13.3).

More so than PD or ED, physical parameters like number of pulses (PRF * ED) show significance (O'Brien et al. 2005, Song et al. 2002). But, by varying ED, the number of pulses is also varied. The next chapter provides an assessment of the number of pulses and duty factor to determine the effect of the combined terms with US-UCA induced angiogenesis.

CHAPTER 14: COMMENTARY ON NUMBER OF PULSES AND DUTY FACTOR

Previous chapters discussed the role of UCAs, PRF and ED in the induction of bioeffects and subsequent angiogenesis. Chapter 13 briefly discussed the possibility that combination terms such as number of pulses (NP) and duty factor (DF) may also play a role in the response. These parameters, while not directly examined, were assessed, by varying the intrinsic parameters. The two equations below describe the intrinsic parameters of NP and DF.

$$NP = ED * PRF \quad (14.1)$$

$$DF = PD * PRF \quad (14.2)$$

where ED is exposure duration, PRF is pulse repetition frequency and PD is pulse duration. Because PRF was varied in Chapter 12 and ED in Chapter 13, this chapter will discuss the implications of those results to NP and DF.

14.1 Number of pulses

Number of pulses has not been directly explored with respect to US-induced angiogenesis and only limited work is available for bioeffects when UCAs are used. While the NP is a non UCA effect, the more pulses generated would likely increase the incidence of bioeffects. One study using EDs ranging from 100 to 10000 ms, and PRFs ranging from 10 to 1000 Hz compared only two NPs (100 and 250) *in vitro* (Samuel et al. 2009). A NP = 250 created a smaller area of extravasation than did NP = 100 (Samuel et al. 2009), when only PRF was decreased, suggesting that more pulses causes a lesser effect. Samuel et al. (2009) states that "the reduced effect at high PRF may indicate that there is a required ED (>10 ms but < 100ms) for an effect. In cross comparing studies, one finds that bioeffects such as hemorrhage, cell lysis, and cell death are correlated to NP. One study, assessed the influence of the PRF on extravasation, and found that

as PRF decreased from 1 to 0.1 Hz, the extravasation points increased by 2000% at 0.2 Hz (Song et al. 2002)! Another study that used a PRF of 0.25 Hz and reported an increase in vascular permeability that was 100% higher than leakage measured in a group without UCAs (Bohmer et al. 2010). Unfortunately, Song et al.(2002) nor Bohmer et al.(2010) provide information about the ED; but with the given material there is a notable disagreement in the level of bioeffect reported from their studies.

Chappell et al. (2008) used a NP of 54 (PRF = 0.2 Hz, ED = 4.5 min) and showed 100% greater flow and increased arteriogenesis with respect to the study's control, and Fuji et al. (2009) used 2400 pulses (PRF = 2 Hz, ED = 20 min) to demonstrate 150% increases in capillary density and a 400% increase in arteriolar density with respect to the experimental control associated with US-UCA exposure, but neither study provides information regarding the acute effects.

A decrease in PRF is analogous to decrease in NP, thus this study leads one to the conclusion that NP is negatively correlated with bioeffects. However, when ED was assessed, the amount of cardiomyocytes injured increased when increasing ED from 5 min to 20 min exposures, as did the number of petechiae (Miller et al. 1998, 2005). An increase in ED also corresponds to an increase in NP and thus, these studies show NP to be positively correlated with bioeffects.

The studies in Chapter 12 and 13 used NP = 300 to 12000. When combining the data, for the acute bioeffect we find that there is no discernable trend across NP for 0 DPE capillary density, but EBD leakage (vascular permeability) increases up to 1500 pulses, and then decreases, suggesting an optimal number of pulses for increases in permeability (Figure 14.1, Figure 14.2, Table 14.1).

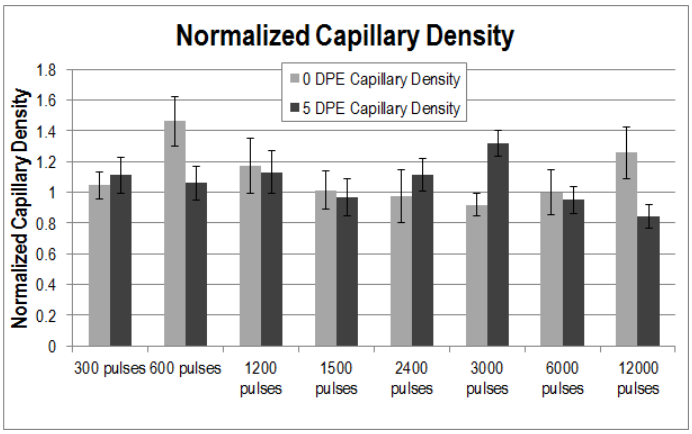

Figure 14.1: Normalized capillary density at 0 DPE (light grey) and 5 DPE (dark grey) from Chapters 12 and 13 across the total number of pulses.

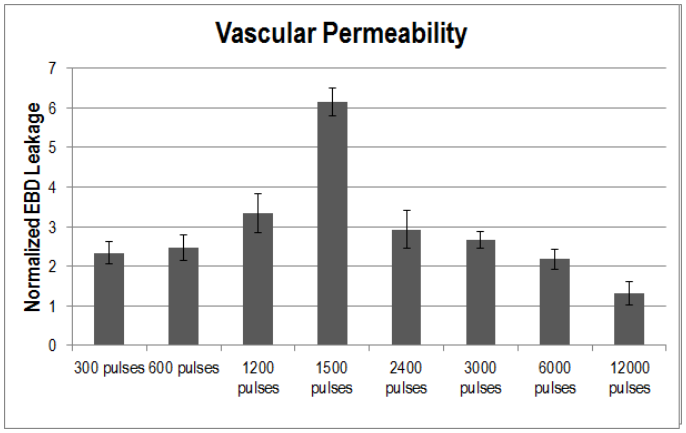

Figure 14.2: Normalized Evans blue dye as a marker for permeability at 0 DPE from Chapters 12 and 13 across the total number of pulses.

Table 14.1: Combination of acutely measured bioeffects seen in Chapter 12 and 13 across the total number of pulses: Normalized 0 DPE capillary density and normalized EBD leakage.

NP	Normalized Capillary Density (0 DPE)	Normalized EBD leakage (permeability)
300	1.0 ± 0.1	2.3 ± 0.3
600	1.5 ± 0.2	2.5 ± 0.3
1200	1.2 ± 0.2	3.4 ± 0.3
1500	1.0 ± 0.1	6.2 ± 0.5
2400	1.0 ± 0.2	2.9 ± 0.3
3000	0.9 ± 0.1	2.7 ± 0.5
6000	1.0 ± 0.1	2.2 ± 0.2
12000	1.3 ± 0.2	1.3 ± 0.3

Because bioeffects were not the end goal of this study, but rather determining the potentiator of US-UCA-induced angiogenesis, examining how the NP affects the acute effects with respect to the response seen at 5 DPE is important. Thus far it has appeared that, to some extent, angiogenesis is driven by increases in acute permeability, but it should be noted that this increase is not without limitation. As shown in Chapter 7, when permeability was very high (at 0 DPE) the subsequent measure of VEGF expression at 5 DPE was low.

When observing the therapeutic response, we find that 1500 pulses is not necessarily effective for inducing angiogenesis (Table 14.2, Figure 14.3).

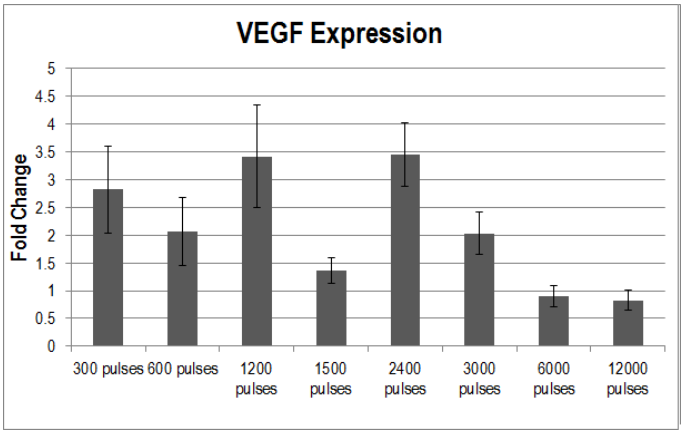

Figure 14.3: Relative VEGF expression (in fold change) across the total number of pulses.

Table 14.2: Combination of 5 DPE assessments for the angiogenic responses seen in Chapter 12 and 1 across the total number of pulses: Normalized 5 DPE capillary density and VEGF expression in fold change.

NP	Normalized Capillary Density (5 DPE)	VEGF (angiogenesis)
300	1.1 ± 0.1	2.8 ± 0.8
600	1.1 ± 0.1	2.1 ± 0.6
1200	1.1 ± 0.1	3.4 ± 0.9
1500	1.0 ± 0.1	1.4 ± 0.2
2400	1.1 ± 0.1	3.5 ± 0.6
3000	1.3 ± 0.1	2.0 ± 0.4
6000	1.0 ± 0.1	0.9 ± 0.2
12000	0.8 ± 0.1	0.8 ± 0.2

The trend across capillary density remains relatively constant across NP, peaking at 3000 pulses. VEGF expression however varies, being generally higher at lower NP. Thus, there appears to be a range of NP for which angiogenesis is optimal, with a preference for lower NP.

Therefore, the data suggests that NP $\leq$ 3000 is sufficient for angiogenesis induction, which further reinforces the notion that there is an optimal amount of vascular perturbation required to elicit an angiogenic response.

14.2 Duty factor

This thesis did not directly address PD due to its relationship to output pressure. An *in vitro* calibration (see Chapter 5) of several power output settings at PD = 1, 5 or 10 µs, and for PRF = 1, 10 and 100 Hz was conducted to determine how these parameters affected Pr (Figure 14.4). This calibration revealed a trend for Pr with PD. As PD was increased from 1 to 10 µs, regardless of PRF and power setting, the calibrated pressure was higher with higher PD. The trends across the power output remains relatively constant with varying PRF, although at higher power settings variation appears with PD = 10 µs.

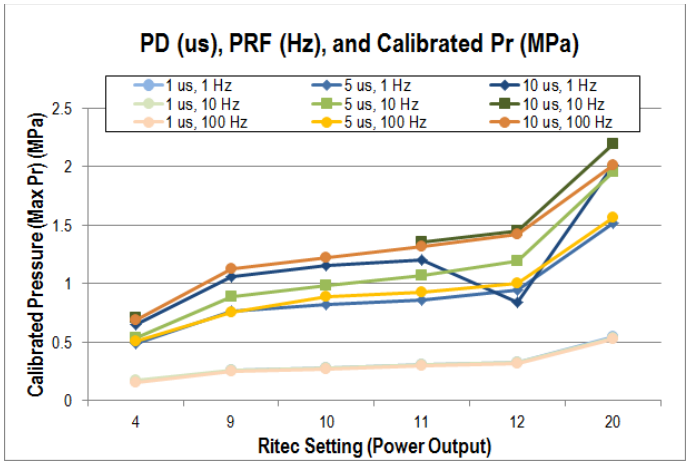

Figure 14.4: Pulse duration, pulse repetition frequency and calibrated pressure. The PD = 1 µs groups were very similar and overlay one another.

Interestingly, if we look at this same data in terms of duty factor (DF), a clear trend with duty factor can be seen as well (Figure 14.5). Literature has shown that the 'total time on' or the duty factor is related to intensity, power and pressure, and this experiment attributes the relationship to PD. A few studies have directly examined DF in terms of bioeffects. It is expected that a higher DF (ie. more "on" time) would cause an increase in the amount of bioeffects reported, because UCAs are perturbed for longer durations with for a fixed ED, as seen in the *in vitro* study (Figure 14.5).

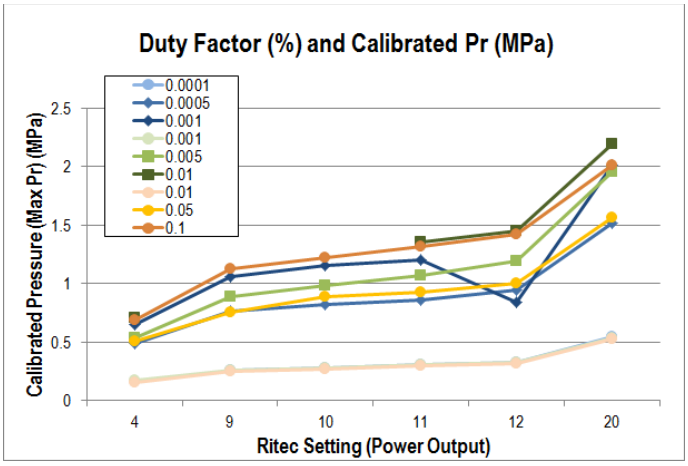

Figure 14.5: Duty Factor vs. Calibrated pressure. Figure 14.4 represented in terms of DF (%).

One study showed that the number of petechiae induced by US-UCA exposure increased with increasing duty factor (DF = 0.1 to 1%) (Miller and Gies 1998). However, further increases in DF showed no difference from 1% (Miller and Gies 1998). The more closely spaced pulses were speculated to cause significant changes in the bioeffect, because it increases the Pr. Another study examined 5, 10 and 15% DF and found counterintuitive results as well. Higher DF caused more cell lysis than a 10% DF, but this effect did not hold true for sonoporation (increases in cellular permeability) activity (Ward et al. 1999). In the same study, however, the

5% DF case demonstrated significantly higher percentage of cellular lysis than the 10% DF case (Ward et al. 1999).

Duty factors ranging from 2 x 10^{-3} to 0.5% (Chappell et al. 2005, Hwang et al. 2005) have been used for bioeffects as well as therapeutic studies. Vascular endothelial cell effects including increased calcium permeability, reactive oxygen species generation, and cytoskeleton rearrangements were reported using a DF = 0.2% (Juffermans et al. 2009). These effects were confirmed by a different study *in vivo* that found extravasation and endothelial cell damage with a DF = 0.22% (Hwang et al. 2005). Other therapeutic studies found increased healing of varicose ulcers at DF = 2%, enhanced cardiac function (with increased vascular density) with DF = 50%, and increased angiogenesis at DF = 2 x 10^{-3}% (Dyson et al. 1976, Chappell et al. 2005, Song et al. 2008). This thesis uses a DF = 1 x 10^{-2}% for most of the studies, varying only in Chapter 12 when PRF was assessed (DF = 5 x 10^{-3}% – 4 x 10^{-2}%). This range was quite small to prevent the reported effects of heating (PD effect) and allow UCA refill (PRF effect) (Table 14.3). The range of DFs capable of inducing an angiogenic response suggests that the optimal range for this parameter is on the order of 10^{-2}% (Figure 14.6—14.8).

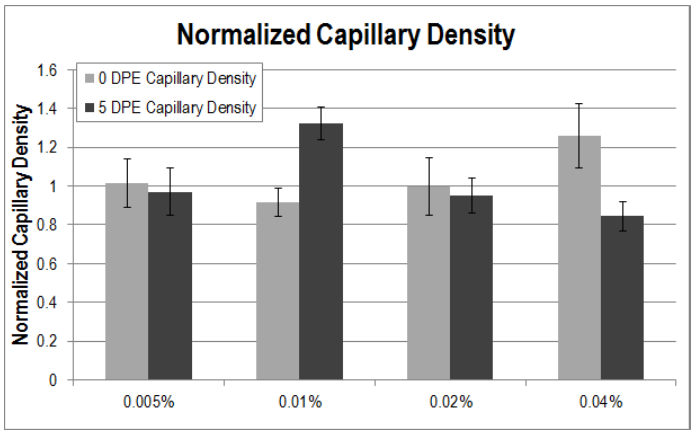

Figure 14.6: Normalized capillary density at 0 DPE (light grey) and 5 DPE (dark grey) across DF (%)

Table 14.3: DF's effect on US-UCA-induced bioeffects and angiogenesis				
DF (%)	Normalized Capillary Density (0 DPE)	Normalized EBD leakage (permeability)	Normalized Capillary Density (5 DPE)	VEGF (angiogenesis)
5×10^{-3}	1.0 ± 0.1	6.15 ± 0.3	1.0 ± 0.1	1.4 ± 0.2
1×10^{-2}*	0.9 ± 0.1	3.0 ± 0.2	1.3 ± 0.1	2.9 ± 0.4
2×10^{-2}	1.0 ± 0.1	2.2 ± 0.2	0.9 ± 0.1	0.9 ± 0.2
4×10^{-2}	1.3 ± 0.2	1.3 ± 0.3	0.8 ± 0.1	0.8 ± 0.2

* average normalized value across parameter matched studies in Chapters 7-13.

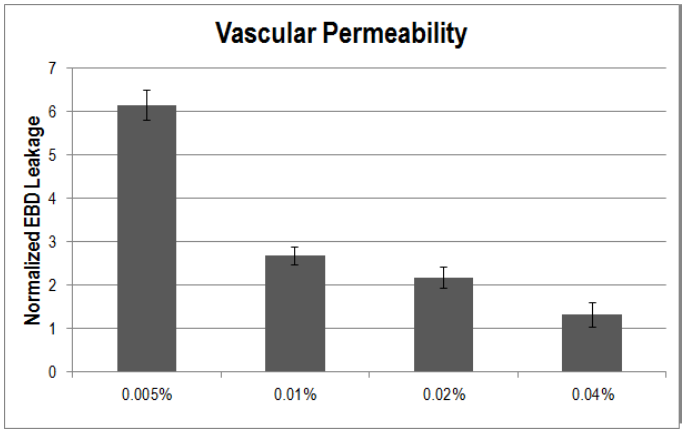

Figure 14.7: Normalized Evans blue dye as a marker for permeability at 0 DPE across DF (%).

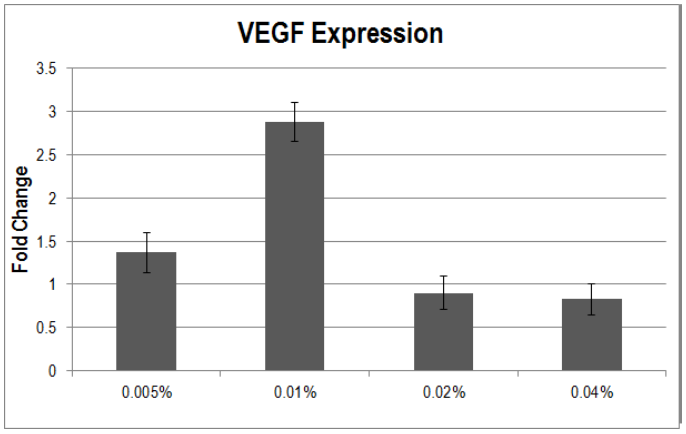

Figure 14.8: Relative VEGF expression (in fold change) across DF (%).

CHAPTER 15: CONCLUSIONS

All of the data gathered herein lead to several conclusions: 1) UCAs increase the angiogenic response, 2) UCA collapse is required for the increased angiogenic response, 3) increases in vascular permeability occur acutely with collapse, 4) shear stresses during exposure are likely involved in the induction of acute bioeffects, 5) Prs equal to or greater than 1.3 MPa demonstrate a deleterious effect, and 6) the coincidence of increased VEGF expression and capillary density at 5 DPE corresponds relatively well to the increases in capillary permeability. These findings suggest there is an appropriate [UCA], Pr, PRF, and bioeffect level that yields optimal angiogenesis. This compilation of studies not only provides some biophysical mechanistic information but also a bit of predictive information when determining appropriate settings for US-UCA induced angiogenesis.

Ultrasound exposure has the potential to stimulate an angiogenic response. When UCAs are added, the progression of the response is disturbed, particularly when collapse occurs. The results in chapter 6 suggested that a mechanical effect of US and UCAs elicit angiogenesis via inflammation and increased VEGF expression. It, however, was of particular interest to determine the role that the [UCA] played in the response, because some of the responses of US-UCA exposure were close to the control value.

Chapter 7 indicated that [UCA] demonstrates a significant effect not only in the acute bioeffects, but also in the subsequent angiogenic response. Both initial and angiogenic responses are positively correlated with the concentration of microbubbles (0x, 1x, 5x, and 10x, see Chapter 7) present during infusion. Beginning with a suggested mechanically induced 3 fold increase in permeability, almost a 20% increase in capillary density between the 0 DPE and 5

DPE group at 10x [UCA] and a 3 fold increase in VEGF expression was found (Figure 15.1). With these findings the acoustic pressure response was revisited in Chapter 8.

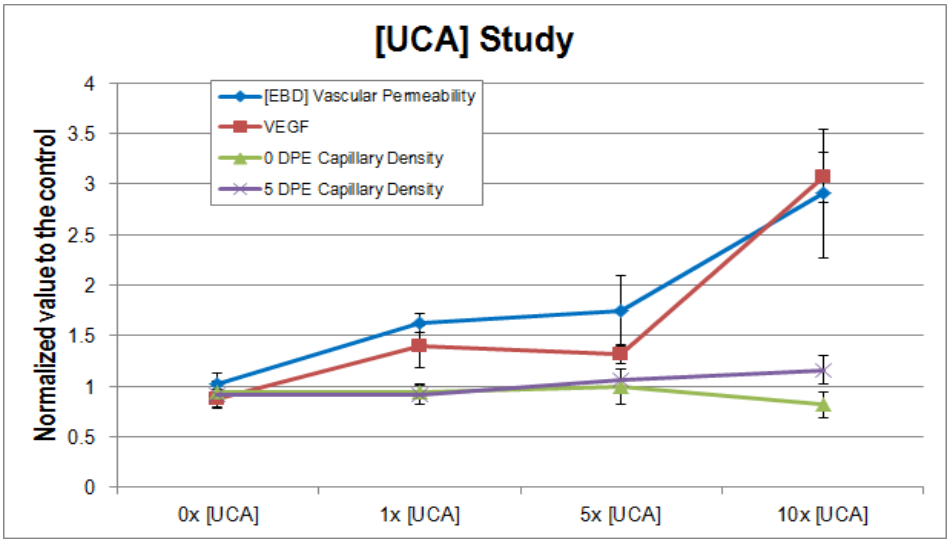

Figure 15.1: Normalized EBD, VEGF, and capillary density mean values. A value of 1 indicates the experimental group was equivalent to the control. Pr = 0.7 MPa, PRF = 10 Hz, PD = 10 µs, ED = 5 min.

The angiogenic response is dependent upon Pr. Once Pr approaches established mechanical index limits, the angiogenic response is stifled and shows reduced levels of VEGF expression. While acute capillary density was unaffected, increases in acute permeability seem to potentiate increases in capillary density at 5 DPE and increased VEGF expression at mid-range Prs (Figure 15.2). This study demonstrated up to a 9 fold increase in vascular permeability (EBD) that corresponded with decreases in VEGF expression at 1.9 MPa. However when VEGF expression peaks, at 0.7 MPa, we also see a significant increase in the 5 DPE capillary density. Because angiogenesis was measured at 0.7 MPa, but not 0.1 MPa this study suggests that a particular amount of UCA collapse is required. Further investigation was required to examine the necessity of collapse.

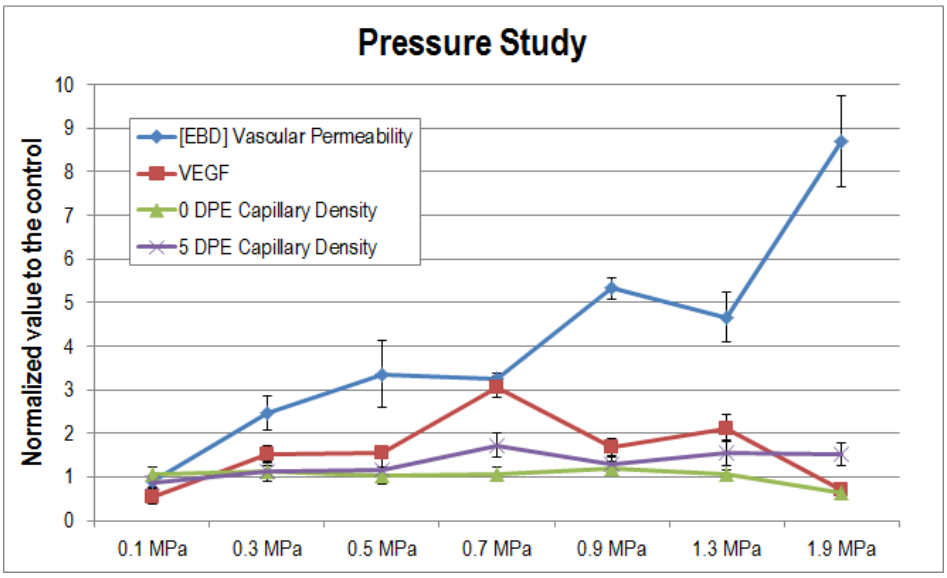

Figure 15.2: Normalized EBD, VEGF, and capillary density mean values. A value of 1 indicates the experimental group was equivalent to the control. [UCA] = 10x, PRF = 10 Hz, PD = 10 µs, ED = 5 min.

Chapter 9 took a closer look at collapse by narrowing the range of Prs. An increase in acute permeability does not necessarily mean that a measurable amount of angiogenesis will occur, however, the vascular permeability trend does agree with the collapse threshold of the UCA used in this study. This suggests that UCA collapse causes an increase in vascular permeability, and that it is collapse that mechanistically motivates the angiogenic response. The angiogenic response was not detected until 0.7 MPa was reached, which suggests that the UCA collapse occurrence must reach approximately 60% for this therapeutic purpose. The UCA collapse may produce minor disruption to the vascular endothelium, but it does not result in a decrease in capillary density.

Also, in comparing the increases in VEGF and EBD at corresponding Pr, there is agreement between separate studies. Whereas the normalized values for 0.1 MPa tend to cluster around the control value for all measurements, and 0.7 MPa demonstrates approximately a 3 fold increase in vascular permeability and VEGF expression. When studying a range of Pr, it is important to ensure that temperature increases remain low. Table 15.1 shows the approximate

maximal temperature increases with all of the pressures used. The temperature estimates are calculated for the total time on and thus do not take into consideration the pulsed nature of the exposure. The estimates also assume that there is no heat removal process which is not necessarily the case for a 5 minutes exposure. Because UCAs are being infused, and the rat cardiac output is approximately 200 mL/min (Gotshall et al. 1987), there is about 500 mL of blood that passes the exposed region during the experiment.

Pr (MPa)	**ΔT_{max} (^{0}C)**
0	0
0.1	0.01
0.3	0.09
0.5	0.24
0.7	0.47
0.9	0.78
1.3	1.62
1.9	3.45

Table 15.1: ΔT_{max} for all pressures used in Chapters 6, 7, 8 and 9.

Chapter 10 examined the biophysical mechanisms behind the acute bioeffects and angiogenic response, while relating biological events to specific UCA dynamics. The trends for UCA collapse and vascular permeability were confirmed to be similar, and the onset of radial expansion beyond two, corresponded with the Pr where VEGF expression demonstrated significant decreases. In an effort to correlate oscillation and collapse to tissue-level effects, a histological study was completed. By looking at several time points one can not only gather information regarding a risk/benefit analysis, but also bioeffects that are not acutely present can be evaluated.

Therefore, the next chapter measured the effects of US and UCA exposure at several time points. Chapter 11 showed a histological study assessing tissue effects at 0, 8, 16 and 24 HPE.

Coagulative necrosis, nucleus internalization and contraction bands were all present when Pr $\geq$ 1.3 MPa. This histological study confirmed the suggestions made by previous chapters in that there exists a range of US exposure parameters that facilitate angiogenesis induction, beyond which tissue-level damage becomes apparent.

The exposures are pulsed; therefore pulse repetition frequency was tested to determine if it was an important modulator of bioeffects when UCAs are used. Because research suggests, and Chapter 12 supports, that these bioeffects potentiate therapy, PRF may play an important role in the induction of an angiogenic response. The data in Chapter 12 indicates that lower PRFs results in both higher acute permeability and VEGF expression at 5 DPE. The data in Figure 15.4 is normalized to the 5 Hz data set because the objective was to determine if the PRF value was a significant factor. The EBD leakage decreases with respect to 5 Hz when 10 Hz is used, but we can see that capillary density (5 DPE – 0 DPE) increases at this time point. VEGF expression also declines with PRFs above 10 Hz (Figure 15.3). Temperature estimates were also calculated for this study and are displayed in Table 15.2 below.

PRF (Hz)	**ΔT_{max} (^{0}C)**
5	0.23
10	0.47
20	0.94
40	1.88

Table 15.2: ΔT_{max} for all pressures used in Chapter 12.

Chapter 13 focused on the exposure duration to investigate its effect on angiogenesis. This study showed that ED is not a significant parameter for US-UCA-induced angiogenesis. ED is, as reported by other studies, significant for eliciting bioeffects acutely, however.

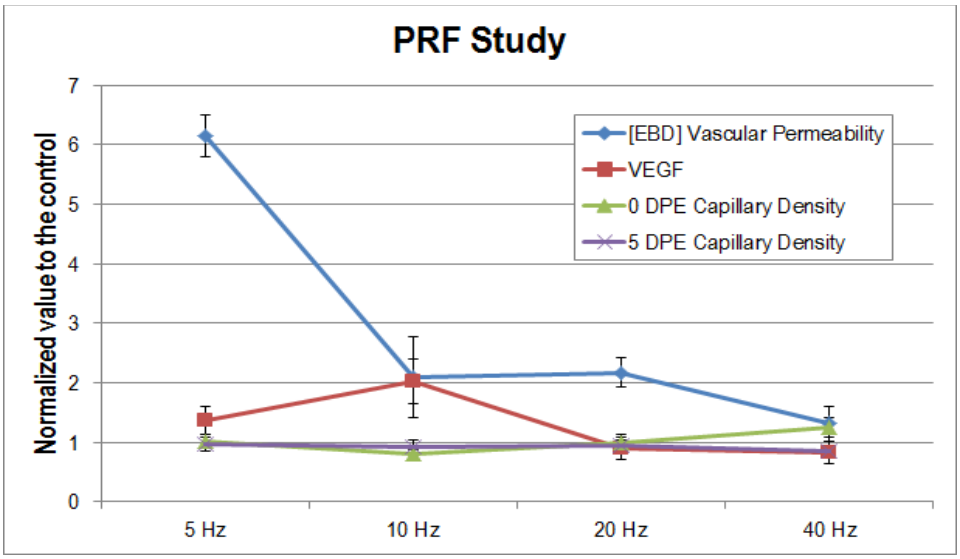

Figure 15.3: Normalized EBD, VEGF, and capillary density mean values. A value of 1 indicates the experimental group was equivalent to the control. Pr = 0.7 MPa, [UCA] = 10x, PD = 10 μs, ED = 5 min.

Figure 15.4 shows the trends in data with respect to the lowest time for exposure, 30 seconds (0.5 min). The EBD leakage increases at 2 min of exposure with respect to the 30 second exposure, but the capillary density and VEGF expression do not reach significance.

Because exposure duration also affects the maximal temperature increase, the estimates are reported in Table 15.3. None are sufficient for effects to be attributable to heating.

ED (s)	ΔT_{max} (^{0}C)
30	0.05
60	0.09
120	0.20
240	0.38

Table 15.3: ΔT_{max} for all pressures used in Chapter 10.

Finally, Chapter 14 discussed the total number of pulses and duty factor with respect to the acute and angiogenic responses. For the studies conducted herein, the optimal window for the angiogenic response was a NP $\leq$ 3000 and a DF on the order of 10^{-2}%.

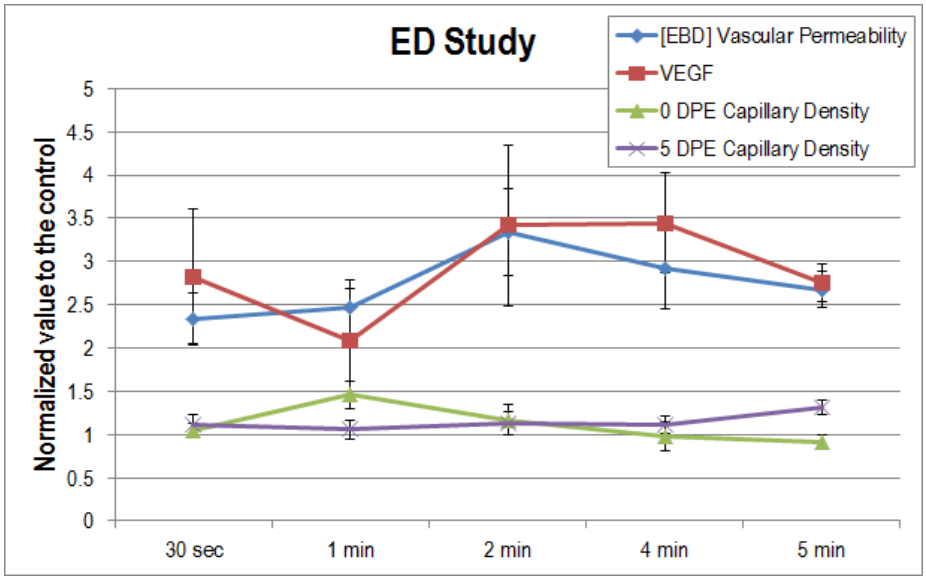

Figure 15.4: Normalized EBD, VEGF, and capillary density mean values. A value of 1 indicates the experimental group was equivalent to the control. Pr = 0.7 MPa, [UCA] = 10x, PD = 10 μs, PRF = 10 Hz.

According to all findings, a Pr ~ 0.7 MPa, PRF ~ 10 Hz, and ED between 2 to 5 minutes demonstrates the greatest angiogenic response. The theoretical simulations, in vitro experiments and in vivo angiogenic experiments agree that at pressures in excess of 0.9 MPa, vascular permeability increases significantly and VEGF expression decrease significantly. Further, the histological study shows that once pressure levels reach 1.3 MPa there are significant deleterious effects. Thus all the results support that it is not necessarily damage, but rather an increase in permeability, caused by a combination of UCA oscillation and collapse eliciting mechanical disturbances to the vasculature, that potentiate the increases in VEGF expression (and capillary density at 5 DPE) noted herein.

CHAPTER 16: SPECULATION

The work presented herein verified that US and UCAs can be used to induce noninvasive and spatially specific an angiogenic response. In doing so, the mechanisms of US-UCA-induced angiogenesis were explored connecting ultrasound, the underlying physics of the ultrasound contrast agents to the bioeffects and then relating those bioeffects to the end goal of an angiogenic response. Thus, the work addressed two of the cited reasons for slow clinical transition: connection of the acute bioeffects to subsequent angiogenic response and exploring a physical mechanism.

It was originally hypothesized that: [UCA] increases would increase (enhance) the angiogenic response above that of saline only infusion, that IC would acutely reduce capillary density cause hemorrhage and tissue damage leading to angiogenesis, that microstreaming would cause increases in permeability, but not angiogenesis, and that TNP, but not ED or PRF would be positively correlated to the angiogenic effect. The study found that UCAs do, in fact, enhance the angiogenic response, and that IC is required for the response, but permeability, hemorrhage or tissue damage could elicit the angiogenic response. It was also found that IC caused increased acute permeability, not necessarily microstreaming, though shear stresses from oscillation reached sufficiently high values to perturb vascular endothelial cells. Pressure was also found to be correlated with the acute and angiogenic response with pressures greater than 1.3 MPa causing significant tissue damage. Optimization parameters PRF and TNP, but not ED demonstrated significance for the angiogenic response.

This examination also revealed two types of therapeutic treatments: one set of parameters optimal for drug delivery, demonstrating increased vascular permeability without significant tissue damage (low Pr), and another set of parameters optimal for secondary-wound healing

angiogenesis, where damage is created (at high Pr) (Figure 16.1). These findings make the work relevant to not only researchers attaching growth factors, stem cells, and other therapeutic agents to contrast agents for site specific delivery, but also to those who use US and UCAs for ablation or cancer treatment applications.

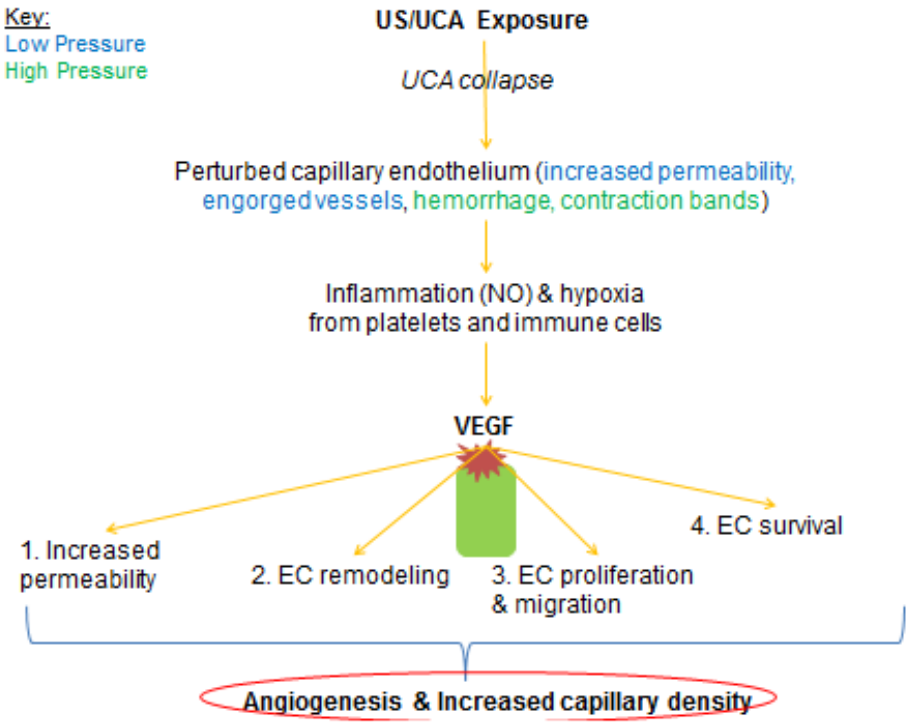

Figure 16.1: Two-fold flow of US-UCA induction of angiogenesis contingent upon UCA collapse.

This work found that low pressures (0.3 to 0.7 MPa) increase vascular permeability, and this range of pressures were also correlated to 15 to 60% collapse, therefore it is speculated that low levels of inertial cavitation (or UCA collapse) is required for increased permeability. This finding agrees with the work of Miao et al (2008) with generated stress exceeding capillary strength leading to vascular perturbation. For drug delivery purposes, it is important to be able to either increase vessel porosity or increase the size of pores *without* destroying the tissue or the agent that is bound to the UCA. Lower pressures could possibly facilitate uptake of therapeutic

agents into the desired location, and if the parameters are kept below the values used in this thesis, heating would not be a competing (perhaps deleterious?) factor.

For secondary wound healing angiogenesis, pressures above 1.3 MPa should be used according to the findings herein. The normal animal model was able to recover from the damage caused (hemorrhage, contraction bands, inflammatory infiltrate, and nucleus internalization). How a diseased model would react to the treatment was not tested, but if this treatment is applied to healthy tissue on the periphery of ischemic tissue, it could cause an ingrowth of capillaries to the hypoxic area. Likewise, because angiogenesis is largely a system of checks and balances between pro- and anti-angiogenic factors, using US and UCAs to cause local, minor damage may be sufficient to offset the balance and boost the body's normal response to injury.

The benefit of therapeutic US over exiting clinical techniques to treat ischemia are plentiful. US-UCA treatment is noninvasive, site specific, temporally specific, can be repeated with minimal additional risks, has been proven to increase vascularity up to 50% when growth factors or stem cells are used, and is associated with very low risk. Surgical interventions carry the risk of death during operation, and, while initially minimally invasive, sometimes end in open heart by-pass surgery. To demonstrate the amount of risk involved in this type of therapy with respect to cellular damage, intravascular hemolysis is considered with a relative relationship to levels of hemolysis occurring in endurance sports.

Commonly in endurance sports like running intravascular hemolysis occurs, reportedly from impact with hard surfaces, as in the case of heel-strike (Telford et al. 2003). Literature states that running for 1 hour causes a ~30% decrease in red blood cells (RBCs) due to intravascular hemolysis (Telford et al. 2003). This decrease is commonly measured by a reduction in haptoglobin, a molecule that binds free hemoglobin released from damaged RBCs.

The number of RBCs injured when UCA collapse is the cause of intravascular hemolysis is a function of Pr, the focal region of the transducer and exposure duration. Previously we established that the volume of blood in the rat is ~ 2 x 10^{14}μm^3, if we consider the volume of the rat approximated as an ellipsoid (with height = 8 in., width = 3.5 in, and depth = 2.5 in.), we find that the volume of the rat, V_{rat} = 5 x 10^{15} μm^3. From these quantities we can determine the percentage of the body that is blood.

$$\% = \frac{V_{blood}}{V_{rat}}(100)$$

where V_{blood} is the volume of blood in the rat. (% = 4%). Next we need to determine the ultrasound focal volume. Approximated by a cylinder with radius of 2.5 mm and depth of 50 mm (because the focus is aligned at the surface of the gracilis muscle, but the beam extends beyond the gracilis muscle), the US focal volume (USFV) is , V_{focus} = 1.3 x 10^8 μm^3.

With the calculations above we can assume that blood is equally and evenly distributed for any portion of the body, 4% of the body is blood and as established in Chapter 5, that 0.00008% of blood is UCA. Therefore 4% of V_{focus} is blood in the USFV (B = 5 x 10^6 μm^3), and 0.00008% of the blood volume (5 x 10^6 μm^3) is comprised of Definity® = 4 μm^3. So the maximum infusion at steady state: 5 x 10^{-3} microbubbles/min/ μm^3 is multiplied by the volume of Definity® (4 μm^3) to determine the number of microbubbles/minute there are in the USFV: $N_{D\text{-}USFV}$ = 2 x 10^{-2} microbubbles/min. This is relative to the $N_{R\text{-}USFV}$ = 6.5 x 10^3 RBCs/min in the USFV. [This quantity was determined by multiplying B by the hematocrit, and dividing by the volume of one RBC.]

This is a simplified estimate of how the volume fraction of both UCAs and RBCs are distributed in vivo. It should be noted that not every RBC is in contact with a UCA, thus

intravascular hemolysis as a result of inertial cavitation affects only a small percentage of RBCs ($N_{D\text{-}USFV}/N_{R\text{-}USFV}$ = 0.0003%). This percentage is *significantly* less than damage caused during intense exercise, which, as stated previously, causes a 30% decrease in RBCs with 60 minutes of exercise. For the 5 minute ED used in most of the studies presented, there would be an adjusted 2.5% decrease in RBCs from running induced intravascular hemolysis. [30%/60 min ≈ 2.5%/5 min]. On a per-minute basis, running causes a 0.5% and US-UCA therapy causes a 0.0003% decrease in RBCs from intravascular hemolysis.

While these calculations do not take into consideration the Pr used during exposure, it does assume 100% collapse is occurring. Therefore it is speculated that even at high Pr, the intravascular hemolysis attributable solely to IC is nominal. Thus, while hemolysis does occur, it does not pose a substantial risk concern.

REFERENCES

AIUM 2000. Section 2—Definitions and description of nonthermal mechanisms. American Institute of Ultrasound in Medicine. J Ultrasound Med. 200; 19: 77-84, 154-168.

AIUM 2000. Section 6--Mechanical bioeffects in the presence of gas-carrier ultrasound contrast agents. American Institute of Ultrasound in Medicine J Ultrasound Med 2000; 19: 120-142.

AIUM/NEMA. Acoustic Output Measurement Standard for Diagnostic Ultrasound Equipment. American Institute of Ultrasound in Medicine, Laurel, MD and National Electrical Manufacturers Association, Rosslyn, VA, 1998.

Ammi AY, Cleveland RO, Mamou J, Wang GI, Bridal L, O'Brien, WD Jr. Ultrasonic contrast agent shell rupture detected by inertial cavitation and rebound signals. IEEE Trans Ult Ferro & Freq. 2006; 53(1): 126-136.

Apfel RE, Holland CK. Gauging the likelihood of cavitation from short-pulse, low-duty cycle diagnostic ultrasound. Ultrasound in Medicine and Biology 1991; 17:179-85.

Assmus B, Schachinger V, Teupe C. Transplantation of progenitor cells and regeneration enhancement in acute myocardial infarction (TOPCARE-AMI). Circulation. 2002; 106: 3009-3017.

Atchley AA, Frizzell LA, Apfel RE, Holland CK, Madanshetty S, Roy RA. Thresholds for cavitation produced in water by pulsed ultrasound. Ultrasonics. 1988 Sep; 26(5):280-5.

Augustin H. Tubes, branches, and pillars: the many ways of forming a new vasculature. *Circ Res.* 2001; 89:645-647.

Baker KG, Robertson VJ. A review of therapeutic ultrasound: biophysical effects. Phys Ther 2001; 81 (7):1351-8.

Barrientos S, Stojadinovic O, Golinko M, Brem H, Tomic-Canic M. Growth factors and cytokines in wound healing. Wound Repair & Regeneration. 2008; 16(5): 585-601.

Barzelai S, Sharabani-Yosef O, Holbova R, Castel D, Walsen R, Engelberg S, Scheinowitz M. Low intensity ultrasound induces angiogenesis in rat hind limb ischemia. Ultrasound in Med & Biol. 2006; 32:139-145.

Bates DO, Pritchard-Jones RO. The role of vascular endothelial growth factor in wound healing. Intl. J of Lower Ext. Wounds. 2003; 2: 107-120.

Bednarski M, Lee J, Callstrom M, Li K. In vivo target-specific delivery of macromolecular agents with MR-guided focused ultrasound. Radiology. 1997; 204:263-268.

Bohmer MR, Chlon CHT, Raju BI, Chin CT, Shevchenko T, Kilbanov AL. Focused ultrasound and microbubbles for enhanced extravasation. J Controlled Release. 2010; 148: 18-24.

Bouakaz A, Versluis M, de Jong N. High speed optical observations of contrast agent destruction. Ultrasound Med Biol. 2005; 33:391-399.

Braddock M, Schwachtgen J, Houston P, Dickson M, lee M, Campbell C. Fluid shear stress modulation of gene expression in endothelial cells. News Physiol. Sci. 1998; 13: 241-246.

Bridges CR. Guidelines for the clinical use of transmyocardial laser revascularization. Thoracic and Cardiovascular Surgery. 2006; 18: 68-73.

Brown LF, Yeo KT, Berse B, Yeo TK, Senger DR, Dvorak HF, van de Water L. Expression of vascular permeability factor (vascular endothelial growth factor) by epidermal keratinocytes during wound healing. J Exp Med. 199 ;176: 1375–1379.

Brujan EA, Ikeda T, Matsumoto Y. Jet formation and shock wave emission during collapse of ultrasound-induced cavitation bubbles and their role in the therapeutic applications of high intensity focused ultrasound. Phys Med Biol. 2005; 50: 4747-4809.

Buldakov MA, Hassan MA, Zhao QL, Feril LB, Kudo N, Kondo T, Litvyakov NV, Bolshakov MA, Rostov VV, Cherdyntseva NV, Riesz P. Influence of changing pulse repetition frequency on chemical and biological effects induced by low-intensity ultrasound in vitro. Ultrason Sonochem. 2009 Mar;16(3):392-7

Burkhoff D, Fisher PE, Apfelbaum M, et al. Histologic appearance of transmyocardial laser channels after 4 ½ weeks. Ann Thoracic Surg 1996; 61: 1532-1539.

Cavicchi TJ, O'Brien WD Jr. Heat generated by ultrasound in an absorbing medium. J. Acoust. Soc. Amer. 1984; 70: 1244-1245.

Carroll VA, Ashcroft M. Targeting the molecular basis for tumor hypoxia. Expert Rev Mol Med. 2005; 7: 1-16.

Chappell J, Kilbanov A, Price R. Ultrasound Microbubble Induced Neovascularization in mouse skeletal muscle. Ultrasound in Med & Biol. 2005;31: 1411-1422.

Chappell J, Song J, Burke C, Kilbanov A, Price R. Ultrasonic microbubble destruction stimulates therapeutic artiogenesis via the CD18-dependent recruitment of bone marrow derived cells. Arterioscler. Throm. & Vasc Biol. 2008; 28: 1117-1122.

Cherwek DH, Hopkins MB, Thompson MJ, Annex BH, Taylor DA. Fiber type-specific differential expression of angiogenic factors in response to chronic hindlimb ischemia. Am J Physiol Heart Circ Physiol. 2000 Sep;279(3):H932-8.

Chen H, Li X, Wan M. Spatial-temporal dynamics of cavitation bubble clouds in 1.2 MHz focused ultrasound field. Ultrasonics Sonochem. 2006; 13: 480.486.

Choi JJ, Wang S, Tung YS, Morrison B 3rd, Konofagou EE. Molecules of various pharmacologically-relevant sizes can cross the ultrasound-induced blood-brain barrier opening in vivo. Ultrasound Med Biol. 2010; 36: 58-67.

Chomas J, Dayton P, Allen J, Morgan K. Mechanisms of contrast agent destruction. IEEE Trans Ultrason Ferr Freq Control. 2001; 48: 232-248.

Chu V, Kuang J, McGinn A, Angiogenic response induced by mechanical transmyocardial revascularization.J Thorac Cardiovasc Surg. 1999;118:849-56.

Chen H, Brayman A, Bailey M, Matula T. Blood vessel rupture by cavitation. Urol Res. 2010; 38: 321-326.

Church C, Carstensen E. "Stable" inertial caviataion. Ultrasound Med Biol. 2001; 27: 1435-1437.

Church CC. Frequency, pulse length, and the mechanical index. Acoustics Research Letters Online 2005; 6:162-8.

Coakley W, Nyborg W. Fry F (Ed). Ultrasound, it's applications in medicine and biology part I. Elsevier Scientific, Amsterdam. Oxford. 1978.

Cochran S, Prausnitz M. Sonoluminescence as an indicator of cell membrane disruption by acoustic cavitation. Ultrasound Med Biol. 2001; 27: 841-850.

Dalecki D, Raeman C, Carstensen E. Effects of pulsed ultrasound on the frog heart I: Thresholds for changes in cardiac rhythm and aortic pressure and II: an investigation of heating as a possible mechanism. Ultrasound Med Biol. 1993; 19: 385-398.

Dalecki D, Raeman C, Child S, Carstensen E. Intestinal hemorrhage from exposure to pulsed ultrasound. Ultrasound in Med & Biol. 1995; 21:1067-1072.

Dalecki D, Child SZ, Raeman CH, Bioeffects of positive and negative acoustic pressures in mice infused with microbubbles. Ultrasound Med & Biol. 2000;26: 1327–1332.

Dallan LAO, Gowdak LH, Lisboa LAF, Cell therapy plus transmyocardial laser revascularization: a proposed alternative procedure for refractory angina. Rev Bras Cir Cardiovasc 2008; 23: 46-52.

Davidson B, Riley N. Cavitation microstreaming. J Sound Vib. 1971; 15: 217-233.

Davies P, Remuzzi A, Gordon E, Dewey C, Gimbrone Jr M. Turbulent fluid shear stress induces vascular endothelial cell turnover in vitrol. Proc Natl Acad Sci USA. 1986; 83: 2114-2117.

Dayton P, Morgan K, Kilbanov A, Bradenburger G, Nightingale K, Ferrara K. A preliminary evaluation of the effects of primary and secondary radiation forces on acoustic contrast agents. IEEE Trans Ultrasonic Ferr. Freq Control. 1997b; 44:1264-1277.

Definity [package insert]. N. Billerica, MA: Lantheus Medical Imaging; April 2008.

DeForrest J, Hollis T. Relationship between low intensity shear stress, aortic histamine formation and aortic albumin uptake. Exp. Mol. Pathol. 1980; 32:217-225.

De Jong N, Hoff L. Ultrasound scattering properties of albunex microspheres. Ultrasonics. 1993; 31: 175-181.

Dicker S, Mleczko M, Schmitz G, Wrenn S. Determination of microbubble cavitation threshold pressure as a function of shell chemistry. Bubble Sci Engr Tech. 2010; 2: 55-64.

Didenko Y, McNamara III W, Suslick K. Hot spot conditions during cavitation in water. J Am Chem Soc. 1999; 121:5817-8.

Doan N, Reher P, Meghji S, Harris M. In vitro effects of therapeutic ultrasound on cell proliferation, protein synthesis, and cytokine production by human fibroblasts, osteoblasts, and monocytes. J Oral Maxillofac Surg. 1999; 57: 409-419.

Draper D, Mahaffey C, Kaiser D, Eggett D, Jarmin J. Thermal ultrasound decreases tissue stiffness of trigger points in upper trapezius muscle. Physiother Theory Pract. 2010; 26: 167-172.

Dvorak DW, Abbas G, Ali T Stevenson S, Welling DB. Repair of chronic tympanic membrane performations with long term epidermal growth factor. Laryngoscope. 1995; 105: 1300-1304.

Dyson M, Pond J, Joseph J, Warwick R. The stimulation of tissue regeneration by means of ultrasound. Clin Sci. 1968; 35: 273-285.

Dyson M, Franks C, Suckling J. Stimulation of healing of varicose ulcers by ultrasound. Ultrasonics. 1976; 14: 232-236.

Dyson M, Niinikoski J. Stimulation of tissue repair by therapeutic ultrasound. Infect. In Surg. 1982; 37-44.

Dyson, M., Joseph. J, Pond, J. and Warwick, R. The stimulation of tissue regeneration by

means of ultrasound. Clin. Sci., 1968;35: 273-285.

Efthimiadou A, Asimakopoulos B, Nikolettos N, et al. Angiogenic effect of intramuscular administration of basic and acidic fibroblast growth factor on skeletal muscles and influence of exercise on muscle angiogenesis. *Br J Sports Med* 2006; 40:35-39.

Elder SA. Cavitation microstreaming. Journal of the Acoustical Society of America 1959; 30: 54-64.

Eller A, Flynn H. Rectified diffusion during nonlinear pulsations to cavitation bubbles. J Acous. Soc. Am. 1965; 37: 493-503.

Emmer M, Van Wamel A, Goertz D, de Jong N. The onset of microbubble vibration. Ultrasound Med Biol. 2007; 33: 941-949.

Estvold SK, Mordini F, Zhou Y, Yu ZX, Schadev V, Arai A, Horvath KA. Does laser type impact myocardial function following transmyocardial laser revascularization. Lasers Surg Med 2010; 42(10): 746-751.

Ferrara N, Carver-Moore K, Chen H, Dowd M, Lu L, O'Shea KS, Powell-Braxton L, Hillan KJ, Moore MW. Heterozygous embryonic lethality induced by targeted inactivation of the VEGF gene. *Nature* 1996 Apr 4; 380(6573): 439-42.

Ferrara N, Kerbel R. Angiogenesis as a therapeutic target. Nature. 2005; 438: 967-974.

Flectcher D, Palanker D, Huie P, Miller J, Marmor M, Blumenkranz M. Intravascular drug delivery with a pulsed liquid microjet. Arch Opthalmol. 2002; 120: 1206-1208.

Flynn HG. Cavitation dynamics. II. Free pulsations and models for cavitation bubbles. J Acoust Soc Am. 1975; 58:1160-70.

Flynn H, Church C. Transient pulsations of small gas bubbles in water. J Acoust Soc. Am. 1988; 84: 985-998.

Forbes M. The role of ultrasound contrast agents in producing sonoporation. (PhD Dissertation, University of Illinois, 2009), 1-166.

Forbes MM, Steinberg RL, O'Brien WD Jr. Frequency –dependent evaluation of the role of definity in producing sonoporation of Chinese hamster ovary cells. J Ultrasound Med. 2011; 30: 61-69.

French, L.A., Wild, J.J., and Neal, D. The experimental application of ultrasonics to the localization of brain tumors. J. Neurosurg.1951; 8:198–203.

Frey R, Ushio-Fukai M, Malik A. NADPH oxidas-dependent signaling in endothelial cells: role in physiology and pathophysiology. Antioxid Redox Signal. 2009; 11: 791-810.

Frenkel V, Oberoi J, Stone MJ, Park M, Deng C, Wood B, Neeman Z, horne M 3rd, Li K. Pulsed high intensity focused ultrasound enhances thrombolysis in an in vitro model. Radiology. 2006; 239: 86-93.

Fry, W.J., Fry, R.B. Temperature changes produced in tissue during ultrasonic irradiation. J. Acoust. Soc. Am. 1953; 25: 6–11.

Fuji H, Sun Z, Li S, et al. Ultrasound-targeted gene delivery induced angiogenesis after a myocardial infarction in mice. JACC: Cardiovasc. Imag. 2009; 7: 869-879.

Fujikura K, Otsuka R, Kalisz A, Ketterling JA, Jin Z, Sciacca RR, Marboe CC, Wang J, Muratore R, Feleppa EJ, Homma S. Effects of ultrasonic exposure parameters on myocardial lesions induced by high intensity focused ultrasound. J. Ultrasound Med. 2006; 11:1375-86.

Gavard J, Gutkind JS. Vascular endothelial growth factor controls endothelial cell permability by promoting the beta-arrestin-dependent endocytosis of VE-cadherin. Nat Cell Biol. 2006; 8: 1223-1234.

Geis N, Mayer C, Kroll R, Hardt S, Katus H, Bekeredjian R. Spatial distribution of ultrasound targeted microbubble destruction increases cardiac transgene expression but not capillary permeability. Ultrasound in Med & Biol. 2009; 35: 1119-1126.

Girard PR, Nerem RM. Shear stress modulates endothelial cell morphology and F-actin organization through the regulation of focal adhesion-associated proteins. J Cell Physiol. 1995; 163: 179-193.

Goertz D, de Jong N, van der Steen A. Attenuation and size distribution measurements of definity and manipulated definity populations. Ultrasound Med Biol. 2007; 33: 1376-1388.

Gormley G, Wu J. Acoustic streaming near Albunex spheres. Journal of the Acoustical Society of America 1998; 104: 3115-3118.

Gotshall, R. W., Breay-Pilcher, J. C., & Boelcskevy, B. D. Cardiac output in adult and neonatal rats utilizing impedance cardiography. Am J Physiol Heart Circ Physiol,1987; 253: 1298-1304.

Grines CL, Watkins MW, Helmer G, Penny W, Brinker J, Marmur JD, West A, Rade JJ, Marrott P, Hammond HK, Engler RL. Angiogenic Gene Therapy (AGENT) trial in patients with stable angina pectoris. Circulation. 2002 Mar 19;105(11):1291-7.

Grines C, Rubanyi GM, Kleiman N, Marrott P, Watkins M. Angiogenic gene therapy with

adenovirus 5 fibroblast growth factor-4 (Ad5FGF-4): a new option for the treatment of coronary artery disease. Am J Cardiol. 2003; 92: 24N-31N.

Guzman H, Nguyen D, Khan S, Prausnitz M. Ultrasound-mediated disruption of cell membranes I: quantification of molecular uptake and cell viability. And II: heterogeneous effects in cells. J Acoust Soc Am. 2001; 110: 588-606.

Haak A, O'Brien WD, Jr. "Detection of Microbubble Ultrasound Contrast Agent Destruction Applied to Definity®." Proceedings of the International Congress on Ultrasound, Paper Number 1719. Available at http://papers.icultrasonics.org/. (2007).

Halkos ME, Zhao ZQ, Kerendi F, et al. Intravenous infusion of mesenchymal stem cells enhances regional perfusion and improves ventricular function in a porcine model of myocardial infarction. *Basic Res Cardiol.* 2008; 103:525-536.

Hansen D, Dendale P, van Loon LJ, Meeusen R. The impact of training modalities on the clinical benefits of exercise intervention in patients with cardiovascular disease or type 2 diabetes. Sports Med. 2010; 40(11):921-940.

Harkins H, Harkins W. The surface tension of blood serum, and the determination of the surface tension of biological fluids. J Clin Inves. 1929; 7: 263-281.

Harvey E. Biological aspects of ultrasonic waves: a general survey. Biol. Bull. 1930; 59:306-25.

Hasuike A, Sato S, Udagawa A, Ando K, Arai Y, Ito K. In vivo bone regenerative effect of low-intensity pulsed ultrasound in rat calvarial defects. Oral Surg Oral Med Oral Pathol Oral Radiol Endod. 2011 Jan;111(1):e12-20.

Hernot S, Cosyns B, Droogmans S, Garbar C, Couck P, Vanhove C, Caveliers V, Van Camp G, Bossuyt A, Lahoutte T. Effect of high-intensity ultrasound-targeted microbubble destruction on perfusion and function of the rat heart assessed by pinhole-gated SPECT. Ultrasound Med Biol. 2010; 36:158-65.

Hershey JC, Baskin EP, Corcoran HA, Vascular endothelial growth factor stimulates angiogenesis without improving collateral blood flow following hindlimb ischemia in rabbits. Heart Vessels. 203; 18:142-149.

Hissa K, Ishibashi M, Ohtani K, et al. Gene transfer of stromal cell-derived factor-1alpha enhances ischemic vasculogenesis and angiogenesis via vascular endothelial growth factor/endothelial nitric oxide synthase-related pathway: next generation chemokine therapy for therapeutic neovascularization. *Circulation* 2004;109:2454-2461.

Hitchcock KE, Holland CK. Ultrasound-assisted thrombolysis for stroke therapy: better thrombus break-up with bubbles. Stroke. 2010 Oct;41(10 Suppl):S50-3.

Hoff, L., 2001. Acoustic Characterization of Contrast Agents for Medical Ultrasound Imaging. Kluwer Academic Publishers, Dordrecht,Netherlands, 2001.

Hoff L, Sontum P, Horem J. Osciallations of polymeric microbubbles: effect of the encapsulating shell. J Acoust Soc Am. 2000; 107: 2272-2280.

Hogan R, Burke K, Franklin T. The effect of ultrasound on microvascular hemodynamics in skeletal muscle: effects during ischemia. Microvasc Res. 1982; 23: 370-379.

Holland C, Deng C, Apfel R, Alderman J, Fernandez L, Taylor K. Direct evidence of cavitation in vivo from diagnostic ultrasound. Ultrsound in Med & Biol. 1996; 22: 917-925.

Holland, C, Apfel, R. An improved theory for the prediction of microcavitation thresholds. IEEE Trans. Ultrasonics Ferroelectrics Frequency Control 1989: 36; 204–208.

Hughes D, Nyborg W. Streaming and other activity around sonically induced bubbles is a cause of damage to living cells. Science. 1962; 138: 108-114.

Hunt F. Electroacoustics: the analysis of transduction, and its historical background. 1982; New York: Acoustical Society of America.

Hudlicka O, brown M, May S, Zakrzewicz A, Pries A. Changes in capillary shear stress in skeletal muscles exposed to long term activity: role of nitric oxide. Microcirculation. 2006; 13: 249-259.

Hwang JH, Brayman AA, Reidy MA, Vascular effects induced by combined 1-MHz ultrasound and microbubble contrast agent treatments in vivo. Ultrasound in Med & Biol. 2005; 31(4):553-564.

Idris NM, Haier HKH, Goh MWK, et al. Therapeutic angiogenesis for treatment of peripheral vascular disease. Growth Factors 2004; 22:269-279.

Iwaguro H, Yamaguchi J, Kalka C. Endothelial progenitor cell vascular endothelial growth factor gene transfer for vascular regeneration. Circulation 2002;105: 732-738.

Jackiewicz T, McGeachie J, London R, Tennant M. Evans blue dye modifies the ultrastructure of normal and regenerating arterial endothelium in rats. Microsurgery. 1998; 18: 47-54.

Jancar S, Sirois MG, Carrier J, Braquet P, Siros P. PAF induces rat plasma extravasation and releases eicosanoids during anaphylaxis. Inflam. 1991; 15: 347-354.

Jimenez C, Portela R, Mellado M, Rodriguez-Frade J, Collard J, Serrano A, Martinez-A C, Avila J, Carrera A. Role of the PI3K regulatory subunit in the control of actin organization and cell migration. J Cell Biol. 2000; 151: 249-262.

Jimenez-Fernandez J, Crespo A. Bubble oscillation and inertial cavitation in viscoelastic fluids. Ultrasonics. 2005; 43: 643-651.

Jin ZG, Ueba H, Tanimoto T, Lungu A, Frame M, Berk B. Ligand-independent activation of VEGFR2 by fluid shear stress regulates activation of endothelial nitric oxide synthase. Circ Res. 2003; 93: 354-363.

Johns L. Nonthermal effects of therapeutic ultrasound: the frequency resonance hypothesis. J Athl Train. 2002; 37: 293-299.

Johnson CA, Miller RJ, O'Brien WD, Jr. Ultrasound Contrast Agents Affect Angiogenic Response. J Ultrasound Med. 2011, in press.

Johnson CA, Sarwate S, Miller RJ, O'Brien WD, Jr. A temporal study of ultrasound contrast agent-induced changes in capillary density. J Ultrasound Med. 2010; 29:1267-1275.

Jones GE. Cellular signaling in macrophage migration and cemotaxis. J Leukoc Biol. 2000; 68: 593-602.

Juffermans LJ, Kamp O, Dijkmans PA, Visser CA, Musters RJ. Low-intensity ultrasound-exposed microbubbles provoke local hyperpolarization of the cell membrane via activation of BK(Ca) channels. Ultrasound Med Biol. 2008 Mar;34(3):502-8.

Juffermans LJ, van Dijk A, Jongenelen CA, Drukarch B, Reijerkerk A, de Vries HE, Kamp O, Musters RJ. Ultrasound and microbubble-induced intra- and intercellular bioeffects in primary endothelial cells. Ultrasound Med Biol. 2009 Nov;35(11):1917-27.

Kang SW, Lim HW, Seo SW, et al. Nanosphere-mediated delivery of vascular endothelial growth factor gene for therapeutic angiogenesis in mouse ischemic limbs. *Biomaterials.* 2008; 29:1109-1117.

Kasten A, Muller P, Bulnhelm U, Groll J, Bruellhoff K, Beck U, Steinhoff G, Moller M, Rychly J. Mechanical intergrin stress and magnetic forces induce biological responses in mesenchymal stem cells which depend on environmental factors. J Cell Biochem. 2010; 111: 1586-1597.

Keller J Miksis M. Bubble oscillations of large amplitude. J Acoust Soc Am. 1980; 68: 628-633.

King D, Malloy M, Roberts A, Haak A, Yoder C, O'Brien WD, Jr. Determination of

postexcitation thresholds for single ultrasound contrast agent microbubbles using double passive cavitation detection. J. Acoust. Soc. Am 2010; 127: 3449-3455.

King D, O'Brien WD, Jr. Comparison between maximum radial expansion of ultrasound contrast agents and experimental post excitation signal results. J. Acoust Soc Am. 2011; 129:114-121.

Kinsler LE, Frey AR, Fundamentals of Acoustics. New York, NY: John Wiley & Sons, Inc., 2002.

Klemke R, Cai S, Ciannini A, Gallagher P, de Lanerolle P, Cheresh D. Regulation of cell motility by mitogen-activated protein kinase. J Cell Biol. 1997 ; 137 : 481-492.

Kobayashi N, Yasu T, Yamada S, Endothelial cell injury in venule and capillary induced by contrast ultrasonography. Ultrasound Med & Biol. 2002;28:949 –956.

Kobulnik J, Kuliszewski MA, Stewart DJ, Lindner JR, Leong-Poi H. Comparison of gene delivery techniques for therapeutic angiogenesis ultrasound-mediated destruction of carrier microbubbles versus direct intramuscular injection. J Am Coll Cardiol. 2009 Oct 27;54(18):1735-42.

Kodama T, Takayama K. Dynamic behavior of bubbles during extracorporeal shock-wave lithotripsy. Ultrasound Med Biol. 1998; 24: 723-738.

Kondo T, kano E. Effect of free radicals induced by ultrasonic cavitation on cell killing. Int. J Radiat Biol. 1988; 54: 475-486.

Korosuglu G, Hardt S, Bekeredjian R, Jenne J, Konstantin M, Hagenueller M, et al. Ultrasound exposure can increase the membrane permeability of human neutrophil granulocytes containing microbubbles without causing complete cell destruction. Ultrasound Med & Biol. 2006; 32(2): 297-303.

Korpanty G, Grayburn P, Shohet R, Brekken R. Targeting vascular endothelium with avidin microbubbles. Ultrasound in Med & Biol. 2005; 31: 1279-1283.

Korpisalo P, Hytonen J, Laitinen J, Laidinen S, Parviainen H, Karvinen H, Siponen J, Marjomaki V, Vajanto I, Rissanen T, Yla-Herttuala S. Capillary enlargement, not sprouting angiogenensis determines beneficial therapeutic and side effects of angiogenic gene therapy. Euro Heart J 2010; [Epub ahead of print].

Krasovitski B, Kimmel E. Shear stress induced by a gas bubble pulsating in an ultrasonic field near a wall. IEEE Trans Ultrason Ferr Freq Control. 2004; 51: 973-979.

Kost J. Ultrasound-assisted insulin delivery and noninvasive glucose sensing. Diabetes

Technol Ther. 2002;4(4):489-97. Review.

Kruse D, Mackanos M, O'Connell-Rodwell C, Contag C, Ferrara K. Ahort duration-focused ultrasound stimulation of HSP70 expression in vivo. Phys Med Biol. 2008; 53: 3641-3660.

Kumar S, Brennen CE. Nonlinear effects in the dynamics of clouds of bubbles. J Acoust Soc Am. 1991; 89: 707-14. Erratum in: J Acoust Soc Am 1991 Nov;90(5):2854.

Landolfo CK, Landolfo KP, Hughes GF Intermediate-term clinical outcome following transmyocardial laser revascularization in patient with refractory angina pectoris. Circulation 1999;100: II128-133.

LauterbornW. Numerical investigation of nonlinear oscillations of gas bubbles in liquids. J Acoust Soc Am. 19976; 59: 28-293.

Lebherz C, von Degenfeld G, Karl A, Therapeutic angiogenesis/arteriogenesisin the chronic ischemic rabbit hindlimb: effect of venous basic fibroblast growth factor retroinfusion. Endothelium. 2003;10: 257-265.

Leighton TG. The Acoustic Bubble. San Diego: Academic Press; 1994.

Leighton TG. The Rayleigh plesset equation in terms of volume with explicit shear losses. Ultrasonics. 2008; 48: 85-90.

Leon MB, Baim DS. DMR in regeneration endomyocardial channels trial. 12th Annual Transcatheter Cardiovascular Therapeutic, Washington DC, 17-22 Oct. 2000.

Leong-Poi H, Kuliszowski M, Lekas M. Therapeutic arteriogenesis by ultrasound-mediated VEGF165 plasmid gene delivery to chronically ischemic skeletal muscle. Circ. Res. 1007; 101: 295-303.

LeVeen H, Fishman W. Combination of evans blue with plasma protein: its significance in capillary permeability studies, blood dye disappearance curves and its use as a protein tag. Am J. Physiol. 1947; 151: 26-33.

Lewin P, Bjorno L. Acoustically induced shear stress in the vicinity of microbubbles in tissue. J Acoust Soc Am. 1982; 71: 728-734.

Li VW, Kung EF, Li WW. Molecular Therapy for Wounds: Modalities for stimulating angiogenesis and granulation. Manual of Wound Management (Bok Lec, Editor) McGraw Hill, 2004, p. 17-43.

Li W, Talcott K, Zhai A, Kruger E, Li V. The Role of Therapeutic Angiogenesis in Tissue Repair and Regeneration Adv Skin Wound Care 2005; 18: 491-500.

Liekens S, De Clercq E, Neyts J. Angiogenesis: regulators and clinical applications. Biochem

Pharmacol 2001; 61: 253–70.

Lloyd-Jones D, Adams R, Carnethon M, et al. Heart Disease and Stroke Statistics—2009 Update: A report from the American heart association statistics committee and stroke statistics subcommittee. Circulation. 2009; 119: e21-e181.

Lucas LC, Mills JL Sr. Critical evaluation of endovascular surgery for limb salvage. Plast. Reconstr. Surg. 2001; 127 Suppl 1: 174S-176S.

MacRobbie AG, Raeman CH, Child SZ, Dalecki D. Thresholds for premature contractions in murine hearts exposed to pulsed ultrasound. Ultrasound in Med & Biol. 1997; 23: 761-765.

Mari J, Hibbs K, Tang M. A non-linear ultrasonic scattering approach for microbubble concentration quantification. Proc Am Intl Conf IEEE EMBS. 2007; 2183-2186.

Mariotti M, Maier J. (eds) Angiogenesis: an overview. New frontiers in Angiogenesis. Netherlands: Springer, 2006: 2-4.

Marmottant P, van der Meer S, Emmer M, Versluis M, de Jong N, Hilgenfeldt S, Lohse D. A model for large amplitude oscillations of coated bubbles accounting for buckling and rupture. J Acoust Soc Am. 2005; 118: 3499-3505.

Martynov S, Stride E, Saffari N. The natural frequencies of microbubble oscillation in elastic vessels. J Acoust Soc Am. 2009; 126: 2963-2972.

Maxwell AD, Wang TY, Yuan L, Duryea AP, Xu Z, Cain CA. A tissue phantom for visualization and measurement of ultrasound-induced cavitation damage. Ultrasound Med Biol. 2010 Dec;36(12):2132-43.

Medinger M, Fischer N, Tzankov A. Vascular endothelial growth factor-related pathways in hemato-lymphoid malignancies. J Oncol. 2010; 2010:1-14.

Medwin H. Counting bubbles acoustically: a review. Ultrasonics. 1997; 15: 7-13.

Merouani S, Hamdaoui O, Saoudi F, Chiha M. Inflammation of experimental parameters on sonochemical dosimeteries: KI oxidation, Fricke reaction and H2O2 production. J Hazard Mater. 2010; 178: 1007-1014.

Mettin R, Akhatov I, Parlitz V, Ohl C, Lauterborn W. Bjerknes forces between small cavitation bubbles in a strong acoustic field. Physical Rev E. 1997; 56: 2924-2931.

Messina LM, Breveiti LS, Chang DS, Paek R, Sarkar R. Therapeutic angiogenesis for critical limb ischemia. Invited commentary. J Controlled Release. 2002; 78:285-294.

Miao H, Gracewski S, Dalecki D. Ultrasonic excitation of a bubble inside a deformable tube:

Implications for ultrasonically induced hemorrhage. J Acoust Soc Am.2008; 124 :2374-2384.

Miller D. Microstreaming shear as a mechanism of cell death in elodea leaves exposed to ultrasound. Ultrasound Med Biol. 1985; 11: 285-292.

Miller D, Thomas R. A comparison of hemolytic and sonochemical activity of ultraosonic cavitation in a rotating tube. Ultrasound Med Biol. 1993; 19: 83-90.

Miller DL, Thomas RM, Buschbom RL. Comet assay reveals DNA strand breaks induced by ultrasound cavitation in vitro. Ultrasound in Medicine and Biology 1995; 21:841-8.

Miller D, Gies RA. Gas-body-based contrast agent enhances vascular bioeffects of 1.09 MHz ultrasound on mouse intestine. Ultrasound Med & Biol. 1998c;24: 1201–1208.

Miller D, Quddus J. Diagnostic ultrasound activation of contrast agent gas bodies induces capillary rupture in mice. Proc Natl Acad Sci USA. 2000; 97: 10179-10184.

Miller D, Dou C. Theroetical gas body pulsation in relation to empirical gas-body destabilization and to cell membrane damage thresholds. J Acoust Soc Am. 2004; 116: 3742-3749.

Miller D, Dou C, Armstrong W. The influence of agent delivery mode on cardiomyocytes injury induced by myocardial contrast echocardiography in rats. Ultrasound Med boil. 2005;31: 1257-1263.

Miller D, Li P, Dou C, Armstrong W, Gordon D. Evans blue staining of cardiomyocytes induced by myocardial contrast echocardiography in rats: evidence for necrosis instead of apoptosis. Ultrasound Med Biol. 2007; 33: 1988-1996.

Miller D. Overview of experimental studies of biological effects of medical ultrasound caused by gas body activation and inertial cavitation. Biophys. & Molec. Biol. 2007; 93:314-30.

Miller D, Averklou M, Brayman A, Everbah E, Holland C, Wible J, Wu J. Bioeffects considerations for diagnostic ultrasound contrast agents. J Ultrasound Med. 2008; 27: 611-632.

Miller D, Dou C, Wiggins R. Frequency dependence of kidney injury induced by contrast-aided diagnostic ultrasound in rats. Ultrasound Med & Biol. 2008; 34(10):1678-87.

Miller D, Dou C, Lucchesi B. Cardiac arrhythmia and injury induced in rats by burst and pulsed mode ultrasound with gas body contrast agent. J Ultrasound Med. 2009; 28: 1519-1526.

Miller DL, Dou C, Wiggins RC. Contrast enhanced diagnostic ultrasound causes renal tissue damage in a porcine model. J Ultrasound Med. 2010; 29: 1391-1401.

Minones J Jr, Rodriguez Patino J, Minones J, Dynarowicz-Latka P, Carrera C. Structural and topographical characteristics of dipalmitoyl phosphatidic acid in Langmuir monolayers. J Colloid Interface. Sci. 2002; 249: 388-397.

Miri A, Mitri F. Acoustic radiation force on a spherical contrast agent shell near a vessel porous wall-theory. Ultrasound Med Biol. 2011; 37: 301-311.

Miyake Y, Ohmori K, Yoshida J, et al. Granulocyte colony-stimulating factor facilitates the angiogenesis induced by ultrasonic microbubble destruction. Ultrasound in Med. & Biol. 2007; 33: 1796-1804.

Mirahi N, Seliktar D, Kimmel E. Ultrasound-induced angiogenic response in endothelial cells. Ultrasound Med Biol. 2007; 33: 1818-1829.

Monsen T, Lougren E, Widerstrom M, Wallinder L. In citro effect of ultrasound in bacteria and suggested protocol for sonication and diagnosis of prosthetic infections. J Clin Microbiol. 2009; 47: 2446-2501.

Moran CM, Anderson T, Pye SD, Sboros V, McDicken, WN. Quantification of microbubble destruction of three fluorocarbon-filled ultrasonic contrast agents. *Ultrasound in Med & Biol*. 2000:26; 629-639.

Moran CM, Watson RJ, Fox KAA, McDicken WN. In vitro acoustic characterization of four intravenous ultrasonic contrast agents at 30 MHz. *Ultrasound in Med & Biol.* 2002: 28:785-791.

Mukherjee S, Tessema M, Wandinger-Ness A. Vesicular trafficking of tyrosine kinase receptors and associated proteins in the regulation of signaling and vascular function. Circ Res. 2006; 98: 743-756.

Nakajima H, Sakakibara Y, Tambara K, Iwakura A, Doi K, Marui A, Ueyama K, Ikeda T, Tabata Y, Komeda M. Therapeutic angiogenesis by controlled release of basic fibroblast growth factor for ischemic limb and heart injury; toward safety and minimal invasiveness. J Artif Organs. 2004; 7: 58-61.

NEMA. Acoustic output measurement standard for diagnostic ultrasound equipment, rev 3. American Institute of Ultrasound in Medicine, Laurel, MD and National Electrical Manufacturers Association, Rosslyn, VA, 2009a.

NEMA. Standard for the real-time display of thermal and mechanical acoustic output indices on diagnostic ultrasound equipment, rev 2. American Institute of Ultrasound in Medicine, Laurel, MD and National Electrical Manufacturers Association, Rosslyn, VA, 2009b.

NCRP. Exposure criteria for medical diagnostic ultrasound: II. Criteria based on all known

mechanisms. Report No. 140. Bethesda, MD: National Council on Radiation Protection and Measurements; 2002

NDFS. Centers for disease control and prevention. National diabetes fact sheet: national estimates and general information on diabetes and pre-diabetes in the US, 2011. Atlanta, GA: US department of health and human services, CDC and prevention 2011.

Nightingale, K.R., Kornguth, P.J., Walker, W.F., McDermott, B.A., Trahey, G.E., 1995. A novel ultrasonic technique for differentiating cysts from solid lesions: preliminary results in the breast. Ultrasound Med. Biol. 21, 745–751.

Nyborg W. Acoustic streaming In: Mason, WP, ed Physical acoustics, Vol 2B. New York:Academic Press; 1965:265-331.

Nyborg W. Biological effects of Ultrasound: Development of Safety Guidelines. Ultrasound Med & Biol. 2000; 26(6):911-64.

Nyborg W. Biological effects of Ultrasound: Development of Safety Guidelines. Part II: General Review. Ultrasound Med & Biol. 2001; 27(3):301-33.

Nyborg WL. Acoustic streaming near a boundary. Journal of the Acoustical Society of America 1958; 30: 329-339.

Nyborg, W.L. Acoustic streaming due to attenuated plane waves. J. Acoust. Soc. Am. 1953; 25: 68–75.

Nyborg, W.L. Acoustic streaming. In: Mason, W.P. (Ed.), Physical Acoustics, vol. 2B. Academic Press, New York, NY, 1965; 265–331.

Nyborg, W. Intermediate Biophysical Mechanics. Cummings Publishing Co., Menlo Park, CA, 1975.

Nyborg, W.L. Heat generation by ultrasound in a relaxing medium. J. Acoust. Soc. Am. 1981; 70, 310–312.

O'Brien WD Jr, Zachary J. Mouse lung damage from exposure to 30 kHz ultrasound. Ultrasound Med. & Biol. 1998; 20(3):287-97.

O'Brien WD Jr. Assessing the risks for modern diagnostic ultrasound imaging. JJAP. 1998; 37(5B):2781-2788.

O'Brien WD Jr, Simpson DG, Frizzell LA, Zachary JF. Age-dependent threshold and superthreshold behavior of ultrasound-induced lung hemorrhage in pigs. Proc Ultrason Symp IEEE. 2001;2: 1315 – 1318.

O'Brien WD, Frizzell LA, Schaeffer DJ, Zachary JF. Superthreshold behavior of ultrasound-

induced lung hemorrhage in adult mice and rats: role of pulse repetition frequency and exposure duration. Ultrasound Med. Biol. 2001; 27:267–77.

O'Brien WD, Simpson DG, Frizzell LA, Zachary JF. Threshold estimates and superthreshold behavior of ultrasound-induced lung hemorrhage in adult rats: role of pulse duration. Ultrasound Med. Biol. 2003; 29:1625–1634.

O'Brien WD Jr, Simpson DG, Frizzell LA, Zachary JF. Effect of contrast agent on the incidence and magnitude of ultrasound-induced lung hemorrhage in rats. Echocardiography. 2004; 21(5):417-422.

O'Brien, Jr. WD, Simpson DG, Frizzell LA and Zachary JF. Superthreshold Behavior of Ultrasound-induced Lung Hemorrhage in Adult Rats: Role of Pulse Repetition Frequency and Exposure Duration Revisited. Journal of Ultrasound in Medicine, 2005; 24:339-348.

O'Brien WD Jr. Ultrasound-biophysics mechanisms. Biophys & Molec Biol. 2007; 93: 212-255.

Oguz H, Prosperetti A. The natural frequency of oscillation of gas bubbles in tubes. J Acoust Soc Am. 1998; 103; 3301-3308.

Ohl CD, Ikin R. Shock-wave induced jetting of micron sized bubbles. Physical Review Letters. 2003; 90:2145-2202.

Optison [package insert]. Princeton, NJ: Amersham Health; June 2003.

Overvelde M, Garbin V, Sijl J, Dollet B, de Jong N, Lohse D, Versluis M. Nonlinear shell behavior of phospholipid coated microbubbles. Ultrasound Med Biol. 2010; 36: 2080-2092.

Paliwal S, Mitragotri S. Therapeutic opportunities in biological responses of ultrasound. Ultrasonics. 2008; 48: 271-278.

Pang KH, Bate GR, Darvall KA, Adam DJ, Bradbury AW. Healing and recurrence rates following ultrasound-guided foam sclerotherapy of superficial venous reflux in patients with chronic venous ulceration. Eur J Vasc Endovasc Surg. 2010 Dec;40(6):790-795.

Paszkowiak J, Dardik A. Arterial wall shear stress: observations from the bench to the bedside. Vasc Endovasc Surg. 2003; 37: 47-57.

Plesset M. The dynamics of cavitation bubbles. J Appl Mech. 1949; 16: 277-282.

Porter TR, Xie F. Therapeutic ultrasound for gene delivery. Echocardiography. 2001 May;18(4):349-53. Review.

Postema M, van Wamel A, Lancee C, de Jong N. Ultrasound-induced encapsulated microbubble phenomena. Ultrasound Med Biol. 2004; 30: 827-840.

Postema M, van Wamel A, ten Cate FJ, de Jong N. High-speed photography during ultrasound illustrates potential therapeutic applications of microbubbles. Med Phys. 2005 Dec;32(12):3707-11.

Pugh C, Ratcliffe P. Regulation of angiogenesis by hypoxia: role of the HIF system. Nat Med. 2003; 9:677-684.

Prosperetti A. Bubble phenomena in sound fields: part one. Ultrasonics. 1984; 22:69-77.

Prosperetti A. Bubble phenomena in sound fields: part two. Ultrasonics. 1984; 22:115-124.

Prosperetti A. A new mechanism for sonoluminescence. J Acoust Soc Am. 1997;101: 2003-2007.

Qiagen. Platinum Q PCR Package Insert. 2006 Qiagen GmbH Hilden, Germany.

Qiagen. RNeasy mini handbook, 4th ed. 2006 Qiagen GmbH Hilden, Germany.

R&D Systems, Inc. Cytokines in Wound Healing. Minneapolis: R&D Systems, 2002.

Rayleigh JW. The theory of sound. 1945; New York: Dover.

Reher P, Doan N, Bradnock B, Meghji S, Harris M. Effect of ultrasound on the production of IL-8, basic FGF and VEGF. Cytokine 1999; 11: 416–423.

Reynolds L, Redmer D. Expression of the angiogenic factors, basic fibroblast growth factor and vascular endothelial growth factor, in the ovary. J Anim Sci. 1998; 76: 1671-1681.

Riederer-Henderson MA, Olerud JE, O'Brien, WD Jr. Biochemical and Acoustical Parameters of Normal Canine Skin. IEEE Transactions on Biomed.l Eng, 1988; 35: 967-972.

Roberts W, Hall T, Ives K, Ives K, Wolf J Jr, Fowlkes J, Cain C. Pulsed cavitational ultrasound: a noninvasive technology for controlled tissue ablation (histotripsy) in the rabbit kidney. J Urol. 2006; 175: 734-738.

Robbins & Cotran. Pathological Basis of Disease, Seventh Ed. Philadelphia, Pa: WB Saunders Co, 2005.

Roger V, Go A, Lloyd-Jones D, Adams R, berry J, brown T, Carnethon M, Dai S, deSimone G, Ford E, Foz C, Fullerton H, Gillespie C, greenlund K, Hailpern S, Heit J, Ho P, Howard V, Kissela B, Kittner S, Lackland D, Litchtman J, Lisabeth L, Makvic d, Marcus G, Marelli A, Matchar D, McDernott M, Meigs J, Moy C, Mozaffarian D, Mussolino M, Nichol G, Paynter N, Rosamond W, Solvie P, Stafford R, Turan T, Turner M, Wong N, Wylie-Rosett J. Heart

disease and stroke statistics 2011. Update: a report from the American heart association.

Rooney J. Hemolysis near an ultrasonically pulsing gas buble. Science. 1970; 169: 869-871.

Rooney J. Shear as a mechanism for sonically induced biological effects. J Acoust Soc Am. 1972; 6: 1718-1724.

Rota C, Raeman CH, Child SZ, Dalecki D. Detection of acoustic cavitation in the heart with microbubble contrast agents in vivo: a mechanism for ultrasound-induced arrhythmias. J Acoust Soc Am. 2006 Nov;120(5 Pt 1):2958-64.

Sabti HA. Therapeutic angiogenesis in cardiovascular disease. *J Cardiothoracic Surg.* 2007; 2:49-56.

Sapareto S, Dewey W. Thermal dose determination in cancer therapy. Int J Radiat Oncol. Biol Phys. 1984; 10: 787-800.

Samuel S, Cooper M, Bull J, Fowlkes B, Miller D. An ex vivo study of the correlation between acoustic emission and microvascular damage. Ultrasound in Med & Biol. 2009; 35: 1574-1586.

Samuel S, Miller DL, Fowlkes JB. The relationship of acoustic emission and pulse repetition frequency in the detection of gas body stability and cell death. Ultrasound Med Biol 2006; 32:439–447.

Santin M, King D, Foiret J, Haak A, O'Brien WD Jr, Bridal SL. Encapsulated contrast microbubble radial oscillation associated with postexcitation pressure peaks. J Acoust Soc Am. 2010; 127: 1156-1164.

Sarkar K, Katiyar A, Jain P. Growth and dissolution of an encapsulated contrast microbubble: effects of encapsulation permeability. Ultrasound Med & Biol. 2009; 35:1385-1396.

Sassaroli E. Hynynen K. Forced linear oscillations of microbubbles in blood capillaries. J Acous Soc Am. 2004; 115: 3235-3243.

Sboros V. "Response of contrast agents to ultrasound." Adv. Drug Delivery Rev. 2008; 60: 1117-1136.

Sempsrott JM and O'Brien WD Jr. Experimental Verification of Acoustic Saturation. Proceedings of the 1999 IEEE Ultrasonics Symposium. 1999;1287-1290.

Shang X, Wang P, Liu Y, Zhang Z, Xue Y. Mechanism of low-frequency ultrasound in opening blood-tumor barrier by tight junction. J Mol Neurosci. 2011; 143: 364-369.

Shay-Salit A, Shushy M, Wolfovitz E, Yahav H, Breviario F, Dejana E, Resnick N. VEGFR2 and the adherens junction as a mechanical transducer in vascular endothelial cells. Proc. Natl

Avad Sci USA. 2002; 99: 9462-9467.

Skyba D, Price R, Linka A, Sklak T, Kaul S. Direct in vivo visualization of intravascular destruction of microbubbles by ultrasound and its local effects on tissue. Circulation 1998; 98: 290-293.

Smaje L, Fraser P, Glough G. The distensibility of single capillaries and venules in the cat mesentery. Microvasc Res. 1980; 20: 358-370.

Song J, Chappell J, Qi M, VanGieson E, Kaul S, Price R. Influence of injection site, microvascular pressure, and ultrasound variables on microbubble-mediated delivery of microspheres to muscle. J Am Coll Cardiol. 2002;39: 726-31.

Song J, Cottler PS, Klibanov AL, Kaul S, Price RJ. Microvascular remodeling and accelerated hyperemia blood flow restoration in arterially occluded skeletal muscle exposed to ultrasonic microbubble destruction. Am J Physiol Heart Circ Physiol. 2004; 287: H2754–H2761.

Song X, Zhu H, Jin L, et al. Ultrasound-mediated microbubble destruction enhances the efficacy of bone marrow mesenchymal stem cell transplantation and cardiac function. Clin & Exptl Pharm & Physiol. 2008; 36: 267-271.

Sonovue [package insert]. Milan, Italy. Bracco; May 2001.

Stride E, Saffari N. The potential for thermal damage posed by microbubble ultrasound contrast agents. Ultrasonics 2004; 42:907-13.

Stride E, Saffari N. "Microbubble ultrasound contrast agents: a review." Proc. Instn. Mech. Engrs. Part H: J. Eng. in Med. 2003; 217: 429-447.

Sugita Y. Nitric oxide generation directy responds to US exposure. Ultrasound in Med & Biol. 2008;34: 487-493.

Sunderkotter C, Steinbrink K, Goebeler M, Bhardnaj R, Sorg C. Macrophages and angiogenesis. J of Leukocyte Biol. 1994; 55(3): 410-422.

Suslick K. Ultrasound: its chemical, physical, and biological effects; 1988: New York: VCH Publishers, Inc.

Takeshita S, Weir L, Chen D, Therapeutic angiogenesis following arterial gene transfer of vascular endothelil growth factor in a rabbit model of hindlimb ischemia. Biochem & Bioph Res Com. 1996; 227:628-635.

Tandar A, Saperia GM, Spodick DH. Direct myocardial revascularization and therapeutic angiogenesis. European Heart J. 2002; 23:1492-1502.

Taniyama Y, Tachibana K, Hiraoka K, et al. Development of safe and efficient novel nonviral

gene transfer using ultrasound: enhancement of transfection efficiency of naked plasmid DNA in skeletal muscle. Gene Ther. 2002; 9: 372-80.

Telford R, Sly G, Hahn G, Cunningham R, Bryant C, Smith J. Footstrike is the major cause of hemolysis during running. J Appl Physiol. 2003; 94: 38-42.

ter Haar R, Daniels S, Morton K. Evidence for acoustic cavitation in vivo. Thresholds for bubble formation with 0.75 MHz continuous wave and pulsed beams. IEEE Trans UFFC. 1986; 33: 162-164.

ter Haar G. Therapeutic Ultrasound. Eur J Ultrasound. 1999; 9:3-9.

ter Haar. Safety and bioeffects of ultrasound contrast agents. Med Biol Eng Comput. 2009; 47: 893-900.

Tiidus P. Editor. Skeletal muscle damage and repair. Champaign, IL: Human Kinetics, 2008.

Trilling L. The collapse and rebound of a gas bubble. J Appl. Phys. 1952; 23: 14-17.

Urbich C, Stein M, Reisinger K, Kaufmann R, Dimmeler S, Gille J. Fluid shear stress transcription activation of the VEGFR2 genes requires Sp1-dependent DNA binding. REBS Lett. 2003; 30: 87-93.

Usuba M, Miyanaga Y, Miyakawa S, Maeshima T, Shiraski Y. Effect of heat in increasing the range of knee motion after the development of a joint contracture: an experiment with an animal model. Arch Phys Med Rehanil. 2006; 87: 247-253.

Van Royen N, Hoefer I, Buschmann I, et al. Exogenous application of transforming growth factor beta 1 stimulates arteriogenesis in the peripheral circulation. Federation of American Societies for Experimental BiologyJ 2002;16: 432-434.

Vancraeynest D, Havauz X, Pasquet A, Gerber B, Beauloye C, Rafier P, Bertrand L, Vanovershelde J. Myocardial injury induced by ultrasound-targeted microbubble destruction: evidence for the contribution of myocardial ischemia. Ultrasound in Med & Biol. 2009; 35; 672-679.

Verral R, Sehgal C. Suslick K (Ed.) Sonolumenescence. Chapter 6. Ultrasound: Its chemical, physical, and biological effects. New York, 1988.

Vykhodtseva NI, Hynynen K, Damianou C. Pulse duration and peak intensity during focused ultrasound surgery: theoretical and experimental effects in rabbit brain in vivo. Ultrasound Med Biol. 1994;20: 987-1000.

Wahl SM. Transforming growth factor beta: the good, the bad, and the ugly. J Exp Med. 1994 Nov 1;180(5):1587–1590

Wang F, Kuo Y, Wang C, Yang K, Chang P, Huang Y, Huang H, Sun Y, Yang Y, Chen Y. Nitric oxide mediates ultrasound-induced hypoxia-inducible factor-1alpha activation and vascular endothelial growth factor-A expression in human osteoblasts. Bone. 2004; 35; 114-123.

Ward M, Wu J, Chiu J-F. Ultrasound induced cell lysis and sonoporation enahanced by contrast agents. J Acoust. Soc. Am 1999; 105: 2951-2957.

Watson T. Therapeutic Ultrasound. Electro Ther 2005; 1-11.

Williams A, Hughes D, Nyborg W. Hemolysis near a transversely oscillating wire. Science. 1970; 169: 871-873.

Williams A. Disorganization and disruption of mammalian and amoeboid cells by acoustic microstreaming. J Acoust Soc Am. 1971; 50: 99-100.

Williams AR, Wiggins RC, Wharram BL, Goyal M, Dou C, Johnson KJ, Miller DL. Nephron injury induced by diagnostic ultrasound imaging at high mechanical index with gas body contrast agent. Ultrasound Med Biol 2007;33: 1336–1344.

Wu J, Myborg W. Ultrasound, caviation bubbles and their interaction with cells. Adv. Drug Deliv. Rev. 2008; 60:1103-16.

Xu Z, Fowlkes JB, Ludomirsky A, Cain CA. Investigation of intensity thresholds for ultrasound tissue erosion. Ultrasound Med Biol. 2005;31:1673-82.

Yamamoto N, Gu A, DeRosa CM, Radio frequency transmyocardial revacscularization enhances angiogenesis and causes myocardial denervation in canine model. Lasers Surg Med 2000;27: 18-28.

Yamamoto N, Kohmoto T, Roethy W, Histologic evidence that basic fibroblast growth factor enhances the angiogenic effects of transmyocardial laser revascularization. Basic Res Cardiol 2000; 95:55-63.

Yang FY, Lin YS, Kang KH, Chao TK. Reversible blood-brain barrier disruption by repeated transcranial focused ultrasound allows enhanced extravasation. J Control Release. 2011; 150:111-116.

Yang, X., Church, C. Nonlinear dynamics of gas bubbles in viscoelastic media. Acoust. Res. Lett. Online (ARLO). 2005; 6: 151–156.

Yasui K, Iida Y, Tuziuti T, Kozuka T, Towata A. Strongly interacting bubbles under an ultrasonic horn. Physical Rev E. 2008; 77: 1-10.

Yeh C, Su S. Effects of acoustic insonation parameters on ultrasound contrast agent

destruction. Ultrasound in Med & Biol. 2008; 34:1281-1291.

Yoshida J, Ohmori K, Takeuchi H, Shinomiya K, Namba T, Kondo I, Kiyomoto H, Kohno M. Treatment of ischemic limbs based on local recruitment of vascular endothelial growth factor-producing inflammatory cells with ultrasonic microbubble destruction. J Am Coll Cardiol. 2005; 46: 899-905.

Young S, Dyson M. The effect of therapeutic ultrasound on angiogenesis. Ultrasound in Med & Biol. 1990; 16: 261-269.

Zachary J, Hartleben S, Frizzell L, O'Brien WD, Jr. Contrast agent-induced cardiac arrhythmias in rats. Proc Ultrason Sym IEEE. 2001; 2:1709-1712.

Zachary JF, Hartleben SA, Frizzel LA, O'Brien WD Jr. Arrhythmias in rat hearts exposed to pulsed ultrasound after intravenous injection of a contrast agent. J Ultrasound Med. 2002; 21(12):1347-1356.

Zachary J, Blue J, Miller R, Ricconi B, Eden J, O'Brien WD Jr. Lesions of ultrasound-induced lung hemorrhage are not consistent with thermal injury. Ultrasound Med & Biol. 2006; 32(11):1763-70.

Zen K, Okigaki M, Hosokawa Y, Adachi Y, Nozawa Y, Takamiya M, Tatsumi T, Urao N, Tateishi K, Takahashi T, Matsubara H. Myocardium-targeted delivery of endothelial progenitor cells by ultrasound-mediated microbubble destruction improves cardiac function via an angiogenic response. J Mol Cell Cardiol. 2006;40: 799-809.